



ARISTOTLE UNIVERSITY OF THESSALONIKI
SCHOOL OF GEOLOGY
DEPARTMENT OF GEOLOGY



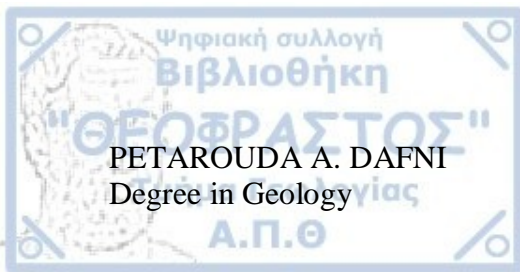
PETAROUDA A. DAFNI
Degree in Geology

REE GEOCHEMISTRY OF PARNASSOS-GIONA ZONE BAUXITES
(GIONA AREA)

MASTER THESIS
*MASTER OF SCIENCE IN 'APPLIED GEOLOGY',
SPECIALISATION: 'MINERAL RESOURCES & ENVIRONMENT'*



THESSALONIKI
2024



REE GEOCHEMISTRY OF PARNASSOS-GIONA ZONE BAUXITES (GIONA AREA)

Submitted to the School of Geology in accordance with the Master of Science 'Applied Geology', Specialization 'Mineral Resources & Environment'

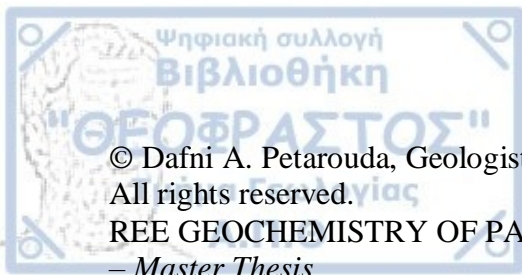
Date of Oral Exam: 11/01/2024

Three-member Committee of Inquiry

Professor Koroneos A., Supervisor

Professor Papadopoulou L., Member of the Three-member Advisory Committee

Professor Kantiranis N., Member of the Three-member Advisory Committee



© Dafni A. Petarouda, Geologist, 2024

All rights reserved.

REE GEOCHEMISTRY OF PARNASSOS-GIONA ZONE BAUXITES (GIONA AREA)

– *Master Thesis*

© Δάφνη Α. Πεταρούδα, Γεωλόγος, 2024

Με επιφύλαξη παντός δικαιώματος.

ΓΕΩΧΗΜΕΙΑ ΣΠΑΝΙΩΝ ΓΑΙΩΝ (REE) ΣΕ ΒΩΞΙΤΕΣ ΤΗΣ ΖΩΝΗΣ ΠΑΡΝΑΣΣΟΥ-ΓΚΙΩΝΑΣ (ΠΕΡΙΟΧΗ ΓΚΙΩΝΑΣ).

– *Μεταπτυχιακή Διπλωματική Εργασία*

Citation:

Petarouda A. D., 2024. – REE geochemistry of Parnassos-Giona Zone Bauxites (Giona area). Master Thesis, Department of Geology, Aristotle University of Thessaloniki, 104 pp.

Πεταρούδα Α. Δ., 2024. – Γεωχημεία σπανίων γαιών (REE) σε βωξίτες της Ζώνης Παρνασσού-Γκιώνας (περιοχή Γκιώνας). Μεταπτυχιακή Διπλωματική Εργασία, Τμήμα Γεωλογίας Α.Π.Θ., 104 σελ.

Απαγορεύεται η αντιγραφή, αποθήκευση και διανομή της παρούσας εργασίας, εξ ολοκλήρου ή τμήματος αυτής, για εμπορικό σκοπό. Επιτρέπεται η ανατύπωση, αποθήκευση και διανομή για σκοπό μη κερδοσκοπικό, εκπαιδευτικής ή ερευνητικής φύσης, υπό την προϋπόθεση να αναφέρεται η πηγή προέλευσης και να διατηρείται το παρόν μήνυμα. Ερωτήματα που αφορούν τη χρήση της εργασίας για κερδοσκοπικό σκοπό πρέπει να απευθύνονται προς το συγγραφέα.

Οι απόψεις και τα συμπεράσματα που περιέχονται σε αυτό το έγγραφο εκφράζουν το συγγραφέα και δεν πρέπει να ερμηνευτεί ότι εκφράζουν τις επίσημες θέσεις του Α.Π.Θ.

Εικόνα Εξωφύλλου: Δείγμα βωξίτη από τις εγκαταστάσεις της Imerys Βωξίτες Α.Ε. στη Φωκίδα.



TABLE OF CONTENTS

ABSTRACT	10
ΠΕΡΙΛΗΨΗ	11
1 INTRODUCTION	12
1.1 BAUXITES	13
1.2 BAUXITE CLASSIFICATION, COMPOSITION AND STRUCTURE	14
1.3 BAUXITE USES	15
1.4 KARSTIC BAUXITES	15
1.4.1 Karstic bauxites' classification.....	16
2 GEOLOGICAL SETTING OF PARNASSOS-GIONA ZONE	18
2.1 PALEOGEOGRAPHY & GEOTECTONICS.....	18
2.2 LITHOSTRATIGRAPHY & TECTOROGENESIS.....	19
3 ANALYTICAL METHODS	22
3.1 SAMPLING.....	22
3.2 MINERALOGICAL ANALYSES.....	24
3.3 CHEMICAL ANALYSES	25
3.3.1 Method of analysis of bauxite by X-Ray fluorescence (XRF).....	25
3.3.2 ICP-MS	27
4 MACROSCOPIC DESCRIPTION	28
4.1 COLOUR CLASSIFICATION.....	28
5 MINERALOGY	38
5.1 CLASSIFICATION	39
5.1.1 Samples classification based on mineralogical composition.	40
6 GEOCHEMISTRY	43
6.1 MAJOR ELEMENTS	43
6.1.1 Samples classification based on major elements.	46
6.2 TRACE ELEMENTS	49



6.2.1	Sample classification based on trace elements.....	54
6.3	RARE EARTH ELEMENTS (REE).....	57
6.3.1	Sample classification based on REE contents.....	59
6.3.2	Chondrite-normalized rare earth elements diagrams (REE).	62
6.4	COMPARISON WITH KARST-BAUXITE SAMPLES FROM PARNASSOS-GIONA ZONE	64
7	BAUXITE DEPOSITS' CORRELATION COMPARISON	67
7.1	PEARSON'S CORRELATION.....	67
7.2	GREECE	68
7.2.1	Correlation between ΣREE, ΣLREE, ΣHREE and major elements, Pisoliths_size, Pisoliths_percent.	71
7.2.2	Boxplots.....	72
7.2.3	ANOVA.....	76
7.3	CHINA	77
7.3.1	Longhe.....	77
7.3.2	Tianyang	80
7.3.3	Western Guangxi.....	82
7.3.4	Henan.....	87
7.4	MONTENEGRO.....	89
8	DISCUSSION	92
9	CONCLUSIONS.....	96
	REFERENCES.....	98



LIST OF FIGURES

Figure 1: Bauxite deposit world map https://www.usgs.gov/media/images/bauxite-deposit-world-map (retrieved 14/02/2022).	14
Figure 2: Structural zones of the Hellenides. Location map and stratigraphic column of the Parnassos-Giona bauxite deposits.	20
Figure 3: Imerys Bauxites S.A. - Fokida. Photographer: Koroneos A.	22
Figure 4: Geographical position of the Imerys Bauxites S.A. mines where the samples were retrieved from, Fokida, Central Greece. The mines are shown with a yellow pushpin on the map.	23
Figure 5: X-ray diffractometer (XRD), Philips PW1820/00-type, Department of Mineralogy-Petrology-Economic geology, Aristotle University of Thessaloniki.	24
Figure 6: Scatter plots of $\text{SiO}_2 - \text{Al}_2\text{O}_3$ and $\text{Al}_2\text{O}_3 - \text{Fe}_2\text{O}_3$. S.3 samples are defined.	46
Figure 7: Chondrite-normalized rare earth elements diagrams (REE) (Sun and McDonough, 1989). Each region is represented by a different colour and the total samples range is presented in the background with grey colour.	63
Figure 8: Chondrite-normalised rare earth elements diagram (REE) from Parnassos-Giona Zone (Sun and McDonough, 1989). The chart area in yellow represents the Fe-rich samples from Parnassos-Giona Zone (Gamaletsos, 2014). The dotted grey area represents sample measurements from the current Master thesis.	66
Figure 9: Box plots of ΣREE , ΣHREE and ΣLREE by colour.	74
Figure 10: Box plots of ΣREE , ΣHREE and ΣLREE by region.	75
Figure 11: Bar graph of the major elements and the total rare earth elements (ΣREE) for every area of study.	94
Figure 12: Bar graph of the major elements and the total light rare earth elements (ΣLREE) for every area of study.	95
Figure 13: Bar graph of the major elements and the total heavy rare earth elements (ΣHREE) for every area of study.	95



LIST OF TABLES

Table 1: Colour classification of the 23 samples of the area of study, BR: brownish-red, OR: orange-red and Y: yellow.	28
Table 2: Bauxite sample photographs - <i>to be continued</i>	29
Table 3: Samples' area, samples' pisoliths area and percentage of the pisoliths of the calculated area.	37
Table 4: Mineralogical composition (wt.%) of the studied samples by X-ray diffraction (XRD).	39
Table 5: Clusters based on mineralogical composition.	41
Table 6: Final cluster centers based on mineralogical composition.	42
Table 7: Cluster membership based on major element wt.% concentration.	47
Table 8: Final cluster centers based on major element wt.% concentration.	48
Table 9: Trace elements concentration (ppm) of bauxite rock samples - <i>to be continued</i>	51
Table 10: Variation and average values of the trace elements concentration (ppm) of bauxite rock samples.	53
Table 11: Clusters based on trace elements content.	54
Table 12: Final cluster centers based on trace element content.	55
Table 13: Rare earth elements concentration (ppm) of bauxite rock samples.	58
Table 14: Variation and average value of the rare earth elements (REE) concentration (ppm) of bauxite rock samples.	59
Table 15: Clusters based on rare earth element content.	60
Table 16: Final cluster centers based on rare earth element content.	61
Table 17: Major (wt.%) and rare earth elements (ppm) concentration of other authors (Gamaletsos, 2014).	64
Table 18: Variation and average values of major (wt.%) and rare earth elements (ppm) concentration of other authors (Gamaletsos, 2014).	65

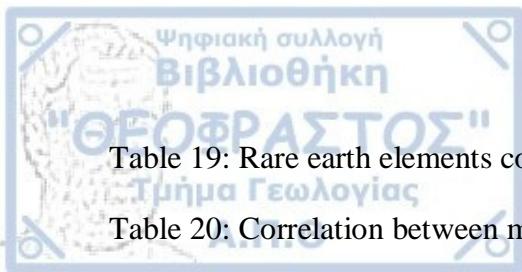


Table 19: Rare earth elements concentrations (ppm) of analyzed samples.	69
Table 20: Correlation between major elements and rare earth elements (REE), Greece.	70
Table 21: Pearson correlation estimates.	71
Table 22: Table of the p-values of the ANOVA test for the categorical data (REGION & COLOUR) and the ΣREE, ΣLREE and ΣHREE.	76
Table 23: Major (wt.%) and rare earth elements (ppm) concentration of analyzed samples of Longhe, China (Liu <i>et al.</i> , 2016).	78
Table 24: Correlation between major elements and rare earth elements (REE), Longhe, China.	79
Table 25: Major (wt.%) and rare earth elements (ppm) concentrations of analyzed samples of Tianyang, China (Liu <i>et al.</i> , 2016).	81
Table 26: Correlation between major elements and rare earth elements (REE), Tianyang, China.	82
Table 27: Major (wt.%) and rare earth elements (ppm) concentrations of analyzed samples of Western Guangxi, China (Liu <i>et al.</i> , 2010) - <i>continued</i>	84
Table 28: Major (wt.%) and rare earth elements (ppm) concentrations of analyzed samples of Western Guangxi, China (Liu <i>et al.</i> , 2010) - <i>continued</i>	85
Table 29: Correlation between major elements and rare earth elements (REE), Western Guangxi, China.	86
Table 30: Major (wt.%) and rare earth elements (ppm) concentrations of analyzed samples of Henan, China (Liu <i>et al.</i> , 2013).	87
Table 31: Correlation between major elements and rare earth elements (REE), Henan, China.	88
Table 32: Major (wt.%) and rare earth elements (ppm) concentrations of analyzed samples of Montenegro (Radusinović and Papadopoulos, 2021).	90
Table 33: Correlation between major elements and rare earth elements (REE), Montenegro.	91



FOREWORD

The present Master thesis was conducted within the framework of the postgraduate program 'Applied Geology' of the Department of Geology, Aristotle University of Thessaloniki, with a specialisation in 'Mineral resources & Environment', under the supervision of Professor Antonios Koroneos.

The analysed samples of this Master thesis were taken from Imerys Bauxites S.A. facilities in Fokida, Central Greece, where the X-Ray fluorescence (XRF) analysis also took place by Dr. Panagiotis Zachariadis, Projects and Bauxite Sourcing Geologist of the company. The X-ray diffraction (XRD) analysis took place at the Faculty of Geology, in the laboratories of the Department of Mineralogy-Petrology-Economic Geology, with the help and supervision of Professor and member of the Three-member Advisory Committee of this thesis, Nikolaos Kantiranis. Inductively coupled plasma mass spectrometry (ICP-MS) was the method that was used for the trace and REE geochemical analysis of the samples. The method was conducted in the Scripps Institution of Oceanography's Scripps Isotope Geochemistry Laboratory in California, USA, by Dr. James Day.

I would like to thank Imerys Bauxites S.A and Dr. Panagiotis Zachariadis, Projects and Bauxite Sourcing Geologist of the company, for providing the samples and executing the XRF analysis of the samples that are used in the current thesis. I would also like to thank Dr. Ioannis Baziotis and Dr. James Day for the help and implementation of the ICP-MS analysis of the samples, as well as Dr. Platon Gamaletsos for his advice and contribution.

In addition, I would like to thank Professor Antonios Koroneos for all the guidance, his patience and help he provided me to complete this Master thesis. I would also like to thank the other members of the Committee of Inquiry, Professor Nikolaos Kantiranis and Professor Lambrini Papadopoulou, for the advice and contribution on this dissertation.

At last, I would like to thank my family, friends, colleagues and cat for the support and love needed for the completion of this thesis.



ABSTRACT

In this thesis, the existence of rare earth elements (REE) in the Parnassos-Giona Zone bauxites, their geochemical value, as well as any possible correlation between the REE, the region and the colour of the bauxites, the samples' major elements content, pisolithic size and the pisoliths' percentage are examined. Twenty-three samples were collected from 6 different mines of the Imerys Bauxites S.A. facilities for macroscopic, mineralogical (XRD) and chemical (XRF, ICP-MS) analyses. Mineralogical analyses reveal that diaspore and boehmite are the major minerals in the bauxite ores, while their pisolithic percentage and colour varies, the latter between yellow, orange-red and brownish-red. The samples from Koromilia mine differentiate from the rest in Li and La values, as well as the sample S.5_1, from 526 mine which presents most of the highest values in traces and rare earth elements. Chondrite-normalized rare earth elements diagrams per region show a positive Ce anomaly. The analysed samples of this research show no statistically significant correlation between the major elements, the region, the bauxitic colour, the size or the percentage of the samples' pisoliths. Finally, the correlation comparison between Greece, China and Montenegro bauxite deposits shows that those from China have the highest positive and negative correlations among the three countries, the Montenegro deposit comes in second place and the Greek deposit show in general the lowest correlation coefficient.



ΠΕΡΙΛΗΨΗ

Στην παρούσα διπλωματική εργασία εξετάζεται η ύπαρξη σπανίων γαιών (REE) στους βωξίτες της Ζώνης Παρνασσού-Γκιώνας, η γεωχημική τους αξία, καθώς και κάθε πιθανή συσχέτιση μεταξύ των REE, της περιοχής και του χρώματος των βωξιτών, καθώς και των κύριων στοιχείων, του μεγέθους και του ποσοστού των πηλολίθων. Το κοίτασμα βωξίτη Παρνασσού-Γκιώνας βρίσκεται στη Φωκίδα, στην κεντρική Ελλάδα, και αποτελεί μέρος της γεωτεκτονικής ζώνης Παρνασσού-Γκιώνας, που περιλαμβάνει τα βουνά Παρνασσός, Γκιώνα, Καλλίδρομο, Ελικώνας και ορισμένα τμήματα του όρους Οίτη. Αυτές οι αποθέσεις φιλοξενούνται μέσα σε ανθρακικά πετρώματα και τοποθετούνται σε τρεις διαδοχικούς λιθοστρωματογραφικούς ορίζοντες, οι οποίοι αντιπροσωπεύουν τρεις διαφορετικές εποχές από το Μέσο-Άνω Τριαδικό έως το Ανώτερο Κρητιδικό. Συλλέχθηκαν 23 δείγματα από 6 διαφορετικά ορυχεία των εγκαταστάσεων της Imerys Βωξίτες Α.Ε. για μακροσκοπικές, ορυκτολογικές (XRD) και χημικές (XRF, ICP-MS) αναλύσεις. Οι ορυκτολογικές αναλύσεις αποκαλύπτουν ότι το διάσπορο και ο μπαιμίτης είναι τα κύρια ορυκτά στα μεταλλεύματα βωξίτη, ενώ το ποσοστό και το χρώμα τους ποικίλλει, το τελευταίο μεταξύ κίτρινου, πορτοκαλοκόκκινου και καστανοκόκκινου. Τα δείγματα από το ορυχείο Κορομηλιάς διαφοροποιούνται από τα υπόλοιπα σε τιμές Li και La, καθώς και το δείγμα S.5_1, από το ορυχείο 526, που παρουσιάζει τις περισσότερες από τις υψηλότερες τιμές σε ιχνοστοιχεία και σπάνιων γαιών. Τα διαγράμματα σπάνιων γαιών, κανονικοποιημένων με χονδρίτη, ανά περιοχή δείχνουν μια απότομη αύξηση στην τιμή Ce. Τα αναλυθέντα δείγματα αυτής της έρευνας δεν δείχνουν στατιστικά σημαντική συσχέτιση μεταξύ των κύριων στοιχείων, της περιοχής, του βωξιτικού χρώματος, του μεγέθους ή του ποσοστού των πηλολίθων των δειγμάτων. Τέλος, η σύγκριση συσχέτισης μεταξύ Ελλάδας, Κίνας και Μαυροβουνίου δείχνει ότι οι περιοχές από την Κίνα έχουν τις υψηλότερες θετικές και αρνητικές συσχετίσεις μεταξύ των τριών χωρών, ενώ το Μαυροβούνιο έρχεται στη δεύτερη θέση.



1 INTRODUCTION

It is no secret that the world is looking, frantically, for a release from China's monopoly in rare earth elements, with all the political aspects which surround this statement. Thankfully, bauxite deposits can be a great source for rare earth elements (REE).

It is important, either positive or negative correlations, to be found between the rare earth elements (REE) abundances and other relative variables eg. colour of bauxites, pisoliths, major element composition, etc. These correlations could create a useful tool for the researchers and the companies that are looking for rare earth elements' exploitation, simultaneously with the bauxites' extraction, the better environmentally friendly approach this relationship could provide, the cover of needs that are becoming more crucial every day in this modern world with its vast necessities of technological items and development. Furthermore, the profit, not only for the mining companies, but for the country's economy in total.

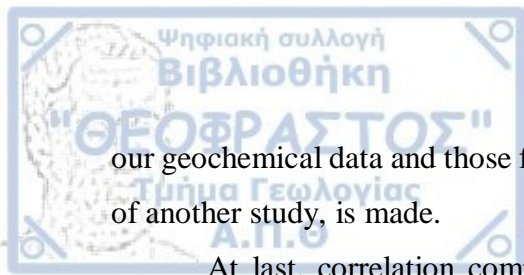
On a genetic basis bauxite deposits are classified in three types: lateritic, karstic and Tikhvin. Well-known karstic bauxite deposits are found in Fokida, Central Greece, which is part of Parnassos-Giona Zone.

The aim of this thesis is to examine the existence of rare earth elements (REE) in the Parnassos-Giona Zone bauxites, their concentration, the mineralogy, the correlation between the REE, the region of the bauxite samples, the colour of the bauxites, the samples' major elements content, the samples' pisolithic size and the pisoliths' percentage.

To begin with, some general information is provided on bauxites, bauxite classification, composition, structure and uses, as well as karstic bauxites in particular and their classification. The geological setting of Parnassos-Giona Zone is described and specifically, the paleogeography, the geotectonics and the lithostratigraphy.

Twenty-three samples were collected from Imerys Bauxites S.A. facilities in Fokida, Central Greece, from 6 different mines. The samples were analysed with the use of X-ray diffraction (XRD), X-Ray fluorescence (XRF), and inductively coupled plasma mass spectrometry (ICP-MS). A macroscopic analysis was conducted to classify the samples by colour, pisoliths' area and pisoliths' percentage. Two-sided photographs of all the samples are provided. The mineralogical analysis of the results that came out of the X-ray diffraction (XRD) and their classification is presented.

Further, in the thesis, the samples are classified based on their geochemistry and chondrite-normalized REE diagrams per region are constructed. A small comparison between



our geochemical data and those from Fe-rich samples, as well, from the Parnassos-Giona Zone of another study, is made.

At last, correlation comparisons between our samples from Greece and some from China (Longhe, Tianyang, Western Guangxi, Henan) and Montenegro with the use of Pearson's correlation are made. Specifically for Greece, ANOVA test was also used for further investigation, as well as visualisation models, such as boxplots.

A brief discussion on the results and the conclusions that arise from this thesis complete this research, leaving more questions that demand their own answer.

1.1 BAUXITES

Bauxite was originally recognized by the French geologist P. Berthier in 1821 as an aluminum (Al) ore in the village of Les Baux in southern France, but it wasn't until 1844 when another French scientist Dufrenoy proposed its current name deriving from the area where it was first found (Gamaletsos, 2014).

Bauxites are formations that consist of large contents of aluminium hydroxide ($\text{Al}(\text{OH})_3$) bearing minerals. They are formed under tropical conditions, such as excessive heat and humidity, due to intense surficial weathering of various rock types of the surrounding area or of the geological substratum (Harder, 1949; Gow and Lozej, 1993). "The main chemical processes that contribute to weathering include dissolution, oxidation, hydrolysis and acid hydrolysis" (Gamaletsos, 2014). Hence, special climatic periods during the Earth's history have played an important role in the formation of bauxites. In the European continent Late Paleozoic, Middle-Late Cretaceous and Upper Jurassic to Eocene are the most important periods for bauxitization processes (Gow and Lozej, 1993; Gamaletsos, 2014).

Various rock types are considered responsible for the formation of bauxites, but the most predominant are the ones that are rich in Al_2O_3 and contain a large quantity of soluble compounds. Along with the climatic conditions, the Eh and pH, the groundwater's composition and the topographic changes affect the bauxitization processes.

Important bauxite deposits (Figure 1) are found in limestones in Europe and the Mediterranean region, bauxites that were formed from basaltic bedrock in India, from clays in U.S.A., igneous, metamorphic or sedimentary rocks in Malaysia, Guyana, Venezuela, schists, phyllites, sandstones in French Guinea, etc. (Harder, 1949; Soler and Lasaga, 1996; Robb, 2005).

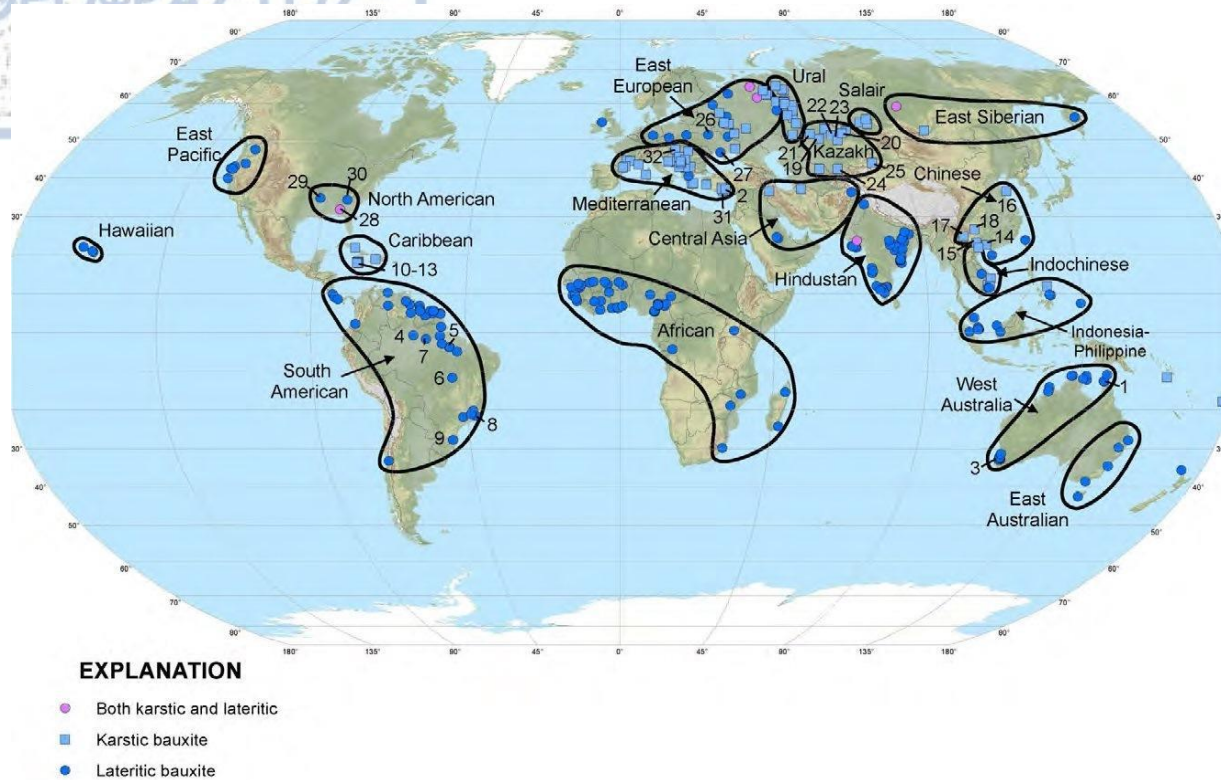


Figure 1: Bauxite deposit world map <https://www.usgs.gov/media/images/bauxite-deposit-world-map> (retrieved 14/02/2022).

1.2 BAUXITE CLASSIFICATION, COMPOSITION AND STRUCTURE

For the bauxites' classification, various criteria can be used such as the mineralogy, the chemical composition, the area's geomorphology and the type of the parent rock (Bárdossy and Aleva, 1990; Gow and Lozej, 1993).

The classification based on the parent rock as well as genetic and paleogeographical characteristics lead to three different types. The first type, known as the 'lateritic' deposits, is created by chemical weathering on top of the parent rock. These are residual deposits deriving from the underlying rocks and they represent 88% of bauxite production worldwide. The second type is the 'karstic' type or the 'terra rossa' deposits, as they're also known, found in karst carbonate rocks like limestones, dolomites and marls, representing 14% of the world's bauxite production. Finally, the third type known as 'sedimentary' type or 'Tikhvin' type, as it's well-known, are detrital bauxite deposits found on eroded aluminosilicate rocks' surfaces, representing only 1% of bauxite production.

Another method to classify the bauxites is based on their colour, as it can reveal the presence of some minerals. Therefore, we can classify them in the following types:



- Red or red-brownish, showing the existence of hematite.
- Yellow, revealing the existence of goethite.
- Grey, showing a small amount of Fe-oxides.
- White that doesn't contain any Fe-oxides.

(Bárdossy and Aleva, 1990; Gow and Lozej, 1993; Bárdossy and Combes, 1999; Nyamsari & Yalcin, 2017).

Bauxites are mostly composed of Al-hydroxides: gibbsite, boehmite and diaspore. Gibbsite is found, particularly, in Tertiary and lateritic deposits, while boehmite and diaspore are found in karstic deposits. In Greece, the bauxite deposits include boehmite and diaspore, while gibbsite is rarely found or completely absent, resulting in a low LOI of the bauxites. They are also, often, composed of kaolinite, Fe-oxyhydroxides, Ti-oxides and Mn-oxides.

The bauxitic structure ranges from granular to pisolithic, stratified or massive, pseudomorphic or even structureless. Generally, the older ones are harder and tend to be composed of boehmite and diaspore, as the ones we have sampled, while the newer ones are softer and composed of gibbsite (Gow and Lozej, 1993; Eliopoulos *et al.*, 2014; Gamaletsos, 2014; Alderton and Elias, 2020).

1.3 BAUXITE USES

Bauxite has several uses. It's an important raw material for the primary aluminium industry. It is also used in non-metallurgical sectors such as cement, Portland type cement, as a refractory, abrasive, making chemicals and steel. In addition, it is used in various industries like dyeing, printing, treating sewage and tannins in water purification. Furthermore, aluminium and its by-products are extensively used in construction, in railings, airports, aircrafts, satellites, in electrical industry in multiple ways, in explosives, rocket fuels and many more. (Patil, 1993; Orescanin *et al.*, 2006; Kehagia, 2010; Gándara, 2013; Mymrin *et al.*, 2017; Verma *et al.*, 2017; Ismail *et al.*, 2019; Bullerjahn and Bolte, 2022; Chao *et al.*, 2022)

1.4 KARSTIC BAUXITES

The karst-bauxite deposits and terra rossa occurrences of the Mediterranean region are found on or within carbonate rocks that were subjected to karstification on mobile platforms or in the orogenic belts and are formed by residual clays that accumulate, following the weathering of different rock types and aluminosilicate minerals. The formation that results

from the chemical processes and the depressions of the regional topography is called ferrillite or terra rossa (ferrillitic soils), is of red colour and rich in iron (Fe) and aluminium (Al). Chronically, the Mediterranean type bauxites developed during the Triassic-Cretaceous-Eocene on Mesozoic carbonate platforms of the European and Adriatic region (Bardossy, 1984; Maksimovic and Pantó, 1991; Gow and Lozej, 1993; Zedef and Doyen, 2009; Gamaletsos, 2014).

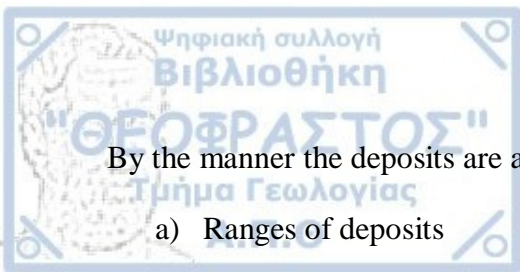
1.4.1 Karstic bauxites' classification

According to Bárdossy (2013) we can subdivide the karst bauxite deposits into six categories by depositological criteria:

- a) Kazakhstan type
- b) Mediterranean type
- c) Tulska type
- d) Ariège type
- e) Salento type
- f) Timan type

Based on deposits' sizes and shapes they are subdivided into:

- a) Stratiform deposits
- b) Blanket deposits
- c) Strip-like deposits
- d) Strip-Valley deposits
- e) Lenticular deposits
- f) Graben deposits
- g) Canyon-like deposits
- h) Sinkhole deposits
- i) Bauxite 'nests' and 'bags'
- j) Flat lenses



By the manner the deposits are arranged:

- a) Ranges of deposits
- b) Fields of deposits

By the relationship of the bauxite:

- a) To its bedrock
- b) To its cover (Bárdossy, 2013)

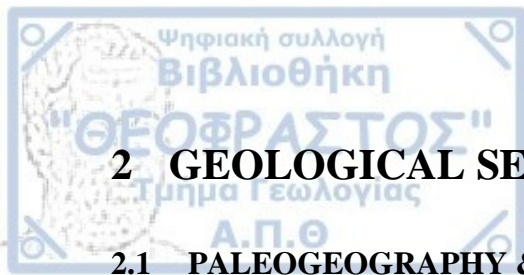
Based on sedimentary sequences along with paleogeographic reconstructions:

- a) Autochthonous
- b) Parautochthonous
- c) Allochthonous
- d) Parallochthonous

Based on paleogeography and the geotectonical position:

- a) Intracontinental
- b) Margin-Continental
- c) Shallow, marine platforms

They could also be classified by the mineralogy, the hydrogeological position, the chemical composition and plenty of other factors. Thus, the bauxites themselves can, as well, be used as indicators in geodynamics, paleoclimate, tectonic instability and eustatic movements (Bárdossy and Combes, 1999).



2 GEOLOGICAL SETTING OF PARNASSOS-GIONA ZONE

2.1 PALEOGEOGRAPHY & GEOTECTONICS

The Parnassos-Giona Zone was labelled by Philippson (1898), who was the first to recognize its distinguishable existence, as the "subzone of Parnassos". In 1940 it was named by Renz (1940) the Parnassos-Giona Zone, respectively to the Parnassos and Giona mountains of central Greece which form the main zone, but it has later been referred to as the Parnassos Zone (Gregou, 1996).

The geotectonic zone of the Parnassos-Giona is of limited geographical extension positioned in central Greece, including the mountains of Parnassos, Giona, Kalidromon, Elikonas and some parts of mountain Iti (Gregou, 1996; Eliopoulos *et al.*, 2014). In the past, it has been claimed, that the "Trapezona unit" in Argolis, NE Peloponnese, represents the southern extension of the Parnassos Zone (Dercourt, 1964; Gregou, 1996). Nowadays, however, the presence of Parnassos-Giona Zone in Peloponnese is considered quite doubtful, and it is believed to be a reef dam or a locally inserted ridge in the ocean of Neo-Tethys, neighboring the Sub-Pelagonian Zone (Mountrakis, 2010). It is stated that the southern extension of Parnassos was interrupted because of the activation of the Corinthiakos transverse fault, after the Triassic-Early Cretaceous. Aubouin (1977) accredited that the zone re-appeared in regard to the northern extension of Parnassos in Albania, as the "nordalbanische tafel" (Nopcsa, 1921), along with the former Republic of Yugoslavia, as the "westmontenegrisch-kroatisch Hochkarstzone" (Kossmat, 1924; Dercourt, 1980; Gregou, 1996).

At present, these zones in Albania and the former Republic of Yugoslavia are considered as the northern extensions of the Gavrovo-Tripolis Zone, although Parnassos-Giona Zone and the "High Karst Zone" do have in common one important characteristic, the karst-bauxite deposits (Gregou, 1996; Mountrakis, 2010).

The activation of the Spercheios's river valley transverse fault, after the Triassic-Early Jurassic is considered responsible for the disappearance of Parnassos-Giona Zone. Therefore, having the Spercheios's fault to the north and the Corinthiakos fault to the south, both of which are being active at the moment, the carbonate platform of Parnassos was affected by the severe transverse faults.

To the western side of the Parnassos-Giona Zone a transition is held by the Vardousia unit towards the Pindos-Olonos Zone, while to the east side the transition is held by the Boetian Zone to the Pelagonian Zone. Basically, the Parnassos-Giona Zone which is the innermost of

the external Hellenides, overthrusts the Pindos-Olonos Zone from the east side through the transitional Vardousia unit, while in the contrary, it is overthrust by the Boetian Zone and the Sub-Pelagonian Zone to the east (Celet et al., 1976; Clement, 1977; Fleury, 1980; Gregou, 1996).

2.2 LITHOSTRATIGRAPHY & TECTOROGENESIS

A distinctive characteristic of this zone are the bauxite deposits that are hosted within carbonate rocks, set in three consecutive lithostratigraphic horizons, each of which represents a different era. The Pre-Alpine basin of the zone is not known, except for the fact that igneous rocks are totally absent.

The Alpine sedimentation is nearly continuous, calcareous, purely neritic, which leads us to the conclusion that the paleogeographic position of the zone was indeed a reef dam or a small underwater platform of epicontinental carbonates from the Upper Triassic to the Upper Cretaceous.

The general stratigraphic column of the Parnassos-Giona Zone consists of the following units (Gregou, 1996; Mountrakis, 2010; Deady *et al.*, 2014; Eliopoulos *et al.*, 2014) (Figure 2):

- **Middle-Late Triassic:** White dolomites grading upwards into greyish dolomites and alternating with thin limestone intercalations (approx. 600 m).
- **Early-Middle Jurassic:** Grey and dark colored dolomitic, bituminous often oolitic and/or pisolithic, limestones (approx. 400 m).
- **Bauxite horizon 1 (B1):** Pisolithic in texture, undissolved (of diasporic type) and of no economic value as of today.
- **Late Jurassic:** Dark, thick-bedded limestones of Kimmeridgian age and limestones with corals of Portlandian-Tithonian age (approx. 300 m).
- **Bauxite horizon 2 (B2):** Based above the Kimmeridgian limestones and extended in a greater geographical area than the previous bauxite horizon (B1), is dissolved (of boehmitic type) and is of great economic value.
- **Tithonian-Cenomanian:** Reddish argillaceous limestones, which change upwards into greyish oolitic limestones with thin bauxite layers of pisolithic type (approx. 300-400 m). The beds of Tithonian-Cenomanian age are known as the "intermediate limestones" because they stand between the two bauxitic horizons: B2-B3 (Mountrakis, 2010), but

another term, "Limestones of Amfissa", has been also proposed and used by some researchers (Carras & Fazzuoli, 1991).

- **Bauxite horizon 3 (B3):** On top of the Tithonian-Cenomanian limestones, of pisolithic texture, undissolved (of diasporic type) like the first bauxite horizon (B1). It is the most intriguing considering the economic aspect.
- **Late Cretaceous:** A thin horizon of dark limestones grading upwards into grey, thick-bedded, rudist-bearing limestones of Turonian-early Campanian age (approx. 200 m). This is followed by transitional nodular limestones and greyish-white, reddish or greyish-green thin-bedded neritic limestones of late Campanian-Maastrichtian age (approx. 150-200 m).
- **Paleocene-Late Eocene:** Transitional red nodular shales of calcareous marl composition (Celet, 1962; Gregou, 1996) that grade upwards into the sediments of the typical Eocenian flysch, evolving in sandy-argillaceous flysch and conglomerates.

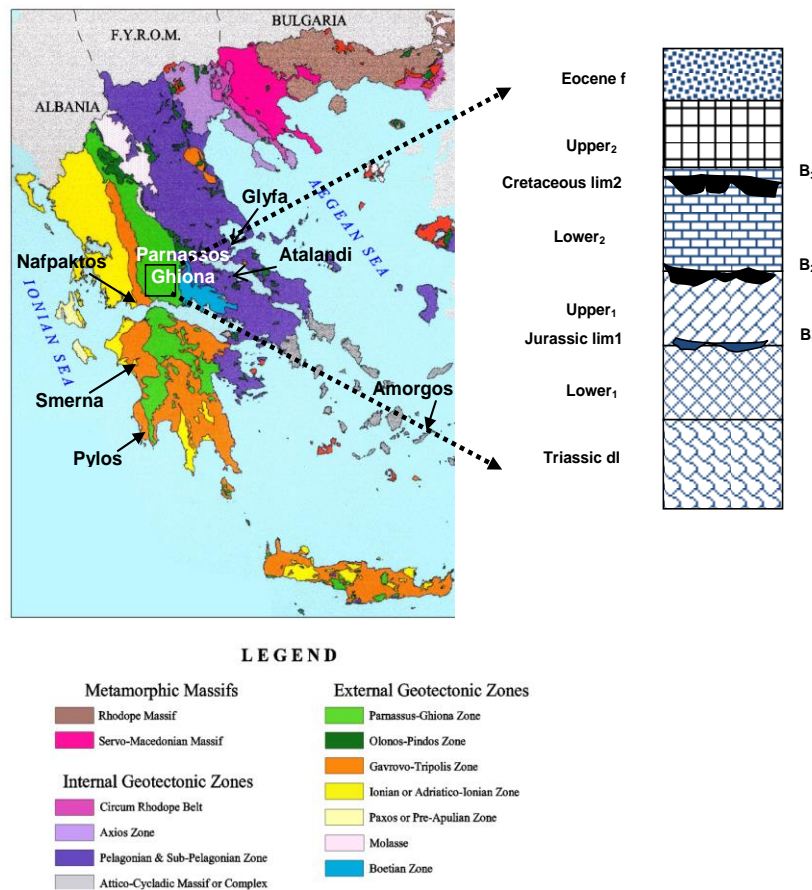
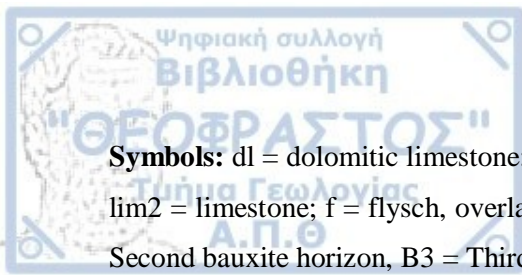


Figure 2: Structural zones of the Hellenides. Location map and stratigraphic column of the Parnassos-Ghiona bauxite deposits.



Symbols: dl = dolomitic limestone; lim1 = grey (Lower) and dark colored (Upper) Jurassic limestone; lim2 = limestone; f = flysch, overlain by Quaternary conglomerates; B1 = First bauxite horizon, B2 = Second bauxite horizon, B3 = Third bauxite horizon (Eliopoulos et al., 2014)

The key element to study the tectogenesis of the Parnassos-Giona Zone is the existence of the three intercalated bauxite horizons to the continuous calcareous unit.

According to many, bauxites are formed during land emerging periods. Therefore, the three bauxite horizons represent the three successive emersions of the zone and the three sedimentation interruptions. During the Mesozoic era, the area consisted of a carbonate platform where neritic sedimentation took place and got interrupted during three main exposure episodes, on which the three different bauxite horizons accumulated. These bauxite deposits were formed from the clastic, ophiolitic sediments that were transferred from the erosion of the internal Hellenides.

The internal Hellenides were affected by the early orogeny, as well as the external ones where the sedimentation was continuous and not interrupted. Specifically, during the Late Cretaceous, the Parnassos-Giona Zone was affected by horst and graben tectonism, when some of these horsts were exposed and subsequently excessively karstified, while in the submarine grabens neritic sedimentation took place. It was the K/T transition (Cretaceous-Tertiary- K from the German word for Cretaceous) that caused the formation of ironphosphate-rich hardgrounds.

Nevertheless, since an important stratigraphic void is not ascertained between the Triassic to Middle-Upper Eocene, which is a typical characteristic of the external Hellenides, it is widely accepted that the Parnassos-Giona Zone belongs to the external Hellenides. (Celet, 1958, 1962, 1977; Papastamatiou, 1960; Pomoni-Papaioannou and Solakius, 1991; Richter et al., 1991; Solakius et al., 1992; Gregou, 1996; Mountrakis, 2010).

3 ANALYTICAL METHODS

3.1 SAMPLING

Twenty-three samples from the three bauxite horizons from the Imerys Bauxites S.A. facilities (Figure 3), from the Parnassos-Giona area, were collected for mineralogical and geochemical analyses. The geographical position of the mines where the samples were retrieved from, is shown on the map displayed below (Figure 4).



Figure 3: Imerys Bauxites S.A. - Fokida. Photographer: Koroneos A.

The samples S.3_1, S.3_2, S.3_3, S.3_4 and S.3_5 were collected from pile S3 of the Koromilia mine and belong to the second bauxite horizon (B2). Sample S.3_1 is a typical bauxite. Sample S.3_2 is a leached spotted bauxite. Sample S.3_3 is a compact bauxite, more solid than sample S.3_1. Sample S.3_4 is leached, of a yellowish colour due to its contact to the roof. Sample S.3_5 is leached and very similar to sample S.3_2.

The samples S.4_1, S.4_2, S.4_3 were collected from the pile S5 of the Nera mine. The first two are intensively fragmented, while sample S.4_3 is slightly more solid.

The samples S.5_1, S.5_2, S.5_3 and S.5_4 were collected from pile 5 of the 526 mine. S.5_1 and S.5_2 represent typical bauxites, sample S.5_3 contains large pisoliths, while S.5_4 looks somehow in between the other three samples.

The samples S.5_5, S.5_6 and S.5_7 were collected from pile S5 of the Koukouvista mine. Sample S.5_5 contains a lot of large pisoliths, sample S.5_6 contains even larger pisoliths than S.5_5 and sample S.5_7 stands in between the previous two.

The samples S.6_1, S.6_2, S.6_3 and S.6_4 belong to pile S6 from the Sila mine. Sample S.6_1 is a typical pisolithic bauxite with a lot of small pisoliths. Sample S.6_2 is whitish and slightly corroded. Sample S.6_3 is a typical white bauxite and sample S.6_4 is a bauxite that contains large pisoliths.

The samples S.7_1, S.7_2, S.7_3 and S.7_4 were retrieved from pile S7 of the Kamara mine that belongs to the third bauxite horizon (B3). Sample S.7_1 is pisolithic bauxite that contains sparsely a few pisoliths. Sample S.7_2 is like S.7_1 but with more pisoliths, while S.7_3 stands in between them considering the pisolithic quantity. Sample S.7_4 is a leached bauxite.

The samples were, firstly, shattered in smaller pieces and subsequently put in a Mixer Mill conducted by the Imerys's personnel, where under hammering and abrasion processes, homogenized powder from each sample was produced.

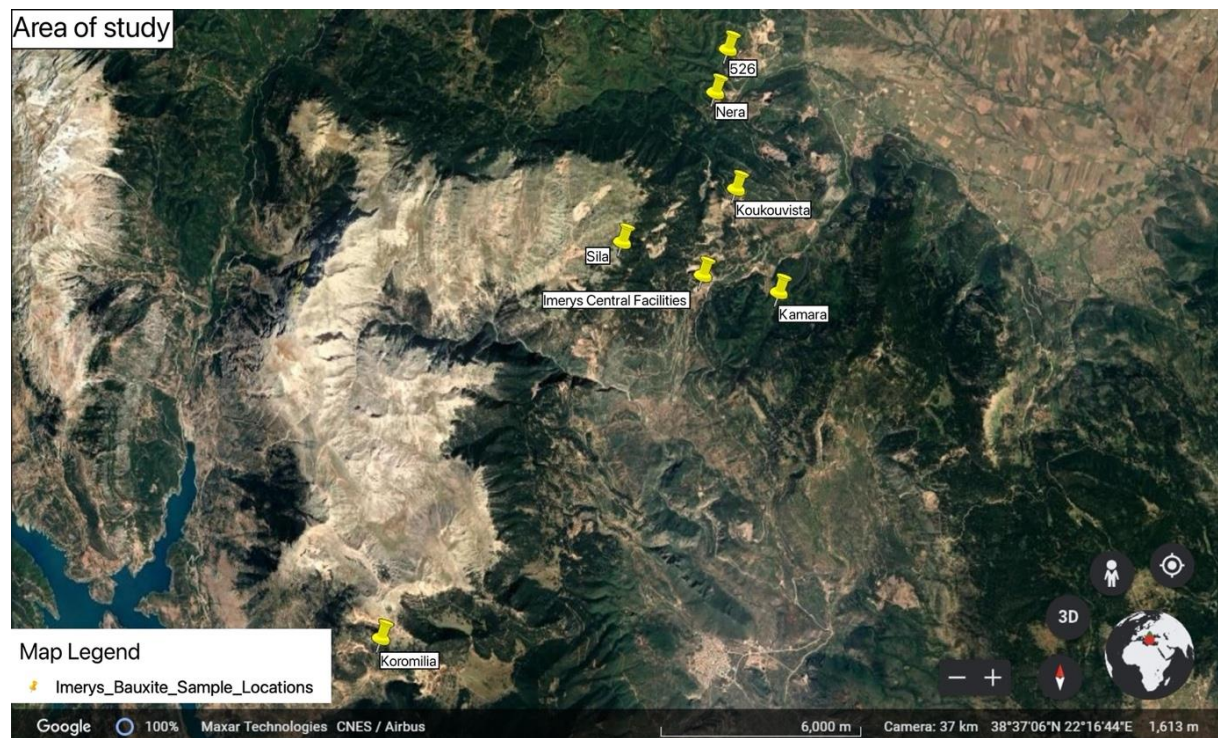


Figure 4: Geographical position of the Imerys Bauxites S.A. mines where the samples were retrieved from, Fokida, Central Greece. The mines are shown with a yellow pushpin on the map.

3.2 MINERALOGICAL ANALYSES

Microscopic studies of the mineralogy and texture of rocks in thin sections and polished blocks were performed at the laboratory of the School of Geology, in Aristotle University of Thessaloniki, Greece. The mineralogical compositions of powdered rock and ore samples were determined at the Faculty of Geology, in the laboratories of the Department of Mineralogy-Petrology-Economic Geology, after being grinded with an agate mortar and pestle by hand. The X-ray diffraction (XRD) analysis was performed using a Philips PW1840 diffractometer, with Ni-filtered CuK α radiation, at 40kV voltage and 30mA amperage, 2θ interval from 3° to 63° degrees, scanning speed of 1° 2θ /min, step size of 0.02° and time per step 5 sec (for more details see (Kantiranis *et al.*, 2004)).



Figure 5: X-ray diffractometer (XRD), Philips PW1820/00-type, Department of Mineralogy-Petrology-Economic geology, Aristotle University of Thessaloniki.

3.3 CHEMICAL ANALYSES

3.3.1 Method of analysis of bauxite by X-Ray fluorescence (XRF)

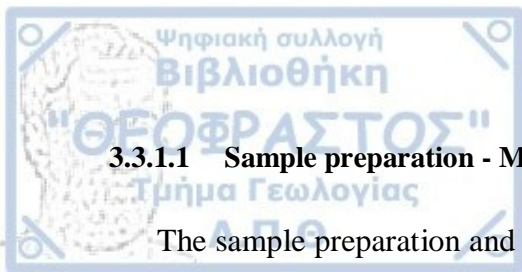
As for the analysis of the bauxite samples, that took place in the Imerys Bauxites S.A. facilities in Fokida, Central Greece, X-Ray Fluorescence (XRF) was used. The subject of this method is to determine the weight percentage concentration of the elements Al, Fe, Si, Ti, Ca, S and Zn in bauxite samples.

The people who were responsible for the observance of the relevant directive are, the quality control manager and the chemistry staff of the Processing and Loading Sector. The information was provided by Dr. Panagiotis Zachariadis, Projects and Bauxite Sourcing Geologist at Imerys Buxites S.A. facilities in Fokida, Central Greece.

For the conduction of this method, specific reagents were used. Specifically, $\text{Li}_2\text{B}_4\text{O}_7$, La_2O_3 , LiNO_3 and KBr . $\text{Li}_2\text{B}_4\text{O}_7$, used for the preparation of glass beads (pearls), was dried at $675\text{ }^\circ\text{C}$ and kept constantly in a desiccator, because of its hygroscopic nature. La_2O_3 was ignited at $1100\text{ }^\circ\text{C}$ overnight and kept in a desiccator. Subsequently, when the reagent was introduced into the oven, anti-thermal gloves and special safety glasses had to be used as a precaution measure.

The necessary equipment that was used is listed below:

- Usual chemical laboratory equipment.
- ARL ADVANT' XP 348 X-ray fluorescence spectrophotometer, with Ar/ CH_4 gas mixture detector.
- Oven set at $675\text{ }^\circ\text{C}$.
- Oven set at $1100\text{ }^\circ\text{C}$.
- Furnace set at $105\text{ }^\circ\text{C}$.
- Analytical scale with a precision of 0.1 mgr.
- Automatic CLAISSE type pearl production device.
- Crucibles with a capacity of 25ml (Pt-Au 5%).
- 32mm diameter pearl molds (Pt-Au 5%).
- Rod.
- Nickel smelters.



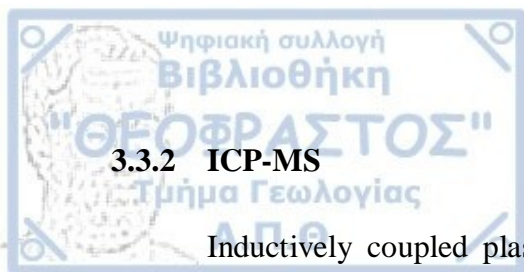
3.3.1.1 Sample preparation - Measurement

The sample preparation and the measurement of the samples that occurred is described in the steps below.

1. Firstly, the identity of each bauxite quality sample that had been received from the preparation plant was noted in a notebook.
2. Secondly, in a nickel crucible dried at 105 °C, reagents were weighed in the below order:
 - 0.3 gr KBr
 - 1 gr LiNO₃
 - 1 gr La₂O₃
 - 6.5 gr Li₂B₄O₇
3. 1 g of bauxite sample dried at 105 °C in a small vessel was weighed.
4. The sample was transferred into the nickel crucible.
5. It was homogenized very carefully with a rod.
6. The mixture was transferred to a Pt-Au 5% crucible, which was adjusted to the special position of the CLAISSE device.
7. Program 3 was selected for the preparation of bauxite pearls in the automatic fusion device and by pressing START the program was completed automatically (automatic fusion completion).
8. With a special suction cup, the pearl was taken from the mold of the device.
9. The pearl was weighed on an analytical scale (accuracy 0.1 mg) and the weight was noted on the point of the notebook corresponding to the specific bauxite sample.
10. Then, the bauxite sample beads were inserted into the numbered positions of the XRF sampler.
11. With the bauxite analysis program that was created during the calibration of the instrument, the analysis / measurement of the samples was performed.

3.3.1.2 Expression of the results

The software of the instrument with the saved calibration equations, gives directly in print the concentration of each oxide expressed in wt%. The results are recorded in an electronic file and where required (e.g. loads, sample shipments) in a specific form.



3.3.2 ICP-MS

Inductively coupled plasma mass spectrometry (ICP-MS) is an elemental analysis technique that is used to measure the elements, rather than the molecules and compounds that are measured by LC/MS and GC/MS, at trace levels in biological fluids (Wilschefski and Baxter, 2019).

At the Scripps Institution of Oceanography's Scripps Isotope Geochemistry Laboratory in California, USA, data on the abundance of minor and trace elements in bulk rocks were calculated. For trace-element abundance measurements, ~50 mg of the received sample powder was digested along with total procedure blanks, terrestrial basalt and andesite standards (BHVO-2, BCR-2, BIR-1a, AGV-2), in a 4:1 Teflon-distilled concentration of 27 M HF and 15 M HNO₃ for more than 72 hours on a hotplate at 150° C. To remove fluorides, samples were successively dried and soaked in pure HNO₃. The samples were thoroughly dissolved, doped with indium to track instrumental drift throughout analysis, and then diluted to a factor of 5,000. Major- and trace-element abundances were determined using a *ThermoScientific* iCAP Qc quadrupole inductively coupled plasma mass spectrometer (ICP-MS) in normal mode. All data are blank-corrected. To determine external reproducibility and accuracy, reference materials that were analyzed as unknowns were examined. In general, reproducibility was better than 5% relative standard deviation. (Day *et al.*, 2022; Day *et al.*, 2022)



4 MACROSCOPIC DESCRIPTION

The descriptive characteristics of the 23 samples have been defined through macroscopic analyses. These characteristics include the colour of the bauxite, whether it is solid, leached or corroded, the existence and the size of its pisoliths and the percentage of the pisoliths on each sample's surface.

4.1 COLOUR CLASSIFICATION

The 23 samples can be classified by colour based on optical observation. Three groups were distinguished based on the colour: brownish-red (BR), orange-red (OR) and yellow (Y). The brownish-red group (BR) consists of 11 samples, the orange-red group (OR) consists of 9 samples and the yellow group (Y) consists of 3 samples. The colour-based classes and the respective samples are displayed below in Table 1 and Table 2 respectively.

Table 1: Colour classification of the 23 samples of the area of study, BR: brownish-red, OR: orange-red and Y: yellow.

BR	OR	Y
S.3_1	S.4_1	S.3_4
S.3_2	S.5_1	S.6_2
S.3_3	S.5_2	S.6_3
S.3_5	S.5_3	
S.4_2	S.5_4	
S.4_3	S.5_6	
S.5_5	S.5_7	
S.6_1	S.7_2	
S.6_4	S.7_3	
S.7_1		
S.7_4		

Table 2: Bauxite sample photographs - *to be continued*



Sample 3_1 (View A)



Sample 3_1 (View B)



Sample 3_2 (View A)



Sample 3_2 (View B)



Sample 3_3 (View A)



Sample 3_3 (View B)

Table 2: Bauxite sample photographs - *continued*



Sample 3_4 (View A)



Sample 3_4 (View B)



Sample 3_5 (View A)



Sample 3_5 (View B)



Sample 4_1 (View A)



Sample 4_1 (View B)

Table 2: Bauxite sample photographs - *continued*



Sample 4_2 (View A)



Sample 4_2 (View B)



Sample 4_3 (View A)



Sample 4_3 (View B)



Sample 5_1 (View A)



Sample 5_1 (View B)

Table 2: Bauxite sample photographs - *continued*



Sample 5_2 (View A)



Sample 5_2 (View B)



Sample 5_3 (View A)



Sample 5_3 (View B)



Sample 5_4 (View A)



Sample 5_4 (View B)

Table 2: Bauxite sample photographs - *continued*



Sample 5_5 (View A)



Sample 5_5 (View B)



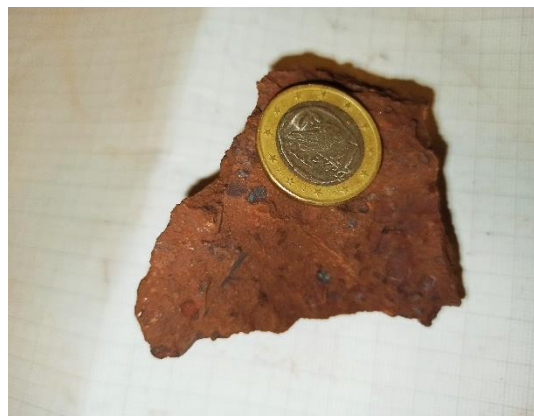
Sample 5_6 (View A)



Sample 5_6 (View B)



Sample 5_7 (View A)



Sample 5_7 (View B)

Table 2: Bauxite sample photographs - *continued*



Sample 6_1 (View A)



Sample 6_1 (View B)



Sample 6_2 (View A)



Sample 6_2 (View B)



Sample 6_3 (View A)



Sample 6_3 (View B)

Table 2: Bauxite sample photographs - *continued*



Sample 6_4 (View A)



Sample 6_4 (View B)



Sample 7_1 (View A)



Sample 7_1 (View B)



Sample 7_2 (View A)



Sample 7_2 (View B)

Table 2: Bauxite sample photographs - *continued*



Sample 7_3 (View A)



Sample 7_3 (View B)



Sample 7_4 (View A)



Sample 7_4 (View B)

The calculation of the percentage of the pisoliths of each sample was conducted by the following steps:

1. Calculation of the surface of each sample on a millimeter paper with the use of rectangles.
2. Use of minimum inscribed rectangles to calculate the surface of the pisoliths, in order to reduce the calculation error.
3. Calculation of the sum of the pisoliths' area.
4. Calculation of the fraction $\text{Sum of the pisoliths' area} / \text{Total area of the sample}$ (based on step 1).
5. Reduction of the result from step 4 to percentage.

The percentages of the pisoliths of the samples are presented in Table 3.

Table 3: Samples' area, samples' pisoliths area and percentage of the pisoliths of the calculated area.

Sample	Total area (cm x cm)	Total pisoliths area (cm x cm)	Pisoliths_percent (%)
S.3_1	37	0,00	0,0
S.3_2	49	1,19	2,4
S.3_3	40	0,00	0,0
S.3_4	28	0,56	2,0
S.3_5	32	4,19	13,3
S.4_1	38	2,25	5,9
S.4_2	60	0,79	1,3
S.4_3	35	1,41	4,1
S.5_1	77	1,48	1,9
S.5_2	54	0,25	0,5
S.5_3	77	6,01	7,8
S.5_4	55	1,09	2,0
S.5_5	55	0,40	0,7
S.5_6	25	0,12	0,5
S.5_7	38	0,36	1,0
S.6_1	71	1,98	2,8
S.6_2	77	3,10	4,0
S.6_3	70	0,60	0,9
S.6_4	48	2,71	5,6
S.7_1	86	0,62	0,7
S.7_2	36	12,23	34,0
S.7_3	59	1,86	3,2
S.7_4	63	4,00	6,3



5 MINERALOGY

The mineralogical analyses of the 23 bauxite samples have shown a dominant presence of either boehmite or diaspore.

The samples S.3_1, S.3_2, S.3_3, S.3_4 and S.3_5 that were collected from pile S3 of the Koromilia mine and belong to the second bauxite horizon (B2) have a minimum of 51 wt.% in boehmite, a maximum of 68 wt.% and an average of 60 wt.%. They also have minimum of 16 wt.% in hematite, a maximum of 28 wt.% and an average of 23 wt.%. In addition, these samples have the highest percentage in amorphous material and S.3_1 specifically, has by far the highest content of calcite with a percentage of 15 wt.% due to external contamination (secondary non-genetic calcite).

The samples S.4_1, S.4_2, S.4_3 that were collected from the pile S5 of the Nera mine have, also, mainly boehmite, with a minimum of 64 wt.%, a maximum of 70 wt.% and an average of 67 wt.%. Hematite ranges between 22 wt.% and 28 wt.%, with an average of 25 wt.%.

The samples S.5_1, S.5_2, S.5_3 and S.5_4 which were collected from pile 5 of the 526 mine, present a minimum of 69 wt.% in diaspore, a maximum of 71 wt.% and an average of 70 wt.%. The range of hematite is between 20 wt.% and 22 wt.%, with an average of 21 wt.%.

The samples S.5_5, S.5_6 and S.5_7 that were collected from pile S5 of the Koukouvista mine have a range of 66 wt.% to 71 wt.% in diaspore, with an average of 69 wt.%, while the range of hematite is between 21 wt.% to 23 wt.% and an average of 22 wt.%.

The samples S.6_1, S.6_2, S.6_3 and S.6_4 belong to pile S6 from the Sila mine. The minimum diaspore is 67 wt.%, the maximum is 71 wt.% and the average is 69 wt.%. Hematite in this sample has a wider range between 5 wt.% and 23 wt.%, with an average of 12 wt.%.

The samples S.7_1, S.7_2, S.7_3 and S.7_4 were retrieved from pile S7 of the Kamara mine, which comes from the third bauxite horizon (B3). These samples provide a range in diaspore between 62 wt.% and 75 wt.%, with an average of 68 wt.%. Hematite has a minimum at 17 wt.%, a maximum at 28 wt.% and an average of 23 wt.%.

Most of the samples have also traces of bayerite, anatase and micas. Goethite is present in samples S.6_2 and S.6_3 at a percentage of 16 wt.% and 17 wt.%, respectively.

Table 4: Mineralogical composition (wt.%) of the studied samples by X-ray diffraction (XRD).

Sample	Boehmite	Bayerite	Diaspore	Hematite	Goethite	Anatase	Quartz	Calcite	Micas	Amorphous
S.3_1	51	0	0	22	0	2	1	15	2	7
S.3_2	65	0	0	24	0	3	0	0	1	7
S.3_3	55	2	0	28	0	2	0	0	0	13
S.3_4	68	2	0	16	0	3	0	0	0	11
S.3_5	60	2	0	25	0	3	0	0	0	10
S.4_1	70	1	0	22	0	3	0	1	0	3
S.4_2	64	0	0	28	0	3	0	0	0	5
S.4_3	68	1	0	25	0	3	0	0	0	3
S.5_1	4	0	69	20	0	3	0	0	0	4
S.5_2	2	1	70	21	0	3	0	0	0	3
S.5_3	1	0	71	22	0	3	0	0	0	3
S.5_4	2	0	69	22	0	3	0	0	0	4
S.5_5	4	0	66	23	0	3	0	0	0	4
S.5_6	1	1	71	21	0	3	0	0	0	3
S.5_7	0	1	70	22	0	4	0	0	0	3
S.6_1	0	0	70	23	0	4	0	0	0	3
S.6_2	1	1	71	5	16	3	0	0	0	3
S.6_3	1	0	68	8	17	3	0	0	0	3
S.6_4	3	1	67	24	0	3	0	0	0	2
S.7_1	3	1	62	28	0	3	0	0	0	3
S.7_2	3	0	70	21	0	2	0	0	0	4
S.7_3	3	0	75	17	0	3	0	0	0	2
S.7_4	3	0	66	26	0	3	0	0	0	2

5.1 CLASSIFICATION

K-means is a widely used clustering algorithm that aims to partition a data set into k non-overlapping groups. The algorithm works by assigning each data point to the nearest cluster based on a distance metric, typically Euclidean distance, then updating cluster centers based on new assignments. The algorithm repeats these two steps until convergence is reached, which is when data is assigned to clusters that don't change. One advantage of the K-means is its simplicity, which makes it easier to use and explain. In addition, K-means can handle large data and is computationally efficient, making it suitable for use in applications that require real-

time processing, but K-means has some limitations that must be considered when being used for data analysis. A limitation of k-determination is that the number of k clusters is specified in advance, which can be difficult when the optimal number of clusters is not known in advance. Choosing an inappropriate value for k may result in an inadequate number of clusters or complex models. Several methods have been developed to determine the optimal value of k, such as the fingerprint method, silhouette score, and interval statistics. Another limitation of K-means is its sensitivity to the initial detection of centroids, which can lead to different clustering results depending on initial conditions. One approach to this problem is to use the algorithm in a loop. It will repeatedly go through different initializations and select the clustering result with the lowest objective-function value.

The objective function $W(S, C) = \sum_{k=1}^K \sum_{i \in S_k} \|y_i - c_k\|^2$ is used by the algorithm, where S is a K-cluster partition in the M-dimensional feature space, consisting of non-empty non-overlapping clusters S_k , each with a centroid c_k ($k = 1, 2, \dots, K$) (MacQueen, 1967; Jain *et al.*, 1999; Kodinariya and Makwana, 2013).

5.1.1 Samples classification based on mineralogical composition.

The 23 samples have been classified in 2 and 4 clusters based on their mineralogical composition, using the K-Means method of classification of IBM® SPSS® software platform for statistical analysis. Examinations of the same classification method using 3, 4 and 5 clusters have been conducted, but the use of 2 clusters has seemed to be more appropriate for the data of the samples used for this dissertation. The results of the classification are presented in Table 5 and Table 6.

Table 5: Clusters based on mineralogical composition.

Case Number	Sample	Cluster	Distance
1	S.3_1	2	24.083
2	S.3_2	2	6.928
3	S.3_3	2	19.079
4	S.3_4	2	10.296
5	S.3_5	2	12.649
6	S.4_1	2	.000
7	S.4_2	2	8.832
8	S.4_3	2	3.742
9	S.5_1	1	22.271
10	S.5_2	1	22.672
11	S.5_3	1	23.367
12	S.5_4	1	23.495
13	S.5_5	1	24.819
14	S.5_6	1	22.627
15	S.5_7	1	23.409
16	S.6_1	1	24.166
17	S.6_2	1	.000
18	S.6_3	1	4.472
19	S.6_4	1	25.259
20	S.7_1	1	29.496
21	S.7_2	1	22.804
22	S.7_3	1	20.543
23	S.7_4	1	26.981

Table 6: Final cluster centers based on mineralogical composition.

	Cluster 1 15 Samples	Cluster 2 8 Samples
Boehmite	2	63
Bayerite	0	1
Diaspore	69	0
Hematite	20	24
Goethite	2	0
Anatase	3	3
Quartz	0	0
Calcite	0	2
Micas	0	0
Amorphous	3	7

Classifying the 23 samples based on their mineralogical composition using 2 clusters, results in cluster 1 consisting of 15 samples and cluster 2 consisting of 8 samples. Cluster 1 includes: S.5_1, S.5_2, S.5_3, S.5_4, S.5_5, S.5_6, S.5_7, S.6_1, S.6_2, S.6_3, S.6_4, S.7_1, S.7_2, S.7_3 and S.7_4. Cluster 2 includes: S.3_1, S.3_2, S.3_3, S.3_4, S.3_5, S.4_1, S.4_2 and S.4_3. Cluster 1 has an average of 69 wt.% diaspore, 20 wt.% hematite, 2 wt.% boehmite, 2 wt.% goethite, 3 wt.% anatase, 3 wt.% amorphous and traces of bayerite, quartz, calcite and micas. Cluster 2 has an average of 63 wt.% boehmite, 24 wt.% hematite, 7 wt.% amorphous, 3 wt.% anatase, 2 wt.% calcite, 1 wt.% bayerite and traces of diaspore, goethite, quartz and micas. Therefore, it is obvious we have two types of bauxite in the region, the diasporic one and the boehmitic one, which agrees with the geological setting of the region.



6 GEOCHEMISTRY

6.1 MAJOR ELEMENTS

The geochemical analyses of the 23 bauxite samples that were carried out to provide the concentrations of the major elements displayed a minimum of 45.56 wt.%, a maximum of 65.03 wt.% and an average of 57.96 wt.% in Al_2O_3 concentration.

The SiO_2 concentration ranges between 0.37 wt.% and 13.18 wt.%, with a relatively low average of 3.33 wt.%.

The concentration in Fe_2O_3 has a minimum of 16.72 wt.%, a maximum of 29.40 wt.% and an average of 23.15 wt.%.

TiO_2 ranges between 1.95 wt.% and 3.51 wt.% with an average of 2.76 wt.%, while CaO ranges between 0.05 wt.% and 7.09 wt.%, with an average of 0.49 wt.% among the 23 bauxite samples.

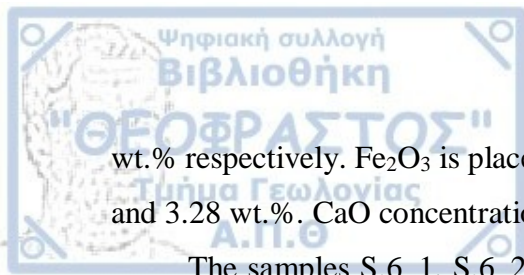
All the samples had a percentage of 0.03 wt.% in S concentration.

The samples S.3_1, S.3_2, S.3_3, S.3_4 and S.3_5 that were collected from pile S3 of the Koromilia mine and belong to the second bauxite horizon (B2) have an Al_2O_3 concentration that ranges between a minimum value of 45.56 wt.% and a maximum of 53.43 wt.%. SiO_2 has a minimum value of 4.69 and a maximum of 13.18 wt.%. Fe_2O_3 ranges between 18.32 and 24.88 wt.%, while TiO_2 ranges between 1.95 and 2.52 wt.%. CaO is between 0.14 and 7.09 wt.%, with sample S.3_1 being the only one among the 23 specimens showing such a CaO concentration.

The samples S.4_1, S.4_2, S.4_3 that were collected from the pile S5 of the Nera mine show a higher concentration in Al_2O_3 compared to the ones from the Koromilia mine, ranging between 53.89 and 63.88 wt.%, while the concentration of SiO_2 is lower, ranging from 1.67 to 3.11. The Fe_2O_3 concentration varies between 19.19 and 28.98 wt.%, TiO_2 between 2.73 and 2.99 and CaO between 0.07 and 0.13.

The samples S.5_1, S.5_2, S.5_3 and S.5_4 which were collected from pile 5 of the 526 mine, present a lower range of Al_2O_3 concentration, between 59.43 and 61.87 wt.%, while SiO_2 is between 1.19 and 3.09 wt.%. The Fe_2O_3 concentration varies between 21.60 and 22.37 wt.%, while TiO_2 ranges from 2.87 to 2.99 wt.%. CaO is low, ranging between 0.09 and 0.11 wt.%.

The samples S.5_5, S.5_6 and S.5_7 that were collected from pile S5 of the Koukouvista mine have an Al_2O_3 and SiO_2 concentration range from 59.21 to 60.24 wt.% and 1.62 to 2.43



wt.% respectively. Fe_2O_3 is placed between 22.57 and 24.09 wt.%, while TiO_2 is between 2.89 and 3.28 wt.%. CaO concentration lays between 0.07 and 0.09 wt.%.

The samples S.6_1, S.6_2, S.6_3 and S.6_4 belong to pile S6 from the Sila mine. The concentration range of Al_2O_3 and SiO_2 is between 56.96 and 60.86 wt.% and 0.91 and 1.56 wt.% respectively. The Fe_2O_3 concentration varies between 22.56 and 27.97 wt.%, while the TiO_2 concentration lays between 2.60 and 3.51 wt.%. CaO concentration has the lowest range among the samples, fluctuating between 0.05 and 0.08 wt.%.

The samples S.7_1, S.7_2, S.7_3 and S.7_4 were retrieved from pile S7 of the Kamara mine, which belongs to the third bauxite horizon (B3). These samples provide a range in Al_2O_3 and SiO_2 concentrations between 54.90 and 65.03 wt.% and 0.37 and 2.32 wt.%, respectively. Fe_2O_3 varies from 16.72 to 29.40 wt.%, while TiO_2 from 2.52 to 2.80 wt.%. CaO concentration lays between 0.12 and 0.26 wt.%.

Table 7: Major element compositions of bauxite rock samples (wt. %).

Samples	SiO ₂	Al ₂ O ₃	Fe ₂ O ₃	TiO ₂	CaO	LOI	Total
S.3_1	8.94	45.56	19.99	1.95	7.09	15.48	99.01
S.3_2	7.13	53.83	24.34	2.44	0.17	11.46	99.37
S.3_3	13.18	51.48	21.36	2.29	0.14	11.43	99.88
S.3_4	10.84	55.08	18.32	2.52	0.22	12.83	99.81
S.3_5	4.69	53.43	24.88	2.33	1.70	11.98	99.01
S.4_1	1.67	63.88	19.19	2.82	0.08	12.13	99.77
S.4_2	3.11	53.89	28.98	2.99	0.13	10.68	99.78
S.4_3	2.05	58.24	25.63	2.73	0.07	11.13	99.85
S.5_1	2.69	60.41	21.92	2.99	0.10	11.73	99.84
S.5_2	3.09	59.43	22.37	2.87	0.11	11.78	99.65
S.5_3	1.19	61.87	21.69	2.94	0.09	12.03	99.81
S.5_4	2.70	60.60	21.60	2.96	0.10	11.91	99.87
S.5_5	2.43	60.24	22.57	2.89	0.09	11.61	99.83
S.5_6	1.95	59.45	24.07	2.95	0.08	11.31	99.81
S.5_7	1.62	59.21	24.09	3.28	0.07	11.42	99.69
S.6_1	1.15	60.86	22.56	3.51	0.05	11.44	99.57
S.6_2	1.56	60.51	22.93	2.92	0.08	11.75	99.75
S.6_3	1.03	56.96	27.97	2.94	0.08	10.9	99.88
S.6_4	0.91	58.58	26.25	2.60	0.06	11.06	99.46
S.7_1	1.46	54.90	29.40	2.53	0.12	11.07	99.48
S.7_2	2.32	60.28	20.23	2.52	0.15	14.31	99.81
S.7_3	0.42	65.03	16.72	2.76	0.16	14.11	99.20
S.7_4	0.37	59.27	25.43	2.80	0.26	11.42	99.55

SiO₂ is relatively constant varying between 0.37 wt.% and 3.11 wt.%, while it is higher in the S.3 samples, varying between 4.69% and 13.18%. Fe₂O₃ decreases with increasing Al₂O₃, although Fe₂O₃ S.3 samples deviate from the general trend (Figure 6).

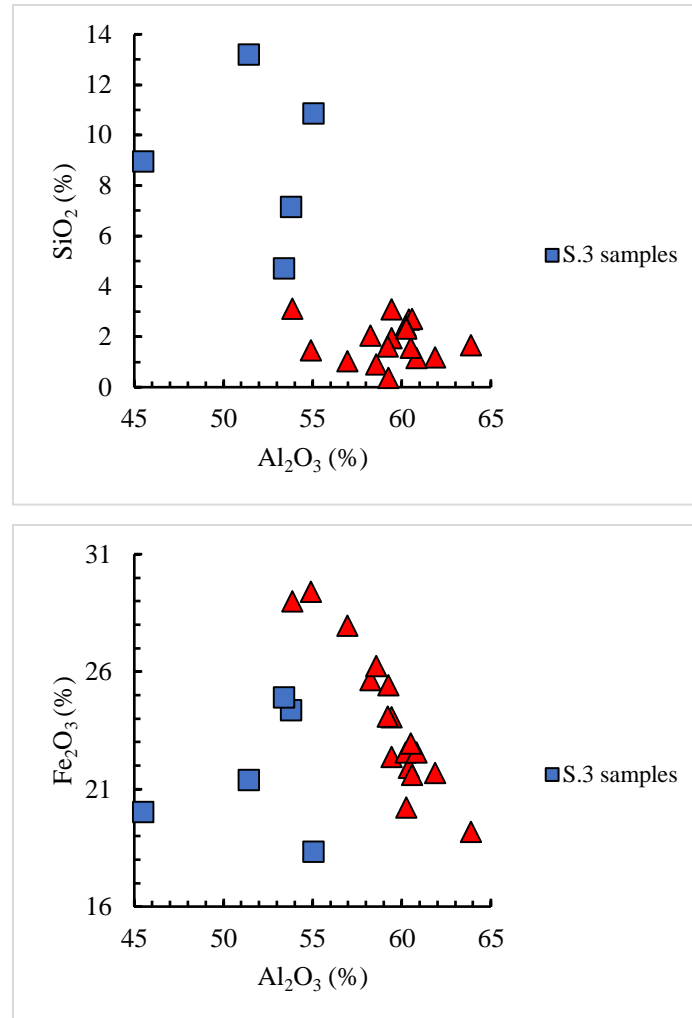


Figure 6: Scatter plots of SiO₂ - Al₂O₃ and Al₂O₃ - Fe₂O₃. S.3 samples are defined.

6.1.1 Samples classification based on major elements.

The 23 samples have been classified in 5 clusters based on their major elements wt.% content, using the K-Means method of classification of IBM® SPSS® software platform for statistical analysis. Examinations of the same classification method using 3, 4 and 6 clusters have been conducted, but the use of 5 clusters has seemed to be more appropriate for the data of the examined samples. The results of the classification are presented in Table 7 and Table 8 along with the average ΣREE, ΣLREE and ΣHREE, respectively, for each cluster.

Table 7: Cluster membership based on major element wt.% concentration.

Case Number	Sample	Cluster	Distance
1	S.3_1	1	.000
2	S.3_2	2	.000
3	S.3_3	4	5.267
4	S.3_4	4	.000
5	S.3_5	2	2.959
6	S.4_1	5	2.999
7	S.4_2	2	6.164
8	S.4_3	3	1.991
9	S.5_1	3	4.366
10	S.5_2	3	4.101
11	S.5_3	3	4.633
12	S.5_4	3	4.682
13	S.5_5	3	3.661
14	S.5_6	3	2.106
15	S.5_7	3	1.905
16	S.6_1	3	3.453
17	S.6_2	3	3.041
18	S.6_3	3	3.504
19	S.6_4	3	1.233
20	S.7_1	3	6.012
21	S.7_2	3	5.653
22	S.7_3	5	.000
23	S.7_4	3	.000

Table 8: Final cluster centers based on major element wt.% concentration.

	Cluster 1	Cluster 2	Cluster 3	Cluster 4	Cluster 5
	1 Sample	3 Samples	15 Samples	2 Samples	2 Samples
Al ₂ O ₃ (%)	45.56	53.72	59.39	53.28	64.46
SiO ₂ (%)	8.94	4.98	1.77	12.01	1.05
Fe ₂ O ₃ (%)	19.99	26.07	23.91	19.84	17.95
TiO ₂ (%)	1.95	2.59	2.90	2.41	2.79
CaO(%)	7.09	.67	.10	.18	.12
ΣLREE	373.00	464.35	219.56	250.30	377.29
ΣHREE	46.26	41.76	23.99	34.51	33.14
ΣREE	419.26	506.11	258.19	284.82	410.43

The 23 samples used for this dissertation have been classified in 5 clusters. Cluster 1 includes only one sample, the sample S.3_1. Cluster 2 includes three samples, the samples S.3_2, S.3_5 and S.4_2. Cluster 3 consists of fifteen samples: S.4_3, S.5_1, S.5_2, S.5_3, S.5_4, S.5_5, S.5_6, S.5_7, S.6_1, S.6_2, S.6_3, S.6_4, S.7_1, S.7_2, S.7_4. Cluster 4 and 5 include two samples each: S.3_3 and S.3_4, S.4_1 and S.7_3, respectively.

Cluster 1 has an average of 45.56 wt.% Al₂O₃, which is the lowest percentage of Al₂O₃ among the 23 samples, 8.94 wt.% SiO₂, 19.99 wt.% Fe₂O₃, 1.95 wt.% TiO₂ and 7.09 wt.% CaO, being the highest percentage of CaO among the 23 samples and the 5 clusters, due to external contamination (secondary non-genetic calcite). Therefore, it is considered as flyer. It also has the highest average in ΣHREE among the 5 clusters. Cluster 2 has an average of 53.72 wt.% Al₂O₃, 4.98 wt.% SiO₂, 26.07 wt.% Fe₂O₃, being the highest percentage of Fe₂O₃ between the 5 clusters, 2.59 wt.% TiO₂ and 0.67 wt.% CaO. ΣLREE and ΣREE averages of cluster 2 have the highest value among all the rest. Cluster 3 has an average of 59.39 wt.% Al₂O₃, 1.77 wt.% SiO₂, 23.91 wt.% Fe₂O₃, 2.90 wt.% TiO₂, which is the highest percentage of TiO₂ among the 5 clusters, while the 0.1 wt.% percentage of CaO is the lowest between them. It also has the lowest average in ΣLREE, ΣHREE and ΣREE among all clusters. Cluster 4 has an average of 53.28 wt.% Al₂O₃, 12.01 wt.% SiO₂, the highest percentage of SiO₂ between the 5 clusters, 19.84 wt.% Fe₂O₃, 2.41 wt.% TiO₂ and 0.18 wt.% CaO. At last, cluster 5 has a cluster centre or average of 64.46 wt.% Al₂O₃, which is the highest percentage of Al₂O₃ of all 5 clusters, an average of 1.05 wt.% SiO₂ and 17.95 wt.% Fe₂O₃, both being the lowest of the 5 clusters, 2.79 wt.% TiO₂ and 0.12 wt.% CaO.

Therefore, it is obvious that samples S.3 differentiate from most of the other samples. Samples S.3 have generally higher values in SiO₂ and CaO, while having generally lower values in Al₂O₃ and TiO₂. Based on the major elements content clustering, the clusters 1, 2, 4 and 5 seem to have higher values in ΣLREE and ΣHREE, thus in ΣREE, than cluster 3 which does not involve any sample from the S.3 category. This relationship will be examined at the rare earth elements clustering for its validity.

Further research is needed on whether the major element content of cluster 3 and the low averages in ΣLREE, ΣHREE and ΣREE are relative or not, as well as, whether the highest average in Fe₂O₃ and ΣLREE of cluster 2 are related.

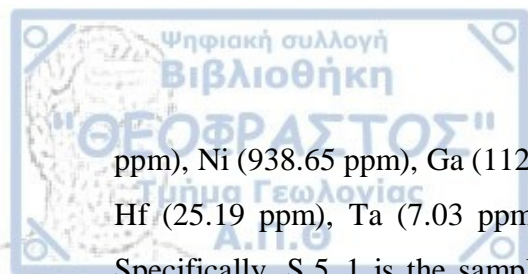
6.2 TRACE ELEMENTS

The geochemical analyses of the 23 bauxite samples that have been carried out to provide the concentrations of the trace elements, as well as their minimum, maximum and average values are presented in Table 9 and Table 10.

Samples S.3_1, S.3_2, S.3_3, S.3_4 and S.3_5, that were collected from pile S3 of the Koromilia mine, show minimum values, compared to all 23 samples, in the following trace elements: Sc (32.60 ppm), Ti (10981.96 ppm), V (241.19 ppm), Cr (292.70 ppm), Zr (385.62 ppm), Nb (37.77 ppm), Sn (8.47 ppm), Hf (10.71 ppm), Ta (2.74 ppm). However, the same samples, show maximum values in the following trace elements: Li (688.81 ppm), B (140.68 ppm), Mn (1388.70 ppm), Cu (76.62 ppm), Zn (196.26 ppm), Rb (14.39 ppm), Sr (148.76 ppm), Y (82.66 ppm), Cs (7.10 ppm), W (71.97 ppm) and Hg (0.55 ppm). Specifically, the samples from Koromilia mine have quite higher average values in Li, B, Mn, Cu, Zn, Rb, Sr, Y, and Cs than all the other mines. As mentioned above in the major elements section, the S.3 samples seem to differentiate from the rest. Similarly, it is obvious that they differ as well when we consider trace element concentrations. S.3_1 differs in CaO content due to external contamination (secondary non-genetic calcite). Therefore, it is considered as flyer. Further research in that mine would be suggested, for Li in particular.

The samples S.4_1, S.4_2, S.4_3 that were collected from the pile S5 of the Nera mine exhibit the minimum value in Ga (50.55 ppm), W (5.75 ppm) and Hg (0.04 ppm).

The samples S.5_1, S.5_2, S.5_3 and S.5_4 which were collected from pile 5 of the 526 mine, show the minimum value of the trace elements B (35.08 ppm), Mn (16.86 ppm), Ni (105.16 ppm), Y (12.71 ppm) and Mo (4.03 ppm), while they show the maximum value of the trace elements Be (12.73 ppm), Si (92.38 ppm), V (1300.96 ppm), Cr (1505.48 ppm), Co (74.70



ppm), Ni (938.65 ppm), Ga (112.41 ppm), Zr (923.59 ppm), Nb (96.81 ppm), Sn (19.57 ppm), Hf (25.19 ppm), Ta (7.03 ppm), Pb (186.55 ppm), Th (81.67 ppm) and U (16.68 ppm). Specifically, S.5_1 is the sample that has most of the highest values in the trace elements mentioned above. Therefore, further research on this area would be suggested in order to distinguish whether this is a random incident or there is a higher content in trace elements somewhere within this mine.

The samples S.5_5, S.5_6 and S.5_7 that were collected from pile S5 of the Koukouvista mine show only one minimum value of the trace element Be (2.46 ppm) and no maximum values for the other trace elements.

The samples S.6_1, S.6_2, S.6_3 and S.6_4 belong to pile S6 from the Sila mine. Minimum values are found for the trace elements: Li (2.83 ppm), Co (4.11 ppm), Cu (6.12 ppm), Zn (50,11 ppm), Rb (0.02 ppm), Sr (5.26 ppm), along with traces of Cs, Ba (4.85 ppm) and Th (31.53 ppm). In these samples the maximum values in Ge (6.79 ppm) and Mo (156.90 ppm) are found.

The samples S.7_1, S.7_2, S.7_3 and S.7_4 were retrieved from pile S7 of the Kamara mine, which comes from the third bauxite horizon (B3). These samples provide the minimum value in Ge (1.59 ppm), Pb (36.26 ppm) and the maximum value in Ba (72.69 ppm).

Table 9: Trace elements concentration (ppm) of bauxite rock samples - to be continued.

Sample	S.3_1	S.3_2	S.3_3	S.3_4	S.3_5	S.4_1	S.4_2	S.4_3	S.5_1	S.5_2	S.5_3	S.5_4
Li	253.09	254.01	343.61	688.81	97.98	85.20	17.44	66.71	36.06	8.03	8.14	11.68
Be	5.89	5.22	5.17	3.75	6.13	7.28	7.64	10.14	12.73	3.75	2.61	2.71
B	117.03	100.79	102.55	140.68	101.35	74.41	58.25	64.06	121.84	45.40	35.08	38.04
Sc	35.08	45.47	51.36	34.83	32.60	57.95	63.54	43.52	92.38	52.63	50.65	54.99
V	241.19	377.84	298.80	308.55	358.69	596.51	555.32	493.67	1300.96	731.14	542.08	543.15
Cr	866.58	390.94	292.70	352.59	402.41	916.66	977.03	755.35	1505.48	899.41	906.89	916.22
Mn	1388.70	462.03	567.33	170.90	1259.87	161.44	138.75	117.78	93.31	38.61	16.86	32.07
Co	51.30	25.59	30.46	26.86	39.39	50.46	42.67	40.34	74.70	9.91	6.08	14.86
Ni	419.18	225.18	256.32	189.74	199.27	535.94	349.13	470.18	938.65	177.00	105.16	344.65
Cu	15.19	76.62	40.17	67.84	18.30	14.04	8.70	8.58	27.51	12.69	7.27	8.95
Zn	196.26	157.55	158.21	131.97	191.74	83.68	68.25	70.69	152.40	71.43	50.61	77.98
Ga	53.06	61.42	58.68	60.25	62.60	59.80	64.42	50.55	112.41	59.55	52.68	52.66
Ge	2.55	3.20	2.32	2.45	2.63	2.12	2.40	1.87	3.84	1.70	1.67	1.88
Rb	14.39	5.04	4.77	1.82	13.24	1.14	0.23	0.33	0.06	0.04	0.06	0.03
Sr	148.76	59.48	26.75	22.14	93.18	12.26	18.95	10.07	49.13	23.51	14.21	18.16
Y	82.66	80.18	63.35	43.37	41.85	35.47	55.78	25.04	60.90	12.71	18.77	34.02
Zr	385.62	464.96	452.36	475.50	461.24	530.21	525.20	438.79	923.59	561.91	511.88	602.60
Nb	37.77	45.43	43.50	46.40	43.73	53.23	54.85	48.31	96.81	57.34	57.66	65.05
Mo	6.18	5.41	4.61	5.15	5.92	9.55	8.80	8.43	6.25	4.94	6.07	4.03
Sn	8.47	10.27	9.45	10.12	10.24	11.50	11.54	9.92	19.57	11.76	11.82	12.91
Cs	7.10	2.03	1.46	0.51	2.24	0.26	0.22	0.15	0.03	0.02	0.05	0.03
Ba	54.62	41.91	28.19	13.58	41.96	22.34	23.29	15.67	53.46	23.70	26.42	33.47
Hf	10.71	12.60	11.78	12.60	12.77	14.29	14.37	12.23	25.19	14.46	14.07	16.40
Ta	2.74	3.21	3.00	3.30	3.20	3.89	4.02	3.58	7.03	3.94	4.20	4.78
W	6.17	6.77	6.15	71.97	6.73	6.43	6.69	5.75	9.46	7.03	6.41	9.88
Hg	0.05	0.05	0.05	0.55	0.05	0.05	0.05	0.04	0.07	0.06	0.05	0.07
Pb	76.14	96.51	75.04	73.25	90.65	104.97	106.59	87.75	186.55	78.11	41.33	77.67
Th	34.88	41.47	34.00	38.89	35.58	50.24	52.11	40.67	81.67	41.33	47.51	44.57
U	4.39	7.10	4.93	6.21	5.92	7.24	6.61	6.52	16.68	7.67	5.75	7.40

Table 9: Trace elements concentration (ppm) of bauxite rock samples – *continued*.

Sample	S.5_5	S.5_6	S.5_7	S.6_1	S.6_2	S.6_3	S.6_4	S.7_1	S.7_2	S.7_3	S.7_4
Li	51.45	42.08	32.04	23.05	17.20	3.80	2.83	15.63	37.59	17.91	28.47
Be	4.04	2.46	4.33	7.73	6.11	8.46	6.51	2.99	5.24	5.17	4.91
B	66.32	48.34	37.63	51.29	56.57	61.69	45.71	42.49	37.82	41.07	46.66
Sc	48.49	69.24	48.67	48.06	58.99	39.11	34.74	37.40	67.80	48.42	51.82
V	769.66	659.01	843.04	661.64	603.40	828.91	640.56	722.75	841.00	750.71	626.92
Cr	959.60	944.63	856.64	815.37	846.79	702.20	775.13	715.11	954.17	805.86	854.72
Mn	78.17	47.67	126.01	25.70	28.88	16.27	18.39	21.67	67.97	58.78	47.70
Co	14.75	12.28	22.91	10.34	66.60	4.11	5.27	14.35	34.87	48.77	43.16
Ni	254.89	228.91	412.08	423.27	748.97	324.82	322.42	192.69	420.30	653.58	573.87
Cu	13.16	12.38	18.45	6.68	6.12	6.66	8.27	19.81	11.40	20.43	11.31
Zn	60.56	101.85	75.53	60.12	59.97	52.36	50.11	50.85	98.20	103.56	88.90
Ga	61.68	58.08	65.31	57.47	65.58	80.54	59.58	58.29	57.37	63.48	62.20
Ge	2.35	2.73	2.29	5.40	3.23	6.79	3.84	1.59	2.65	2.29	2.09
Rb	0.08	0.08	0.04	0.05	0.06	0.03	0.02	0.11	0.12	0.09	0.07
Sr	9.13	12.41	5.71	24.17	5.98	5.26	5.43	23.27	23.34	18.19	24.02
Y	19.65	19.92	12.76	33.83	18.12	23.59	22.60	14.88	49.09	36.39	18.31
Zr	512.83	541.98	481.42	480.37	466.70	518.11	519.41	485.41	559.34	468.68	535.05
Nb	54.52	57.48	49.70	47.70	49.22	52.69	52.86	52.45	57.72	50.89	55.79
Mo	8.87	7.09	6.26	4.89	39.62	156.90	7.75	4.46	5.24	7.87	5.03
Sn	12.95	14.74	11.44	11.58	9.72	11.82	11.62	10.81	12.10	11.01	11.30
Cs	0.01	0.03	0.01	0.00	0.00	0.00	0.00	0.04	0.05	0.02	0.04
Ba	19.41	17.72	13.60	32.66	8.12	5.64	4.85	31.81	72.69	47.55	59.65
Hf	14.22	14.99	12.84	13.22	12.36	14.50	14.24	13.54	15.02	13.05	14.71
Ta	4.04	4.12	3.53	3.45	3.49	3.93	3.90	3.91	4.11	3.79	4.16
W	8.23	7.54	6.81	16.03	6.55	6.11	10.43	5.79	7.86	6.79	7.09
Hg	0.06	0.06	0.05	0.13	0.05	0.04	0.08	0.04	0.06	0.05	0.05
Pb	66.35	63.31	69.84	64.48	47.44	107.10	59.72	36.26	113.52	93.55	62.90
Th	56.79	57.96	45.95	74.72	44.68	31.53	60.65	38.04	52.99	47.75	41.43
U	8.95	8.64	8.82	9.95	13.15	10.03	8.74	6.40	7.03	7.15	6.64

Table 10: Variation and average values of the trace elements concentration (ppm) of bauxite rock samples.

Elements	Min	Max	Average
Li	2.83	688.81	93.17
Be	2.46	12.73	5.69
B	35.08	140.68	66.74
Sc	32.60	92.38	50.77
V	241.19	1300.96	621.54
Cr	292.70	1505.48	800.54
Mn	16.27	1388.70	216.73
Co	4.11	74.70	30.00
Ni	105.16	938.65	381.14
Cu	6.12	76.62	19.15
Zn	50.11	196.26	96.21
Ga	50.55	112.41	62.51
Ge	1.59	6.79	2.78
Rb	0.02	14.39	1.82
Sr	5.26	148.76	28.41
Y	12.71	82.66	35.79
Zr	385.62	923.59	517.53
Nb	37.77	96.81	53.53
Mo	4.03	156.90	14.32
Sn	8.47	19.57	11.59
Cs	0.00	7.10	0.62
Ba	4.85	72.69	30.10
Hf	10.71	25.19	14.09
Ta	2.74	7.03	3.88
W	5.75	71.97	10.38
Hg	0.04	0.55	0.08
Pb	36.26	186.55	81.70
Th	31.53	81.67	47.63
U	4.39	16.68	7.91

6.2.1 Sample classification based on trace elements.

The 23 samples have been classified in 5 clusters based on their trace element content, using the K-Means method of classification of IBM® SPSS® software platform for statistical analysis. Examinations of the same classification method using 3, 4 and 6 clusters have been conducted but the use of 5 clusters has seemed to be more appropriate for studied samples. The results of the classification are presented in Table 11 and Table 12.

Table 11: Clusters based on trace elements content.

Case Number	Elements	Cluster	Distance
1	S.3_1	1	.000
2	S.3_2	5	809.973
3	S.3_3	5	972.027
4	S.3_4	5	1015.051
5	S.3_5	5	1474.275
6	S.4_1	2	363.896
7	S.4_2	2	258.624
8	S.4_3	5	923.879
9	S.5_1	3	.000
10	S.5_2	2	928.053
11	S.5_3	2	681.016
12	S.5_4	4	.000
13	S.5_5	2	.000
14	S.5_6	2	276.329
15	S.5_7	5	1136.976
16	S.6_1	5	.000
17	S.6_2	5	935.868
18	S.6_3	2	797.963
19	S.6_4	2	1105.883
20	S.7_1	2	852.718
21	S.7_2	2	353.803
22	S.7_3	5	1243.304
23	S.7_4	2	548.275

Table 12: Final cluster centers based on trace element content.

	Cluster 1 1 Sample	Cluster 2 11 Samples	Cluster 3 1 Sample	Cluster 4 1 Sample	Cluster 5 9 Samples
Li	253.09	27.33	36.06	11.68	171.26
Be	5.89	5.08	12.73	2.71	5.97
B	117.03	51.11	121.84	38.04	77.33
Sc	35.08	52.13	92.38	54.99	45.77
V	241.19	683.08	1300.96	543.15	521.82
Cr	866.58	873.23	1505.48	916.22	613.18
Mn	1388.70	59.41	93.31	32.07	313.03
Co	51.30	21.63	74.70	14.86	34.58
Ni	419.18	316.83	938.65	344.65	397.62
Cu	15.19	11.43	27.51	8.95	29.24
Zn	196.26	70.62	152.40	77.98	112.15
Ga	53.06	61.29	112.41	52.66	60.59
Ge	2.55	2.72	3.84	1.88	2.85
Rb	14.39	.18	.06	.03	2.82
Sr	148.76	15.62	49.13	18.16	29.52
Y	82.66	26.43	60.90	34.02	39.43
Zr	385.62	527.39	923.59	602.60	465.56
Nb	37.77	55.15	96.81	65.05	47.21
Mo	6.18	20.43	6.25	4.03	9.79
Sn	8.47	12.00	19.57	12.91	10.42
Cs	7.10	.07	.03	.03	.71
Ba	54.62	27.96	53.46	33.47	27.03
Hf	10.71	14.40	25.19	16.40	12.61
Ta	2.74	4.02	7.03	4.78	3.40
W	6.17	7.24	9.46	9.88	14.84
Hg	.05	.05	.07	.07	.11
Pb	76.14	76.38	186.55	77.67	77.61
Th	34.88	48.23	81.67	44.57	44.86
U	4.39	7.61	16.68	7.40	7.75
ΣLREE	373.00	218.09	811.04	371.02	262.46
ΣHREE	46.26	23.19	66.34	28.11	30.10
ΣREE	419.26	264.13	877.38	399.12	292.56

The 23 samples have been classified in 5 clusters based on their trace element concentration. Clusters 1, 3 and 4 consist of one sample, sample S.3_1, S.5_1 and S.5_4, respectively. Cluster 2 consists of the majority of the samples, i.e. 11 samples: S.4_1, S.4_2, S.5_2, S.5_3, S.5_5, S.5_6, S.6_3, S.6_4, S.7_1, S.7_2 and S.7_4. Cluster 5 includes 9 samples: S.3_2, S.3_3, S.3_4, S.3_5, S.4_3, S.5_7, S.6_1, S.6_2 and S.7_3. S.3_1 differs in CaO content due to external contamination (secondary non-genetic calcite). Therefore, it is considered as flyer.

Cluster 1 has the highest values, compared to the other four clusters, in the following trace elements: Li (253.09 ppm), Mn (1388.70 ppm), Zn (196.26 ppm), Rb (14.39 ppm), Sr (148.76 ppm), Y (82.66 ppm), Cs (7.10 ppm) and Ba (54.62 ppm), while it has the lowest value in Hf (10.71 ppm), Ta (2.74 ppm), W (6.17 ppm), Th (34.88 ppm) and U (4.39 ppm).

Cluster 2 has the highest value in Mo (20.43 ppm), compared to the other four clusters, while it has the lowest value in Ni (316.83 ppm), Zn (70.62 ppm), Y (26.43 ppm) and Sr (15.62 ppm). Additionally, it has the second lowest value, after cluster 4, in Mn (59.41 ppm), Co (21.63 ppm) and Cu (11.43 ppm).

Cluster 3, which consists only of sample S.5_1, has the highest concentration value in certain trace elements compared to the other four clusters. Specifically, in Be (12.73 ppm), B (121.84 ppm), Sc (92.38 ppm), V (1300.96 ppm), Cr (1505.48 ppm), Co (74.70 ppm), Ni (938.65 ppm), Ga (112.41 ppm), Ge (3.84 ppm), Zr (923.59 ppm), Nb (96.81 ppm), Sn (19.57 ppm), Hf (25.19 ppm), Ta (7.03 ppm), Pb (186.55 ppm), Th (81.67 ppm) and U (16.68 ppm).

Cluster 4 has the second highest value in the trace elements: Sc (54.99 ppm), Cr (916.22), Zr (602.60 ppm), Sn (12.91 ppm), Ta (4.78 ppm), W (9.88 ppm) and Pb (77.67).

Finally, cluster 5, consisting of nine samples has the highest value in Cu (29.94 ppm), W (14.84 ppm) and Hg (0.11 ppm), while having the second highest value in Li (171.26 ppm), Mn (313.03 ppm), Ge (2.85 ppm), Rb (2.82 ppm), Mo (9.79 ppm) and U (7.75 ppm). On the contrary, it has the lowest value in Cr (613.18 ppm) and Ba (27.03 ppm), while having the second lowest value in Sc (45.77 ppm), Zr (465.56 ppm), Nb (47.21 ppm), Sn (10.42 ppm), Hf (12.61 ppm) and Ta (3.40 ppm).

In conclusion, clusters 1, 3 and 4 that consist of one sample each and have either the highest or the lowest values in most trace elements differentiate from clusters 2 and 5, which include more samples. The former seem to have higher values in ΣLREE and ΣREE, but the validity of this conclusion will be examined with the rare earth elements clustering. In addition, apart from S.3_1, the samples from S.3 are included in cluster 5.

6.3 RARE EARTH ELEMENTS (REE)

The geochemical analyses of the 23 bauxite samples display a wide range in rare earth element (REE) concentrations. The results of the rare earth elements (REE) content, as well as their minimum, maximum and average values, are provided in Table 13 and Table 14. In this thesis, as rare earth elements (REE), are used only the lanthanides, without Sc and Y.

Among the samples S.3_1, S.3_2, S.3_3, S.3_4 and S.3_5, that were collected from pile S.3 of the Koromilia mine, there is only one maximum value found in La (78.48 ppm) and no minimum values found. S.3_1 differs in CaO content due to external contamination (secondary non-genetic calcite). Therefore, it is considered as flyer.

The samples S.4_1, S.4_2, S.4_3 that were collected from the pile S5 of the Nera mine and the samples S.5_5, S.5_6 and S.5_7 that were collected from pile S5 of the Koukouvista mine, show no minimum or maximum values in rare earth elements (REE).

The samples S.5_1, S.5_2, S.5_3 and S.5_4, which were collected from pile 5 of the 526 mine, include most of both, minimum and maximum values in rare earth elements (REE). Specifically, the minimum values were found in the following rare earth elements: La (3.55 ppm), Pr (1.18 ppm), Nd (4.26 ppm), Sm (1.25 ppm), Eu (0.33 ppm), Er (1.95 ppm), Tm (0.31 ppm), Yb (2.19 ppm) and Lu (0.34 ppm). On the contrary, maximum values were found in the rare earth elements (REE): Ce (633.32 ppm), Pr (20.74 ppm), Nd (77.04 ppm), Sm (17.40 ppm), Eu (3.67 ppm), Gd (17.83 ppm), Tb (2.63 ppm), Dy (16.75 ppm), Ho (3.49 ppm), Er (10.38 ppm), Tm (1.66 ppm), Yb (11.87 ppm) and Lu (1.73 ppm).

The samples S.6_1, S.6_2, S.6_3 and S.6_4, that belong to pile S6 from the Sila mine, display only two minimum values in rare earth elements (REE), those of Ce (37.71 ppm) and Ga (1.96 ppm).

The samples S.7_1, S.7_2, S.7_3 and S.7_4, that were retrieved from pile S7 of the Kamara mine, have three minimum values in Tb (0.37 ppm), Dy (2.77 ppm) and Ho (0.64 ppm).

In conclusion, sample S.5_1 has the highest values in all rare earth elements (REE) among all clusters and the S.3 samples seem to have higher values in La than most of the other samples. Therefore, further research is suggested for the 526 mine, where S.5_1 was taken from, as well as for the Koromilia mine, where S.3 samples were taken from, in order to examine the possible financial potentials and advantages.

Table 13: Rare earth elements concentration (ppm) of bauxite rock samples.

Elements	La	Ce	Pr	Nd	Sm	Eu	Gd	Tb	Dy	Ho	Er	Tm	Yb	Lu	ΣLREE	ΣHREE	ΣREE
S.3_1	78.48	198.59	16.40	64.14	12.73	2.66	12.55	1.82	11.52	2.47	7.56	1.18	7.97	1.20	373.00	46.26	419.26
S.3_2	64.85	299.79	15.27	60.74	13.61	2.90	13.19	1.94	12.53	2.70	8.41	1.34	9.12	1.36	457.17	50.58	507.75
S.3_3	42.93	202.23	9.86	38.24	9.04	2.01	9.57	1.51	10.14	2.16	6.84	1.11	7.77	1.17	304.31	40.27	344.58
S.3_4	33.32	126.57	7.40	24.13	4.03	0.83	4.56	0.79	6.52	1.64	5.80	0.99	7.31	1.14	196.29	28.76	225.05
S.3_5	57.41	295.08	12.51	46.00	8.74	1.79	9.05	1.18	7.10	1.46	4.33	0.66	4.46	0.67	421.53	28.91	450.44
S.4_1	23.00	249.40	10.36	40.32	8.96	1.83	8.37	1.28	8.25	1.73	5.59	0.92	6.45	0.95	333.87	33.54	367.41
S.4_2	46.08	378.15	15.32	59.55	12.69	2.58	12.03	1.79	11.49	2.34	7.30	1.17	8.46	1.22	514.37	45.79	560.16
S.4_3	18.84	139.51	9.38	37.17	8.25	1.61	6.41	1.02	6.63	1.38	4.60	0.81	6.18	0.90	214.75	27.92	242.68
S.5_1	58.87	633.32	20.74	77.04	17.40	3.67	17.83	2.63	16.75	3.49	10.38	1.66	11.87	1.73	811.04	66.34	877.38
S.5_2	8.56	113.38	2.33	8.21	1.93	0.45	2.59	0.41	2.95	0.64	1.95	0.31	2.19	0.34	134.87	11.39	146.25
S.5_3	3.55	91.43	1.18	4.26	1.25	0.33	2.12	0.43	3.45	0.81	2.64	0.44	3.15	0.46	102.00	13.50	115.50
S.5_4	15.78	322.83	5.62	20.73	4.92	1.13	6.88	1.04	7.23	1.57	4.78	0.75	5.10	0.75	371.02	28.11	399.12
S.5_5	10.43	150.91	2.64	9.38	2.26	0.53	3.27	0.54	3.94	0.89	2.82	0.46	3.27	0.50	176.16	15.69	191.85
S.5_6	9.66	181.74	2.59	9.67	2.44	0.59	3.84	0.60	4.24	0.90	2.69	0.43	2.90	0.45	206.68	16.04	222.72
S.5_7	8.57	111.97	2.95	10.84	2.33	0.50	2.69	0.41	2.92	0.65	2.13	0.36	2.57	0.38	137.17	12.12	149.29
S.6_1	23.93	89.93	7.93	25.80	5.96	1.38	5.93	1.25	9.14	1.92	6.09	1.03	7.43	1.11	154.94	33.90	188.84
S.6_2	3.83	42.55	1.42	5.35	1.71	0.42	1.96	0.46	3.80	0.88	3.02	0.56	4.33	0.66	55.27	15.67	70.94
S.6_3	5.12	37.87	1.70	6.57	2.03	0.52	2.49	0.60	5.03	1.21	4.24	0.78	5.74	0.87	53.80	20.97	74.77
S.6_4	12.78	37.71	3.21	10.91	2.57	0.66	3.22	0.75	5.85	1.28	4.07	0.65	4.59	0.69	67.83	21.10	88.93
S.7_1	3.84	111.38	1.54	5.91	1.39	0.34	2.26	0.37	2.77	0.64	2.05	0.34	2.42	0.37	124.40	11.23	135.63
S.7_2	37.68	384.41	13.38	50.81	12.88	2.90	13.71	2.13	12.77	2.42	6.72	1.01	6.94	0.99	502.06	46.69	548.75
S.7_3	33.78	323.56	11.74	41.55	8.36	1.72	8.73	1.27	8.24	1.69	5.10	0.84	6.00	0.87	420.72	32.73	453.45
S.7_4	24.43	337.77	7.24	25.47	5.10	1.05	6.26	0.77	4.65	0.92	2.71	0.41	2.93	0.45	401.06	19.10	420.16

Table 14: Variation and average value of the rare earth elements (REE) concentration (ppm) of bauxite rock samples.

Elements	Min	Max	Average
La	3.55	78.48	27.20
Ce	37.71	633.32	211.31
Pr	1.18	20.74	7.94
Nd	4.26	77.04	29.69
Sm	1.25	17.40	6.55
Eu	0.33	3.67	1.41
Gd	1.96	17.83	6.93
Tb	0.37	2.63	1.09
Dy	2.77	16.75	7.30
Ho	0.64	3.49	1.56
Er	1.95	10.38	4.86
Tm	0.31	1.66	0.79
Yb	2.19	11.87	5.62
Lu	0.34	1.73	0.84
ΣLREE	53.80	811.04	284.10
ΣHREE	11.23	66.34	28.98
ΣREE	70.94	877.38	313.08

6.3.1 Sample classification based on REE contents.

The 23 samples have been classified in 4 clusters based on their rare earth element (REE) consistency, using the K-Means method of classification of IBM® SPSS® software platform for statistical analysis. Examinations of the same classification method using 3, 5 and 6 clusters have been conducted, but the use of 4 clusters has seemed to be more appropriate for the studied samples. The results of the classification are presented in Table 15 and Table 16.

Table 15: Clusters based on rare earth element content.

Case Number	Samples	Cluster	Distance
1	S.3_1	1	.000
2	S.3_2	2	89.502
3	S.3_3	1	44.901
4	S.3_4	4	94.971
5	S.3_5	2	92.087
6	S.4_1	1	79.456
7	S.4_2	2	14.050
8	S.4_3	1	89.002
9	S.5_1	3	.000
10	S.5_2	4	75.765
11	S.5_3	4	53.755
12	S.5_4	2	73.413
13	S.5_5	1	101.978
14	S.5_6	1	92.043
15	S.5_7	4	74.445
16	S.6_1	4	59.371
17	S.6_2	4	5.542
18	S.6_3	4	.000
19	S.6_4	4	9.104
20	S.7_1	4	73.672
21	S.7_2	2	.000
22	S.7_3	2	62.277
23	S.7_4	2	57.033

Table 16: Final cluster centers based on rare earth element content.

	Cluster 1 6 Samples	Cluster 2 7 Samples	Cluster 3 1 Sample	Cluster 4 9 Samples
La	30.56	40.00	58.87	11.50
Ce	187.06	334.52	633.32	84.75
Pr	8.54	11.58	20.74	3.30
Nd	33.15	43.55	77.04	11.33
Sm	7.28	9.47	17.40	2.58
Eu	1.54	2.01	3.67	.60
Gd	7.33	9.98	17.83	3.09
Tb	1.13	1.45	2.63	.61
Dy	7.45	9.14	16.75	4.72
Ho	1.59	1.87	3.49	1.07
Er	5.02	5.62	10.38	3.56
Tm	.82	.88	1.66	.61
Yb	5.76	6.14	11.87	4.42
Lu	.86	.90	1.73	.67
ΣLREE	268.13	441.13	811.04	114.06
ΣHREE	29.96	35.98	66.34	18.75
ΣREE	298.09	477.11	877.38	132.81

Classifying the 23 samples based on their rare earth element (REE) composition using 4 clusters, resulted in cluster 1 consisting of 6 samples, cluster 2 consisting of 7 samples, cluster 3 consisting of only 1 sample and cluster 4 of 9 samples. Cluster 1 includes: S.3_1, S.3_3, S.4_1, S.4_3, S.5_5 and S.5_6. Cluster 2 includes: S.3_2, S.3_5, S.4_2, S.5_4, S.7_2, S.7_3 and S. 7_4. Cluster 3 consists of the sample S.5_1. Finally, cluster 4 includes: S.3_4, S.5_2, S.5_3, S. 5_7, S.6_1, S.6_2, S.6_3, S.6_4 and S. 7_1.

Cluster 1 has medium values, measured in ppm, in rare earth elements (REE) compared to the other 3 clusters. All the values of cluster 1 are higher than those of cluster 4 and lower than those of clusters 2 and 3. Ce, specifically, has an average value of 187.06 ppm and Nd of 33.15 ppm. S.3_1, that belongs to cluster 1, differs in CaO content due to external contamination (secondary non-genetic calcite). Therefore, it is considered as flyer.

Cluster 2 has higher average values of rare earth elements (REE) than cluster 1 and 4, but lower than cluster 3. In this cluster Ce reaches an average value of 334.52 ppm, while Nd is 43.55 ppm.

Cluster 3, which consists only of one sample S.5_1, has the highest values in all rare earth elements (REE). Specifically, Ce is 633.32 ppm, Nd 77.04 ppm, La 58.87 ppm, Sm and Gd 17.40 ppm and 17.83 ppm, respectively.

Cluster 4, which consists of 9 samples out of 23, has the lowest average values of rare earth elements (REE). Ce, in this case, is 84.75 ppm, Nd 11.33 ppm, La 11.50 ppm, Sm 2.58 ppm and Gd 3.09 ppm.

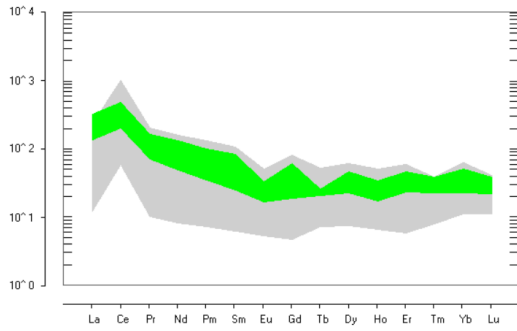
As expected, sample S.5_1 having the highest values in all rare earth elements (REE), is differentiated from all other samples. Further research is suggested for the 526 mine, where S.5_1 was taken from, in order to examine whether the higher values in rare earth elements (REE) of this sample were random or there is a higher concentration in rare earth elements (REE) in this area.

6.3.2 Chondrite-normalized rare earth elements diagrams (REE).

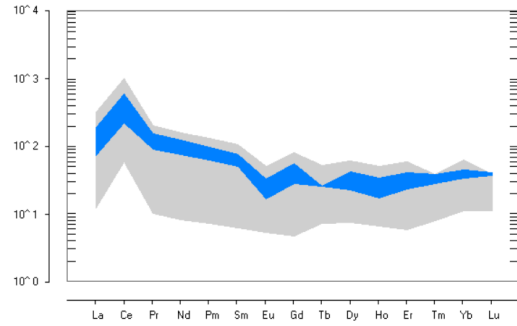
In Figure 7 the chondrite-normalized rare earth elements diagrams (REE) per sampling region are presented (from a-f) with different colours, to better visualise the range of the REE values in the regions, while the combined areas range is presented in the background with grey colour.

Generally, most of the sampling regions seem to have a tendency to contain higher values in HREE than LREE. It appears that there is a peak around the value of Ce in all the regions, while Gd and Er present the lowest values in Sila and 526, respectively.

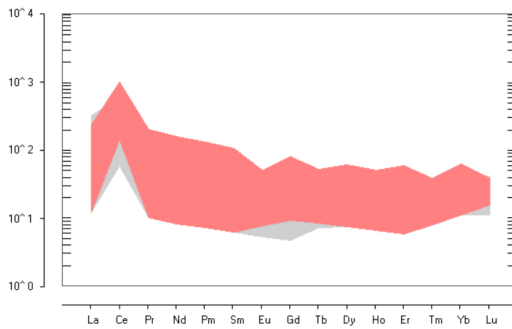
It may be observed that the intervals of REE measurements in samples extracted from Koromilia and Nera regions exhibit lower variance and are placed towards the higher end of the overall sample distribution (grey area). In contrast, REE measurements in Koukouvista and Sila regions are placed near the lower end of the overall sample distribution. REE measurements in 526 and Kamara regions are less clear, with REE concentration values across samples having a large degree of variability, as the coloured areas in the respective diagrams almost fully overlap with the overall sample distribution.



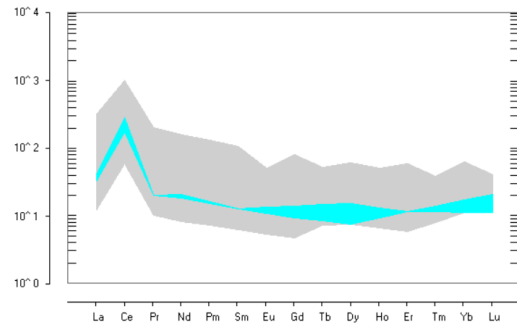
(a) Koromilia



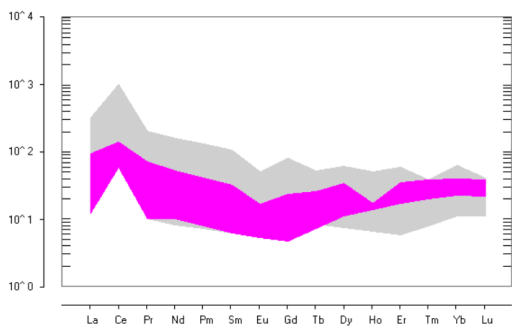
(b) Nera



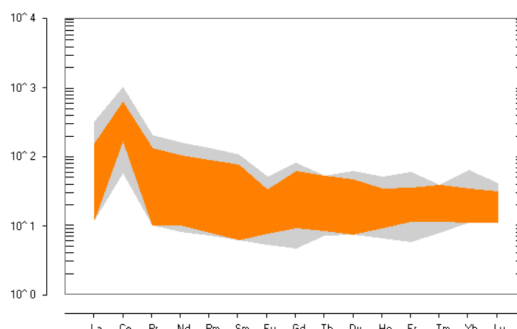
(c) 526



(d) Koukouvista



(e) Sila



(f) Kamara

Figure 7: Chondrite-normalized rare earth elements diagrams (REE) (Sun and McDonough, 1989). Each region is represented by a different colour and the total samples range is presented in the background with grey colour.

6.4 COMPARISON WITH KARST-BAUXITE SAMPLES FROM PARNASSOS-GIONA ZONE

In the present section, a comparative analysis is performed between the analysis results in the present study and the results of the Gamaletsos (2014) thesis 'Mineralogy and Geochemistry of Bauxites from Parnassos-Giona mines and the impact on the origin of the deposits' that studies the same region.

More specifically, in Table 17, the major and rare earth element compositions of 11 (Fe-rich) analyzed samples of the Gamaletsos (2014) study are presented, while Table 18 presents the major, trace and rare earth elements (REE) minimum, maximum and average values.

Our geochemical data present a slightly higher value in La and Pr than those of Gamaletsos (2014) study while the latter's geochemical data present a slightly higher value in Nd, Sm, ΣREE, ΣLREE and ΣHREE. In addition, in Gamaletsos (2014) study as rare earth elements (REE) are considered the lanthanides+Sc+Y.

Table 17: Major (wt.%) and rare earth elements (ppm) concentration of other authors (Gamaletsos, 2014).

	SK_B2	PL1_B1	PL1_B3	PL1_B4	DV_B1	ASV	PL1_B2	KV_B1	2H1	SKR	PL1_B51
SiO ₂ (%)	0,34	1,95	0,75	0,40	1,96	0,50	6,10	13,90	8,57	8,94	1,63
Al ₂ O ₃	67,64	61,53	61,70	56,84	62,49	63,36	55,25	49,70	44,25	52,83	55,28
Fe ₂ O ₃	14,12	20,58	21,95	24,57	19,30	20,29	22,52	20,28	27,66	22,45	27,66
TiO ₂	2,78	2,69	2,63	2,29	3,44	3,36	2,49	2,23	2,58	2,41	2,57
CaO	0,04	0,02	0,08	0,10	0,02	0,05	0,09	0,13	0,21	0,11	0,02
La (ppm)	12,30	32,00	82,70	23,70	106,00	52,20	140,10	167,10	45,90	140,50	22,70
Ce	80,90	216,10	99,10	99,90	655,00	350,50	251,40	286,40	203,40	291,60	83,50
Pr	2,09	6,41	12,10	7,45	25,13	9,83	36,80	23,27	12,97	28,89	6,07
Nd	6,40	21,70	35,20	29,30	90,80	33,30	136,10	79,20	49,10	109,80	22,50
Sm	1,40	6,33	7,82	6,77	19,29	7,57	29,94	14,64	9,69	23,37	4,96
Eu	0,37	1,65	1,90	1,35	3,75	1,63	5,82	2,70	1,61	4,57	1,10
Gd	2,05	7,36	9,14	5,39	12,74	6,72	20,42	9,94	5,49	18,44	4,77
Tb	0,69	2,44	2,76	1,19	2,39	1,85	4,37	2,19	1,36	3,66	1,22
Dy	4,74	16,59	18,33	6,40	12,08	10,85	22,88	12,32	8,70	19,22	7,37
Ho	1,04	3,70	3,87	1,20	2,26	2,23	4,16	2,50	1,68	3,69	1,44
Er	3,26	11,33	12,52	3,60	6,84	6,85	12,24	7,78	5,53	10,98	4,36
Tm	0,56	1,68	2,03	0,60	1,14	1,14	2,06	1,31	0,98	1,75	0,76
Yb	4,01	10,33	13,02	4,04	7,84	7,92	13,25	9,00	7,08	11,71	4,91
Lu	0,63	1,65	2,12	0,64	1,22	1,23	2,05	1,40	1,11	1,82	0,78
Th	32,90	48,30	58,80	44,90	50,70	64,00	48,40	51,00	63,70	53,00	60,40
U	5,10	10,50	11,30	12,40	8,80	7,80	10,00	5,70	11,20	6,70	10,70
Au	0,00	1,60	0,50	3,50	0,00	1,30	6,80	0,00	0,70	1,30	0,90
ΣREE	103,46	284,19	248,00	174,00	913,00	462,00	621,00	583,00	328,00	617,00	146,00
ΣLREE	16,98	55,08	126,00	53,00	123,00	100,00	157,00	126,00	80,00	179,00	64,00
ΣHREE	120,44	339,27	425,00	272,00	1109,00	633,00	835,00	764,00	454,00	853,00	257,00

Table 18: Variation and average values of major (wt.%) and rare earth elements (ppm) concentration of other authors (Gamaletsos, 2014).

	Min	Max	Average
SiO ₂ (%)	0,40	13,90	4,75
Al ₂ O ₃	44,25	63,36	55,74
Fe ₂ O ₃	19,30	27,66	22,96
TiO ₂	2,23	3,44	2,67
CaO	0,02	0,21	0,09
Be (ppm)	4,00	10,00	6,22
Sc	45,00	73,00	55,67
V	271,00	711,00	490,22
Co	6,10	98,90	43,20
Ni	58,00	1142,00	340,11
Cu	1,00	54,60	13,47
Zn	4,00	126,00	36,00
As	0,00	176,70	45,59
Se	0,50	3,60	1,18
Rb	0,50	28,00	6,53
Sr	13,20	271,70	65,26
Y	35,00	126,50	74,70
Zr	353,30	556,40	442,29
Nb	44,90	71,10	52,89
Cd	0,10	0,90	0,27
Mo	0,70	64,80	10,62
Sb	0,60	22,50	8,03
Sn	8,00	17,00	11,56
Cs	0,10	9,40	2,20
Ba	7,80	74,20	29,83
Hf	10,60	16,10	12,53
Ta	2,70	3,70	3,10
W	13,00	133,80	51,12
Hg	0,01	0,77	0,13
Pb	28,00	123,90	83,13
Bi	1,40	2,70	2,14
La	22,70	167,10	86,77
Ce	83,50	655,00	257,87
Pr	6,07	36,80	18,06
Nd	22,50	136,10	65,03
Sm	4,96	29,94	13,78
Eu	1,10	5,82	2,71
Gd	4,77	20,42	10,34
Tb	1,19	4,37	2,33
Dy	6,40	22,88	13,13
Ho	1,20	4,16	2,56
Er	3,60	12,52	7,86
Tm	0,60	2,06	1,31
Yb	4,04	13,25	8,75
Lu	0,64	2,12	1,37
Th	44,90	64,00	54,99
U	5,70	12,40	9,40
Au	0,00	6,80	1,67
ΣREE	140,83	899,97	444,22
ΣLREE	23,06	81,43	47,65
ΣHREE	166,44	946,48	491,87

In Figure 8 the chondrite-normalised rare earth elements diagram (REE) from Parnassos-Giona Zone is presented from both Gamaletsos (2014) and this study. The chart area in yellow represents the Fe-enriched samples from Parnassos-Giona Zone (Gamaletsos, 2014). The dotted grey area represents sample measurements from the current study.

There is a clear difference in the maximum observed values of REE among the samples of the two studies with the maximum REE values of Gamaletsos (2014) being consistently higher than the ones from this study. The difference is accentuated in the cases of the elements Gd, Tm and Lu, where Gamaletsos' measurements are much higher. The only exception is Ce, where maximum values in both studies nearly coincide for the particular element. On the other hand, regarding the lower limit of the REE measurements, the results are miscellaneous. The lowest concentration of elements La and Nd were found in the samples of Gamaletsos study, the lowest value of Er and Yb are similar, while for the remaining elements the lowest value belongs to the samples analysed here. The most extreme difference, between the minimum REE measurements of the two studies, may be found in the elements Pr, Sm, Gd and Dy.

Finally, the spider chart area, corresponding to the Gamaletsos (2014) study results, exhibits peaks that indicate a potential enrichment of the rock samples in Ce, Gd, Tm and Lu. The two studies seem to be aligned with respect to Ce measurements, as our samples have consistently high values as well. On the other hand, the peaks in Gd, Tm and Lu in Gamaletsos (2014) measurements are not supported by our results.

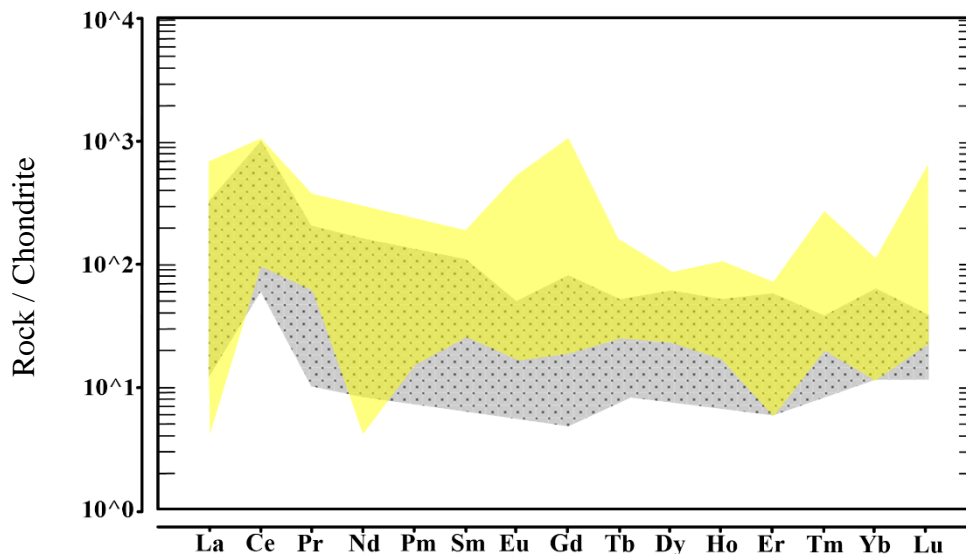


Figure 8: Chondrite-normalised rare earth elements diagram (REE) from Parnassos-Giona Zone (Sun and McDonough, 1989). The chart area in yellow represents the Fe-rich samples from Parnassos-Giona Zone (Gamaletsos, 2014). The dotted grey area represents sample measurements from the current Master thesis.



7 BAUXITE DEPOSITS' CORRELATION COMPARISON

A correlation investigation was conducted using sampling data from Greece, China (Longhe, Tianyang, Western Guangxi, Henan) and Montenegro. The two factors of this analysis were the major elements and the rare earth elements (REE). In order to determine any possible high or low correlation between these factors, Pearson's correlation, ANOVA test and data visualisation methods were used.

In the correlation tables that are presented below (Table 2020, Table 24, Table 26, Table 31 and Table 33), a 3-scale colour grade has been used to present the correlation between the major elements and the rare earth elements of the analysed samples. The correlation with the -1 value is presented with the blue colour, the 0 value is presented with the yellow colour, whereas the $+1$ value is presented with the red colour.

7.1 PEARSON'S CORRELATION.

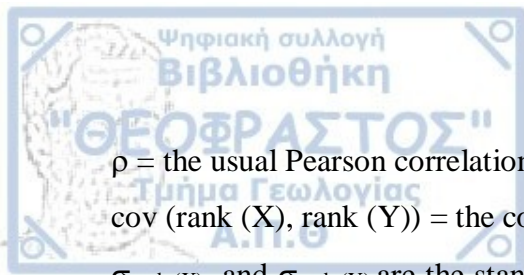
In statistics, Spearman's rank correlation coefficient or Spearman's ρ , named after Charles Spearman and often denoted by the Greek letter ρ (rho) or r_s is a nonparametric rank statistic that measures the strength of the association between two variables.

The nonparametric (distribution-free) rank statistic known as Spearman's rank correlation coefficient was developed as a way to gauge how strongly two variables are related. When the distribution of the data makes Pearson's correlation coefficient unfavorable or inaccurate, it is a measure of a monotone association. Contrary to what some "statisticians" claim, Spearman's coefficient does not measure a linear relationship between two variables. Without assuming anything about the frequency distribution of the variables, it evaluates how well an arbitrary monotonic function can capture the relationship between two variables. It is not necessary to assume that the relationship between the variables is linear or that the variables must be measured, unlike Pearson's product-moment correlation coefficient. Therefore, it was preferred to use the Spearman's rank correlation coefficient for the analysis conducted on this thesis.

If all n ranks are distinct integers, the popular formula used is:

$$\rho = \frac{\text{cov}(\text{rank}(X), \text{rank}(Y))}{\sigma_{\text{rank}(X)} \sigma_{\text{rank}(Y)}}$$

where:



ρ = the usual Pearson correlation coefficient, applied to the rank variables,

$\text{cov}(\text{rank}(X), \text{rank}(Y))$ = the covariance of the rank variables,

$\sigma_{\text{rank}(X)}$ and $\sigma_{\text{rank}(Y)}$ are the standard deviations of the rank variables. (Lehman, 2005; Hauke and Kossowski, 2011)

7.2 GREECE

The Parnassos-Giona Zone was named after the Parnassos and Giona mountains of central Greece. There are three bauxite horizons embedded in the continuous calcareous unit.

The general stratigraphic column consists of the following units in chronological perspective: the Middle-Late Triassic dolomites, the Early-Middle Jurassic dolomitic limestones, the first bauxite horizon (B1), the Late Jurassic limestones, the second bauxite horizon (B2), the Tithonian-Cenomanian limestones, the third bauxite horizon (B3), the Late Cretaceous limestones and the Paleocene-Late Eocene shales and flysch. (Gregou, 1996; Mountrakis, 2010; Deady *et al.*, 2014; Eliopoulos *et al.*, 2014)

Table 19: Rare earth elements concentrations (ppm) of analyzed samples.

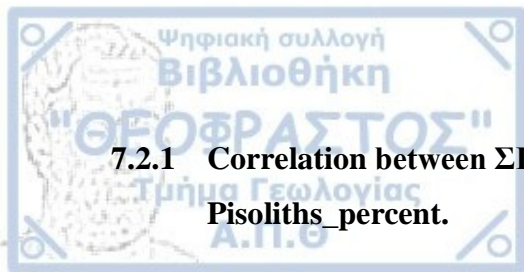
Elements	S.3_1	S.3_2	S.3_3	S.3_4	S.3_5	S.4_1	S.4_2	S.4_3	S.5_1	S.5_2	S.5_3	S.5_4	S.5_5	S.5_6	S.5_7	S.6_1	S.6_2	S.6_3	S.6_4	S.7_1	S.7_2	S.7_3	S.7_4
La	78.48	64.85	42.93	33.32	57.41	23.00	46.08	18.84	58.87	8.56	3.55	15.78	10.43	9.66	8.57	23.93	3.83	5.12	12.78	3.84	37.68	33.78	24.43
Ce	198.59	299.79	202.23	126.57	295.08	249.40	378.15	139.51	633.32	113.38	91.43	322.83	150.91	181.74	111.97	89.93	42.55	37.87	37.71	111.38	384.41	323.56	337.77
Pr	16.40	15.27	9.86	7.40	12.51	10.36	15.32	9.38	20.74	2.33	1.18	5.62	2.64	2.59	2.95	7.93	1.42	1.70	3.21	1.54	13.38	11.74	7.24
Nd	64.14	60.74	38.24	24.13	46.00	40.32	59.55	37.17	77.04	8.21	4.26	20.73	9.38	9.67	10.84	25.80	5.35	6.57	10.91	5.91	50.81	41.55	25.47
Sm	12.73	13.61	9.04	4.03	8.74	8.96	12.69	8.25	17.40	1.93	1.25	4.92	2.26	2.44	2.33	5.96	1.71	2.03	2.57	1.39	12.88	8.36	5.10
Eu	2.66	2.90	2.01	0.83	1.79	1.83	2.58	1.61	3.67	0.45	0.33	1.13	0.53	0.59	0.50	1.38	0.42	0.52	0.66	0.34	2.90	1.72	1.05
Gd	12.55	13.19	9.57	4.56	9.05	8.37	12.03	6.41	17.83	2.59	2.12	6.88	3.27	3.84	2.69	5.93	1.96	2.49	3.22	2.26	13.71	8.73	6.26
Tb	1.82	1.94	1.51	0.79	1.18	1.28	1.79	1.02	2.63	0.41	0.43	1.04	0.54	0.60	0.41	1.25	0.46	0.60	0.75	0.37	2.13	1.27	0.77
Dy	11.52	12.53	10.14	6.52	7.10	8.25	11.49	6.63	16.75	2.95	3.45	7.23	3.94	4.24	2.92	9.14	3.80	5.03	5.85	2.77	12.77	8.24	4.65
Ho	2.47	2.70	2.16	1.64	1.46	1.73	2.34	1.38	3.49	0.64	0.81	1.57	0.89	0.90	0.65	1.92	0.88	1.21	1.28	0.64	2.42	1.69	0.92
Er	7.56	8.41	6.84	5.80	4.33	5.59	7.30	4.60	10.38	1.95	2.64	4.78	2.82	2.69	2.13	6.09	3.02	4.24	4.07	2.05	6.72	5.10	2.71
Tm	1.18	1.34	1.11	0.99	0.66	0.92	1.17	0.81	1.66	0.31	0.44	0.75	0.46	0.43	0.36	1.03	0.56	0.78	0.65	0.34	1.01	0.84	0.41
Yb	7.97	9.12	7.77	7.31	4.46	6.45	8.46	6.18	11.87	2.19	3.15	5.10	3.27	2.90	2.57	7.43	4.33	5.74	4.59	2.42	6.94	6.00	2.93
Lu	1.20	1.36	1.17	1.14	0.67	0.95	1.22	0.90	1.73	0.34	0.46	0.75	0.50	0.45	0.38	1.11	0.66	0.87	0.69	0.37	0.99	0.87	0.45
ΣREE	419.26	507.75	344.58	225.05	450.44	367.41	560.16	242.68	877.38	146.25	115.50	399.12	191.85	222.72	149.29	188.84	70.94	74.77	88.93	135.63	548.75	453.45	420.16
ΣLREE	373.00	457.17	304.31	196.29	421.53	333.87	514.37	214.75	811.04	134.87	102.00	371.02	176.16	206.68	137.17	154.94	55.27	53.80	67.83	124.40	502.06	420.72	401.06
ΣHREE	46.26	50.58	40.27	28.76	28.91	33.54	45.79	27.92	66.34	11.39	13.50	28.11	15.69	16.04	12.12	33.90	15.67	20.97	21.10	11.23	46.69	32.73	19.10
ΣLREE/ΣHREE	8.06	9.04	7.56	6.83	14.58	9.95	11.23	7.69	12.22	11.84	7.55	13.20	11.23	12.88	11.31	4.57	3.53	2.57	3.21	11.08	10.75	12.85	21.00
Ce/Ce*	324.49	489.85	330.44	206.81	482.15	407.51	617.89	227.95	1034.83	185.27	149.39	527.51	246.59	296.95	182.95	146.94	69.52	61.88	61.61	181.99	628.13	528.70	551.92
Eu/Eu*	0.64	0.65	0.66	0.59	0.61	0.64	0.63	0.65	0.63	0.62	0.61	0.59	0.60	0.59	0.61	0.70	0.70	0.70	0.70	0.59	0.66	0.61	0.57
(La/Yb) _N	7.07	5.10	3.96	3.27	9.23	2.56	3.91	2.19	3.56	2.81	0.81	2.22	2.28	2.39	2.39	2.31	0.63	0.64	2.00	1.14	3.90	4.04	5.99
(La/Sm) _N	3.98	3.08	3.07	5.33	4.24	1.66	2.34	1.47	2.18	2.86	1.83	2.07	2.98	2.55	2.37	2.59	1.45	1.63	3.21	1.78	1.89	2.61	3.09
(Gd/Lu) _N	1.29	1.20	1.01	0.49	1.66	1.08	1.22	0.88	1.28	0.94	0.57	1.13	0.81	1.06	0.87	0.66	0.37	0.35	0.58	0.76	1.71	1.24	1.71

As presented in Table 19, the range of the total rare earth elements (Σ REE) is between 70.94 ppm and 877.38 ppm with an average value of 313.08 ppm, while the total light rare earth elements (Σ LRREE) is between 53.80 ppm and 811.04 ppm with an average value of 284.10 ppm and the total heavy earth elements (Σ HREE) is between 11.23 ppm and 66.34 ppm, with an average value of 28.98 ppm.

Table 20: Correlation between major elements and rare earth elements (REE), Greece.

	SiO ₂	Al ₂ O ₃	Fe ₂ O ₃	TiO ₂	CaO
La	0.58	-0.59	-0.24	-0.57	0.58
Ce	0.05	0.04	-0.19	-0.09	0.02
Pr	0.35	-0.31	-0.25	-0.35	0.36
Nd	0.36	-0.34	-0.22	-0.38	0.38
Sm	0.33	-0.29	-0.21	-0.33	0.31
Eu	0.33	-0.28	-0.22	-0.33	0.30
Gd	0.33	-0.27	-0.24	-0.34	0.30
Tb	0.32	-0.24	-0.24	-0.28	0.26
Dy	0.35	-0.25	-0.26	-0.25	0.24
Ho	0.41	-0.28	-0.27	-0.27	0.26
Er	0.45	-0.31	-0.26	-0.26	0.25
Tm	0.45	-0.29	-0.25	-0.23	0.22
Yb	0.43	-0.27	-0.24	-0.19	0.18
Lu	0.46	-0.29	-0.25	-0.20	0.20
Σ LRREE	0.17	-0.09	-0.22	-0.20	0.15
Σ HREE	0.39	-0.28	-0.26	-0.28	0.26
Σ REE	0.19	-0.11	-0.22	-0.21	0.16

As presented in Table 20 it is concluded that there is a medium positive correlation between La and the major elements SiO₂ and CaO, while there is a medium negative correlation with the major elements Al₂O₃ and TiO₂. Er, Tm, Yb and Lu also present a medium positive correlation with SiO₂. The majority of the rare earth elements (REE) demonstrate a low positive correlation with SiO₂ and CaO, while having a low negative correlation with the major elements Al₂O₃, Fe₂O₃ and TiO₂.



7.2.1 Correlation between ΣREE, ΣLREE, ΣHREE and major elements, Pisoliths_size, Pisoliths_percent.

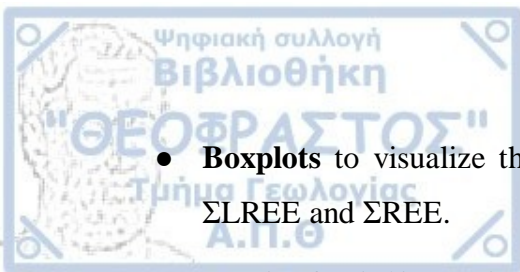
Table 21: Pearson correlation estimates.

	SiO ₂	Al ₂ O ₃	Fe ₂ O ₃	TiO ₂	CaO	Pisoliths_size	Pisoliths_percent
ΣREE	0.19	-0.11	-0.22	-0.21	0.16	0.16	0.25
ΣLREE	0.17	-0.09	-0.22	-0.20	0.15	0.17	0.26
ΣHREE	0.39	-0.28	-0.26	-0.28	0.26	0.06	0.19

The correlations between the rare earth element sums and the rest of the variables reveal both weak and moderate associations. SiO₂ and CaO exhibit weak positive correlations with ΣREE and ΣLREE, suggesting a modest tendency for these elements to increase together. In contrast, Al₂O₃, Fe₂O₃, and TiO₂ show negative correlations with all three rare earth element sums, indicating that higher rare earth element sums tend to be associated with lower levels of these elements, though these correlations are also relatively weak. Notably, there are positive correlations between the rare earth element sums and Pisoliths_size, and Pisoliths_percent, implying that as ΣREE, ΣLREE, and ΣHREE increase, there is a tendency for Pisoliths_size and Pisoliths_percent to increase as well. Among these correlations, ΣHREE exhibits a stronger positive relationship with SiO₂ compared to ΣREE and ΣLREE, while displaying stronger negative correlations with Al₂O₃, Fe₂O₃, and TiO₂. However, it is important to recognize that while these correlations provide valuable insights, they are not extremely strong, and further domain-specific analysis may be required to fully understand the underlying geological processes at play.

To identify any potential correlations between the colour and/or the origin of the samples with the dependent variables ΣHREE, ΣLREE and ΣREE, the estimation of standard correlation measures (e.g., Pearson correlation) would not be appropriate. Correlation is specifically designed to measure the strength and direction of a linear relationship between two continuous variables. Therefore, using correlation between a nominal (categorical) variable and a continuous variable is not appropriate in the standard sense. Nominal variables do not have a quantitative order or a continuous scale, which is a fundamental assumption for calculating correlation coefficients.

Among other indicated methods for estimating the relationship between a nominal (categorical) and continuous variable, the following were used:



- **Boxplots** to visualize the distribution of the dependent variables, namely, ΣΗREE, ΣΛREE and ΣREE.
- The **ANOVA (Analysis of Variance)** technique to assess whether there is a statistically significant difference among the distribution means of ΣΗREE, ΣΛREE and ΣREE across the different groups considering colour and region (i.e., a generalization of the t-test for the difference of means).

It is worth noting that ANOVA results formally indicate the presence or not of correlation compared to boxplots which are used for exploratory purposes.

The analysis using the aforementioned methods will be performed twice, factoring for the sample colour and origin of rock samples independently.

7.2.2 Boxplots

A boxplot, also known as a “box-and-whisker” plot, is a graphical representation that provides a concise summary of the distribution of a dataset. It visually depicts key descriptive statistics, including measures of central tendency, spread, and potential outliers. Here is the anatomy of a boxplot:

- **Box:** The central box in the plot represents the interquartile range (IQR), which encompasses the middle 50% of the data. It spans from the first quartile (Q1) to the third quartile (Q3). The width of the box does not necessarily have a standard definition, but it typically covers the IQR.
- **Median Line:** Inside the box, there is a vertical line that represents the median (Q2), which is the value that separates the lower 50% of the data from the upper 50%.
- **Whiskers:** The whiskers extend from the edges of the box to the data points that are within a certain distance from Q1 and Q3. The distance is often defined as 1.5 times the IQR. Any data points beyond the whiskers are considered potential outliers.
- **Outliers:** Individual data points beyond the whiskers are marked as individual dots or small circles. These are data points that fall outside the typical range of the dataset.

To observe potential differences among the distribution of ΣΗREE, ΣΛREE and ΣREE among the different groups of samples' colour or origin, the following aspects will be checked to consider as indicators of potential significant difference in means among groups:

- High distance among the median lines of boxplots
- High overlap of the "box" areas

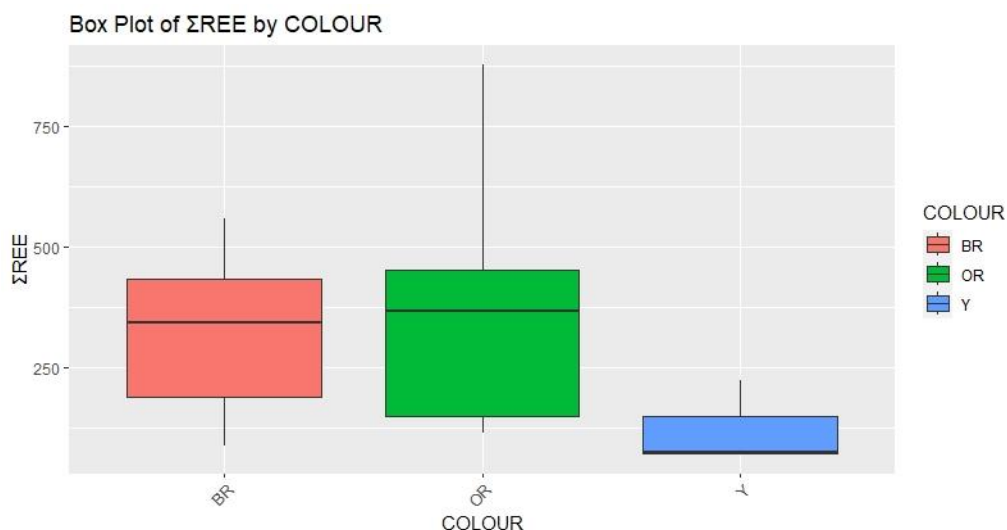
Lengthy "whiskers" might indicate a high level of variability in the distributions, while presence of outliers reduce certainty regarding the difference between the means of two groups.

7.2.2.1 Results

As illustrated in the figures (Figure 9) that follow, the boxplot comparison of ΣREE grouped by colour indicates that yellow rock samples may be associated with lower levels of ΣREE. The median line of the corresponding boxplot is considerably lower than orange and brown rock samples, while there is clear separation of the box areas of the boxplots. The boxplot comparison for ΣLREE is nearly identical.

In contrast, the boxplot of ΣHREE values for different colour groups does not seem to be suggesting any statistically significant difference among the means and distributions of the groups, as the box areas overlap to a great extent, while the median lines are much closer to each other.

The boxplot analysis results suggest that ΣLREE and ΣREE concentrations of yellow rock samples are significantly lower, while we expect the ANOVA test to show a statistically significant difference among the distribution means among different coloured samples (i.e. that the rock sample colour is correlated with the rare earth element concentrations).



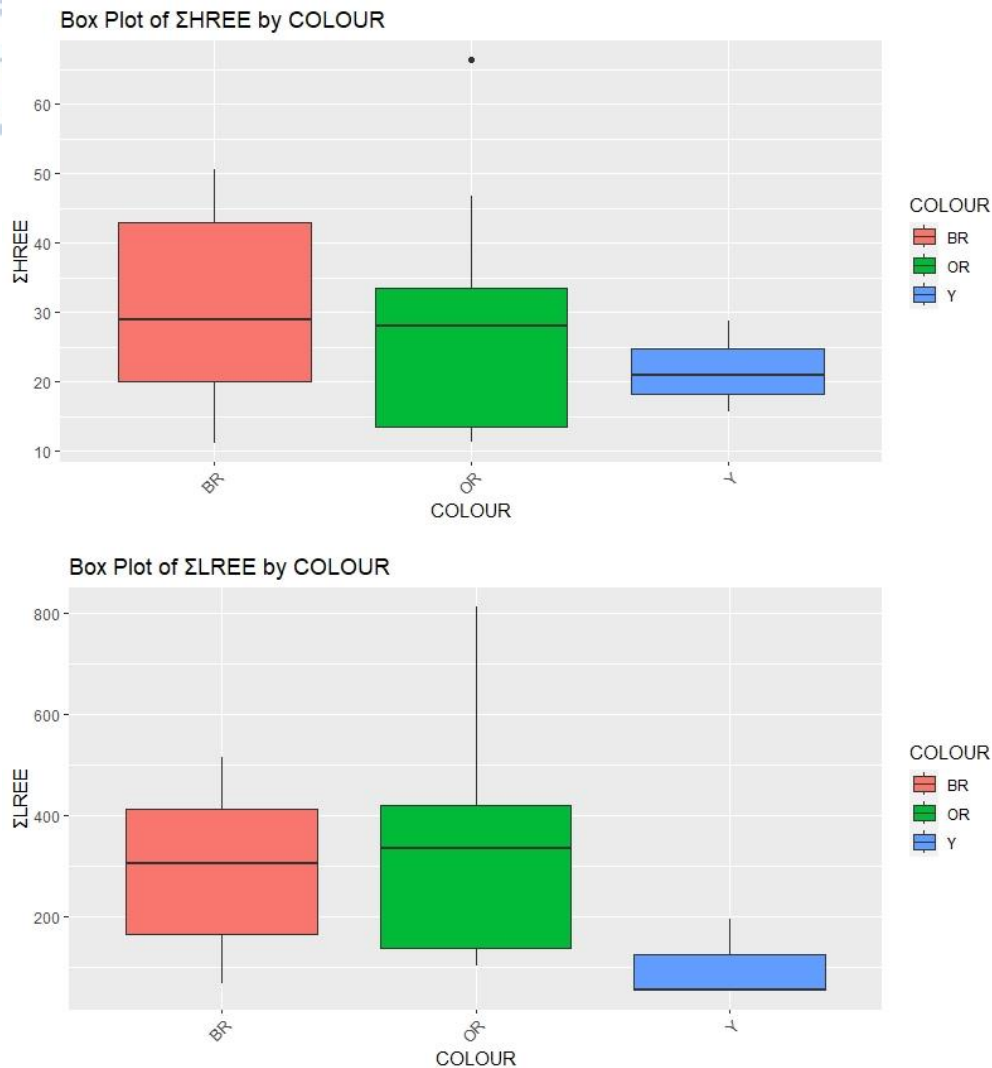


Figure 9: Box plots of ΣREE, ΣHREE and ΣLREE by colour.

The boxplot analysis per region (Figure 10), shows that the distribution of ΣREE, ΣLREE in rock samples from areas Kamara, Koromilia and Nera exhibit nearly identical traits (median line and interquartile range). The distribution of the ΣREE, ΣLREE variables of the “526” region fully overlap with the above regions and it shows more variability. Koukouvista and Sila regions seem to have much lower concentrations of rare earth elements than the rest of the areas with the distribution of Sila overlapping with none of the other areas.

The boxplot analysis of ΣHREE concentrations in the rock sampling areas is quite similar to the results of ΣREE and ΣLREE. In this case, though, the variables of Kamara and “526” regions seem to be more evenly distributed. Koromilia and Nera regions show slightly higher concentrations than Kamara and “526” areas compared to the previous results. The ΣHREE concentrations in Sila region are closer to the Kamara and “526” areas.

Therefore, there is a chance for the ANOVA test to indicate a difference in distribution means for ΣREE and ΣLREE. In the case of ΣHREE, it is *less likely* that the ANOVA test will show any statistically significant difference among the distribution means of the different sampling areas (i.e. the sampling region to be correlated with the rare earth element concentrations).



Figure 10: Box plots of ΣREE, ΣHREE and ΣLREE by region.

7.2.3 ANOVA

The Analysis of Variance (ANOVA) technique is a powerful statistical method used to compare means across multiple groups or treatments. It enables researchers to determine whether the observed differences in group means are significant or if they could have occurred due to random chance. ANOVA works by partitioning the total variation in the data into different sources: variation within each group and variation between groups. By comparing these variations, ANOVA assesses whether the differences between group means are larger than what would be expected from random fluctuations. If the between-group variation is significantly larger, ANOVA indicates that there is likely a real difference in means among the groups.

ANOVA offers several advantages in statistical analysis. Firstly, it allows for efficient comparison of multiple groups simultaneously, reducing the risk of making Type-I errors (false positives) that can occur when conducting multiple pairwise comparisons. Secondly, it provides a framework for quantifying the relative importance of various sources of variability in the data. This is crucial for understanding the factors that contribute to observed differences and for identifying potential interactions between variables. ANOVA is versatile and can be adapted for various study designs, such as one-way ANOVA for single-factor comparisons or two-way ANOVA for examining interactions between two factors. (St and Wold, 1989)

7.2.3.1 Results

Table 22: Table of the p-values of the ANOVA test for the categorical data (REGION & COLOUR) and the ΣREE, ΣLREE and ΣHREE.

Variable	Factor	P_Value
ΣREE	REGION	0.16
ΣREE	COLOUR	0.20
ΣLREE	REGION	0.15
ΣLREE	COLOUR	0.18
ΣHREE	REGION	0.27
ΣHREE	COLOUR	0.66

The ANOVA test matrix presents the results of analyses on three variables (ΣREE, ΣLREE, ΣHREE) concerning two factors (REGION, COLOUR). The corresponding p-values

indicate the statistical significance of mean differences across factor levels. For Σ REE and Σ LREE, p-values (0.16, 0.20 for REGION; 0.15, 0.18 for COLOUR) are higher, suggesting limited evidence for significant differences. Likewise, for Σ HREE, p-values (0.27 for REGION; 0.66 for COLOUR) are elevated, indicating insufficient support for significant mean variation. Overall, the ANOVA outcomes do not strongly substantiate noteworthy mean distinctions among the variables for the considered factors.

7.3 CHINA

7.3.1 Longhe

Various locations in the western Guangxi region, which is located in the southwestern part of the Youjiang Basin in China, have been researched to evaluate the formation of the Permian-Quaternary bauxite deposits, the mineralogy and the geochemistry of the deposits, as well as the type, the mechanisms that resulted in the genesis and the evolution of the rare earth elements (REE) within these bauxite deposits. Due to favorable climate conditions and abundance in ore-forming materials, which originated from the carbonate and magmatic rocks, a large bauxite deposit has been created. After having undergone different stages and conditions throughout the Mesozoic era, these Permian bauxite deposits have been exposed to the surface and formed the Quaternary bauxite found in the karstic depressions.

The samples that were analyzed include both Permian and Quaternary bauxite samples retrieved from the bauxite deposits of Longhe (west part of western Guangxi) and Tianyang (northeast part of western Guangxi), as displayed in Table 23, respectively (Liu *et al.*, 2016).

Table 23: Major (wt.%) and rare earth elements (ppm) concentration of analyzed samples of Longhe, China (Liu *et al.*, 2016).

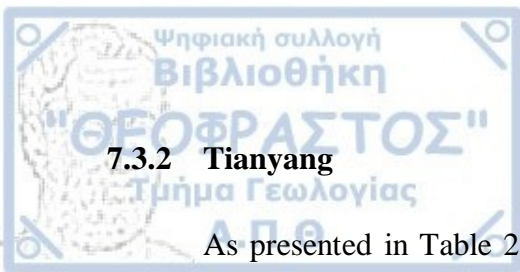
Element	LQ-1	LQ-2	LQ-3	LQ-4	LQ-5	LQ-6	LQ-7	LQ-8	LP-1	LP-2	LP-3
SiO ₂ (%)	7.37	9.96	17.65	1.12	1.89	0.71	0.71	1.93	7.73	7.80	9.82
Al ₂ O ₃	44.95	38.13	39.09	51.80	42.20	51.97	53.58	44.82	57.42	51.24	49.40
Fe ₂ O ₃	26.63	33.57	28.07	30.77	33.79	28.08	25.44	31.42	7.88	9.43	16.98
FeO	0.52	0.15	0.13	0.12	0.12	0.25	0.12	0.24	9.53	12.85	5.30
Fe ₂ O _{3t}	27.21	33.74	28.21	30.90	33.92	28.36	25.57	31.69	18.47	23.71	22.87
MgO	0.13	0.11	0.11	0.08	0.10	0.07	0.09	0.12	0.66	0.29	0.14
CaO	0.08	0.05	0.06	0.05	0.05	0.07	0.06	0.07	0.08	0.21	0.07
Na ₂ O	0.02	0.11	0.08	0.06	0.05	0.02	0.04	0.05	0.03	0.02	0.02
K ₂ O	0.07	0.01	0.01	0.04	0.01	0.01	0.04	0.05	0.01	0.01	0.01
MnO	0.01	0.02	0.01	0.02	0.03	0.02	0.03	0.05	0.02	0.03	0.02
P ₂ O ₅	0.07	0.06	0.17	0.06	0.14	0.06	0.07	0.10	0.04	0.04	0.04
TiO ₂	4.96	3.44	2.07	3.94	5.46	4.51	4.35	5.07	2.45	4.17	3.50
La (ppm)	75.00	70.00	245.00	17.00	158.00	19.00	57.00	124.00	179.00	73.00	75.00
Ce	178.00	190.00	256.00	57.00	233.00	74.00	53.00	212.00	414.00	819.00	236.00
Pr	10.80	14.90	39.80	3.40	22.50	3.80	5.10	15.00	43.60	20.00	18.60
Nd	34.10	57.20	137.20	13.60	70.00	18.30	15.00	39.70	160.90	68.50	65.40
Sm	9.90	12.70	27.10	5.80	17.70	6.60	2.90	6.00	31.80	13.90	14.50
Eu	2.14	2.22	4.12	1.34	3.97	1.34	0.66	1.40	4.90	2.11	2.13
Gd	9.62	11.26	26.74	8.04	18.89	7.53	4.10	6.47	25.78	7.93	11.94
Tb	2.17	2.22	4.39	2.09	3.92	2.00	1.42	1.94	4.68	1.92	2.85
Dy	13.50	13.50	23.70	14.30	24.10	13.50	13.80	14.50	27.20	11.30	18.70
Ho	2.61	2.67	4.46	2.98	4.88	2.87	3.68	3.35	5.67	2.00	3.76
Er	7.93	8.12	12.97	9.43	14.20	8.93	12.77	10.14	17.70	5.74	11.77
Tm	1.38	1.53	2.18	1.96	2.68	1.67	2.36	1.89	3.28	1.11	2.24
Yb	8.90	10.10	13.50	13.10	17.30	11.90	14.20	12.00	20.20	7.60	14.60
Lu	1.28	1.48	2.02	1.94	2.48	1.64	2.20	1.72	2.94	1.12	2.20
ΣREE	357.33	397.90	799.18	151.98	593.62	173.08	188.19	450.11	941.65	1035.23	479.69
ΣLREE	309.94	347.02	709.22	98.14	505.17	123.04	133.66	398.10	834.20	996.51	411.63
ΣHREE	47.39	50.88	89.96	53.84	88.45	50.04	54.53	52.01	107.45	38.72	68.06
ΣLREE/ΣHREE	6.54	6.82	7.88	1.82	5.71	2.46	2.45	7.65	7.76	25.74	6.05

In Table 23 it is noticed that Al_2O_3 values range from 38.13 wt.% to 57.42 wt.% with an average value of 47.69 wt.%, Fe_2O_3t ranges between 22.86 wt.% and 33.92 wt.% with an average of 27.70 wt.% and TiO_2 ranges between 2.07 wt.% and 5.46 wt.% with an average of 3.99 wt.%. The values of the total rare earth elements (ΣREE) range from 151.98 ppm to 1035.23 ppm with an average value of 506.18 ppm. The minimum value of the total light rare earth elements ($\Sigma LREE$) is 98.14 ppm, while the maximum value is 996.51 ppm with an average value of 442.42 ppm. As for the total heavy rare earth elements ($\Sigma HREE$), the values are between 38.72 ppm and 107.45 ppm, with an average of 63.76 ppm.

Table 24: Correlation between major elements and rare earth elements (REE), Longhe, China.

	SiO ₂	Al ₂ O ₃	Fe ₂ O _{3t}	MgO	CaO	Na ₂ O	K ₂ O	MnO	P ₂ O ₅	TiO ₂
La	0.60	-0.36	-0.11	0.36	-0.10	0.26	-0.28	-0.07	0.68	-0.46
Ce	0.36	0.13	-0.44	0.56	0.90	-0.25	-0.37	0.13	-0.20	-0.18
Pr	0.68	-0.11	-0.41	0.67	0.11	0.13	-0.47	-0.20	0.33	-0.66
Nd	0.69	-0.06	-0.45	0.71	0.10	0.13	-0.52	-0.27	0.25	-0.72
Sm	0.68	-0.08	-0.42	0.68	0.06	0.11	-0.54	-0.38	0.25	-0.69
Eu	0.54	-0.17	-0.24	0.60	-0.04	0.14	-0.48	-0.32	0.38	-0.50
Gd	0.63	-0.20	-0.23	0.50	-0.17	0.23	-0.48	-0.42	0.47	-0.64
Tb	0.52	-0.13	-0.24	0.52	-0.20	0.14	-0.49	-0.34	0.44	-0.55
Dy	0.35	-0.03	-0.25	0.50	-0.32	0.08	-0.43	-0.21	0.43	-0.47
Ho	0.15	0.11	-0.26	0.48	-0.43	0.04	-0.32	-0.05	0.38	-0.37
Er	0.07	0.22	-0.33	0.48	-0.46	0.00	-0.26	-0.03	0.28	-0.37
Tm	-0.04	0.30	-0.31	0.49	-0.46	-0.02	-0.27	0.02	0.19	-0.32
Yb	-0.09	0.31	-0.28	0.46	-0.47	-0.04	-0.32	0.01	0.17	-0.29
Lu	-0.06	0.32	-0.31	0.45	-0.47	-0.02	-0.31	0.00	0.16	-0.33
ΣREE	0.57	0.00	-0.46	0.68	0.61	-0.08	-0.47	0.00	0.10	-0.43
$\Sigma LREE$	0.57	-0.01	-0.46	0.67	0.65	-0.09	-0.46	0.01	0.08	-0.41
$\Sigma HREE$	0.34	0.02	-0.28	0.53	-0.35	0.10	-0.43	-0.22	0.39	-0.51

In Table 24 the values of the correlation coefficients between the major elements and the rare earth elements of Longhe region, Western China are displayed. It is obvious that there is a highly positive correlation between Ce and CaO, though there is a highly negative correlation between Nd and TiO_2 .



7.3.2 Tianyang

As presented in Table 25, in the Tianyang bauxite deposit Al_2O_3 ranges from 27.17 wt.% to 75.94 wt.% with an average value of 55.05 wt.%, Fe_2O_3 from 1.47 wt.% to 42.42 wt.% with an average of 18.04 wt.%, while SiO_2 has a value range between 0.29 wt.% and 19.77 wt.%, with an average of 7.88 wt.% and TiO_2 has a minimum value of 2.76 wt.% and a maximum value of 6.86 wt.%, with an average value of 4.65 wt.%. The total concentration of the rare earth elements (ΣREE) ranges between 100.59 ppm and 4491.46 ppm and an average value of 702.57 ppm. The total of the light rare earth elements (ΣLREE) varies between 90.86 ppm and 3901.3 ppm, with an average of 607.99 ppm, while the total of the heavy rare earth elements (ΣHREE) varies between 9.73 ppm and 590.16 ppm with an average value of 94.59 ppm.

Table 25: Major (wt.%) and rare earth elements (ppm) concentrations of analyzed samples of Tianyang, China (Liu *et al.*, 2016).

Element	TQ-1	TQ-2	TQ-3	TQ-4	TQ-5	TQ-6	TQ-7	TQ-8	TQ-9	TQ-10	TQ-11	TQ-12	TQ-13	TQ-14	TQ-15	TQ-16	TQ-17	TP-1	TP-2	TP-3	TP-4
SiO ₂ (%)	1.16	1.33	12.82	6.81	9.09	2.11	5.44	11.16	15.7	0.95	6.36	6.12	13.85	1.44	0.29	7.77	12.78	19.77	12.98	11	6.63
Al ₂ O ₃	71.86	73.98	62.74	50.56	46.72	75.94	64.32	43.54	46.79	75.76	45.69	54.13	49.27	75.75	75.33	42.25	27.15	34.12	38.3	42.71	59.05
Fe ₂ O ₃ t	8.34	4.22	5.07	23.59	25.23	1.97	9.18	27.74	19.01	2.74	32.97	18.88	18.70	1.47	2.20	32.36	42.42	30.47	31.01	25.69	15.51
MgO	0	0	0.32	0	0	0	0	0.32	0	0	0	0	0	0	0	0.13	0	1.1	0.7	0.56	0.8
CaO	0	0	0.24	0.03	0	0	0	0	0	0	0	0	0	0	0	0	0.08	0.05	0	0.01	0
Na ₂ O	0.13	0	0.68	0	0	0.03	0.09	0	0.15	0	0	0	0	0.01	0	0	0.26	0.66	0.14	1.1	0
K ₂ O	0.04	0.01	0.5	0.01	0.02	0.06	0.27	0.01	0.02	0	0	0	0	0.03	0.01	0	1.33	0.79	0.01	0.04	0.01
MnO	0	0	0.36	0.11	0	0	0.03	0.02	0.01	0	0	0	0.01	0	0	0.02	0.01	0.06	0.04	0.04	0.02
P ₂ O ₅	0.04	0.05	0.08	0.15	0.05	0.15	0.05	0.05	0.06	0.03	0.02	0.08	0.16	0.07	0.07	0.08	0.11	0.02	0.04	0.06	0.03
TiO ₂	3.76	4.73	2.76	4.41	4.14	4.71	6.86	4.77	5.76	5.74	3.76	6.05	4.6	4.55	5.53	4.13	4.96	4.18	3.86	4.17	4.21
La (ppm)	22	51	141	87	79	262	54	124	114	23	18	393	42	20	16	36	92	157	299	1006	52
Ce	67	143	563	316	204	90	243	218	270	84	60	223	126	122	89	244	155	446	940	1035	148
Pr	4.7	11	19	15.7	13.9	21.2	11.2	17	12.9	2.8	2.7	38.7	6.5	5.5	3.5	9.3	22.2	47	106.9	321.9	10.8
Nd	17	36	62	49	47	70	37	41	33	8	8	86	23	23	15	35	85	181	420	1254	35
Sm	4	7.9	11.2	10.1	12.1	13.6	9.6	6.8	6	3	1.8	9.9	7.4	6.2	5.9	9.7	20.6	37.5	96.4	244	7.4
Eu	0.79	1.22	2.13	1.84	2.02	3.09	2.14	1.4	1.19	0.81	0.36	1.64	1.73	1.19	1.47	2.19	3.95	6.66	15.77	40.4	1.21
Gd	4.5	6.97	14.17	8.56	11.02	35.02	9.88	8.13	5.67	5.03	1.86	10.37	7.95	5.73	6.1	9.26	17.85	32.03	79.01	187	7.47
Tb	1.23	1.65	2.49	1.54	2.17	10.81	2.27	2.7	0.94	1.49	0.41	2.54	1.77	1.21	1.46	1.99	3.31	5.34	14.09	32.15	1.67
Dy	9.9	11.8	18.4	9.7	13.4	97.5	15.6	22.4	5.9	12.2	2.7	19.8	12.5	8	11.2	13.3	17.7	27.8	74.7	174.9	11.7
Ho	2.19	2.39	4.19	1.81	2.55	23.6	3.03	4.36	1.12	2.67	0.53	4.29	2.52	1.53	2.35	2.64	2.96	4.59	12.17	29.61	2.46
Er	6.81	7.27	12.65	4.88	7.29	64.72	8.72	12.96	3.34	8.03	1.58	12.38	7.5	4.48	7.22	7.79	7.48	11.65	31.48	77.1	7.37
Tm	1.32	1.44	2.22	0.78	1.34	9.05	1.62	2.53	0.63	1.49	0.31	2.05	1.45	0.85	1.38	1.52	1.22	1.76	5.39	11.88	1.38
Yb	8.7	9.57	13.28	4.68	8.54	43.79	10.55	16.98	4.36	9.39	2.04	12.13	9.48	5.79	9.19	9.99	7.24	9.98	33.66	67.78	8.84
Lu	1.27	1.45	2	0.63	1.26	6.43	1.53	2.48	0.64	1.34	0.3	1.78	1.42	0.85	1.34	1.5	1.03	1.36	4.91	9.74	1.32
ΣREE	151.41	292.66	867.73	512.22	405.59	750.81	410.14	480.74	459.69	163.25	100.59	817.58	251.22	206.33	171.11	384.18	437.54	969.67	2133.48	4491.46	296.62
ΣLREE	115.49	250.12	798.33	479.64	358.02	459.89	356.94	408.2	437.09	121.61	90.86	752.24	206.63	177.89	130.87	336.19	378.75	875.16	1878.07	3901.3	254.41
ΣHREE	35.92	42.54	69.4	32.58	47.57	290.92	53.2	72.54	22.6	41.64	9.73	65.34	44.59	28.44	40.24	47.99	58.79	94.51	255.41	590.16	42.21
ΣLREE/ΣHREE	3.22	5.72	11.16	13.93	7.22	1.56	6.45	5.52	18.37	2.86	9	11.23	4.46	6	3.14	6.7	6.04	8.65	6.93	6.19	5.86

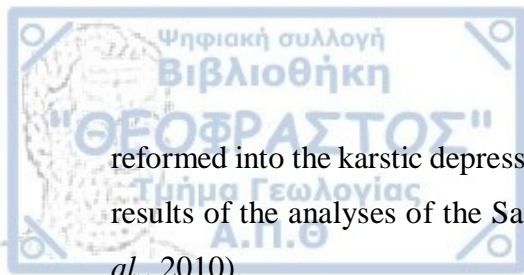
Table 26: Correlation between major elements and rare earth elements (REE), Tianyang, China.

	SiO ₂	Al ₂ O ₃	Fe ₂ O _{3t}	MgO	CaO	Na ₂ O	K ₂ O	MnO	P ₂ O ₅	TiO ₂
La	0.24	-0.27	0.19	0.34	0.01	0.71	-0.04	0.07	0.03	-0.07
Ce	0.51	-0.43	0.31	0.60	0.26	0.74	0.06	0.39	-0.13	-0.32
Pr	0.27	-0.32	0.25	0.43	-0.02	0.76	-0.02	0.05	-0.09	-0.17
Nd	0.27	-0.31	0.25	0.43	-0.02	0.76	-0.01	0.05	-0.09	-0.18
Sm	0.28	-0.33	0.27	0.45	-0.02	0.75	-0.01	0.04	-0.10	-0.20
Eu	0.28	-0.33	0.27	0.45	-0.02	0.76	0.00	0.04	-0.08	-0.19
Gd	0.26	-0.29	0.23	0.45	-0.02	0.75	0.00	0.05	-0.05	-0.20
Tb	0.21	-0.24	0.19	0.42	-0.04	0.71	-0.03	0.02	0.01	-0.18
Dy	0.14	-0.15	0.10	0.36	-0.05	0.64	-0.05	0.01	0.10	-0.16
Ho	0.06	-0.05	0.01	0.29	-0.05	0.56	-0.07	0.00	0.19	-0.14
Er	0.04	-0.02	-0.02	0.27	-0.05	0.55	-0.08	0.01	0.20	-0.13
Tm	0.06	-0.04	0.00	0.29	-0.05	0.56	-0.10	0.02	0.16	-0.14
Yb	0.08	-0.08	0.03	0.33	-0.05	0.58	-0.12	0.02	0.11	-0.15
Lu	0.08	-0.07	0.02	0.32	-0.05	0.58	-0.12	0.03	0.12	-0.15
ΣREE	0.33	-0.33	0.25	0.48	0.06	0.77	-0.01	0.15	-0.06	-0.20
ΣLREE	0.35	-0.36	0.27	0.49	0.08	0.78	0.00	0.16	-0.08	-0.21
ΣHREE	0.16	-0.17	0.11	0.37	-0.04	0.66	-0.05	0.02	0.07	-0.17

In the table of correlations (Table 26) between the major elements and the rare earth elements (REE) of the Tianyang region, it is noticed that there is a highly positive correlation between Na₂O and the majority of the rare earth elements (REE), while the rest present a medium positive correlation. Ce presents a medium positive correlation with the major elements SiO₂ and MgO.

7.3.3 Western Guangxi

Other bauxite deposits in western Guangxi, China, that have been studied are the Dajia Salento-type bauxite deposits, located approximately 75 km southeast of Napo County. The Salento-type bauxite deposit lies dispersedly within Quaternary ferrallitic soils in karstic depressions, according to Bardossy, 1982, Liu et al.,2008. Similarly, to the Longhe and Tianyang regions mentioned above, when the bauxite deposits were exposed to the surface and under different conditions, such as oxidation, erosion and re-sedimentation, the bauxite was



reformed into the karstic depressions and the Salento-type bauxite orebodies were created. The results of the analyses of the Salento-type bauxite samples, are displayed in Table 27 (Liu *et al.*, 2010).

Table 27: Major (wt.%) and rare earth elements (ppm) concentrations of analyzed samples of Western Guangxi, China (Liu *et al.*, 2010) - *continued*.

Element	DJ1130-1	DJ1130-2	DJ1130-3	DJ103024-1	DJ103024-2	DJ1127-1	DJ1127-2	DJ1127-3	DJ222046-1	DJ222046-2	0818-1	0817-1	0817-2	DJ110-1
SiO ₂ (%)	2.22	3.84	2.27	16.48	4.25	2.07	2.59	1.38	1.83	11.06	4.22	11.76	11.58	7.24
Al ₂ O ₃	56.37	51.97	51.57	52.45	58.13	55.58	64.41	54.17	27.13	32.82	68.16	55.47	55.22	41.37
Fe ₂ O _{3t}	23.02	27.84	26.81	13.63	20.74	25.37	13.04	28.52	54.86	35.76	10.58	17.04	16.78	33.06
MgO	0.07	0.08	0.08	0.08	0.06	0.07	0.08	0.06	0.13	0.15	0.09	0.11	0.09	0.26
CaO	0.19	0.112	0.091	0.082	0.082	0.051	0.05	0.072	0.066	0.149	0.062	0.074	0.074	0.063
Na ₂ O	0.022	0.021	0.021	0.022	0.035	0.021	0.02	0.021	0.022	0.051	0.187	0.126	0.067	0.056
K ₂ O	0.01	0.01	0.01	0.01	0.01	0.01	0.01	0.011	0.011	0.2	0.026	0.028	0.013	0.021
MnO	0.017	0.025	0.018	0.017	0.036	0.022	0.021	0.016	0.023	0.026	0.018	0.011	0.015	0.02
P ₂ O ₅	0.04	0.04	0.06	0.04	0.05	0.04	0.05	0.03	0.16	0.16	0.04	0.03	0.03	0.12
TiO ₂	3.53	3.31	3.53	3.26	4.37	3.47	4.5	3.93	3.33	4.19	2.87	1.77	2.6	2.79
La (ppm)	35	35	103	106	39	26	49	15	165	171	62	25	35	802
Ce	192	151	58	85	87	100	181	48	589	380	64	105	65	574
Pr	7.3	5.9	10.6	7.9	5.1	3.9	7.1	1.9	37.9	36	11.1	4.2	6.4	110.7
Nd	24.6	18.8	32.2	21.7	14.5	14.1	27.6	6.1	144.4	109.3	36.5	14.7	21.1	359.4
Sm	6.7	6.1	6.7	3.9	3	5.3	8.9	2.1	29.8	14.5	7.6	4	5.7	59.7
Eu	1.12	1.14	1.42	0.84	0.62	0.98	1.5	0.51	6.16	2.48	1.49	0.87	1.14	10.81
Gd	6.04	5.77	12.96	7.66	4.06	5.59	8.78	2.8	25.92	14.55	9.44	4.12	6.1	64.74
Tb	1.68	1.88	4.81	2.63	1.4	1.72	2.28	1.1	5.19	3.07	3.27	1.17	2	11.31
Dy	11.1	13.8	39.1	21.9	11	12.4	14.4	9.1	30	18.4	31.3	6.5	15.9	59.7
Ho	2.07	2.88	9.02	5.3	2.37	2.66	2.79	1.97	5.58	3.5	8.41	1.23	3.6	10.67
Er	6.71	9.39	29.05	17.18	7.61	8.35	8.95	6.45	16.48	9.98	33.72	3.93	12.29	29.17
Tm	1.37	1.96	5.4	3.17	1.52	1.73	1.86	1.36	2.93	1.84	7.9	0.66	2.69	5.19
Yb	9	14.1	33.8	20	10.1	11.6	13.1	9.6	18.8	11.1	55.8	4.9	19.5	32
Lu	1.22	2.09	5.3	3.05	1.56	1.69	2.01	1.37	2.73	1.67	8.41	0.74	2.88	4.98
ΣREE	306.08	270.18	351.11	306.13	189.21	196.59	328.74	106.97	1079.43	776.67	341.07	176.78	199.35	2134.37
ΣLREE	266.72	217.94	211.92	225.34	149.22	150.28	275.1	73.61	972.26	713.28	182.69	153.77	134.34	1916.61
ΣHREE	39.19	51.87	139.44	80.89	39.62	45.74	54.17	33.75	107.63	64.11	158.25	23.25	64.96	217.76
ΣLREE/ΣHREE	6.78	4.18	1.51	2.78	3.75	3.26	5.05	2.17	8.98	11.09	1.15	6.58	2.05	8.75

Table 28: Major (wt.%) and rare earth elements (ppm) concentrations of analyzed samples of Western Guangxi, China (Liu *et al.*, 2010) - *continued.*

Element	DJ110-2	DJ110-3	23(S)	23(N)	25	21	19	20	26	38	DJC-4	DJC-5	MYC-02
SiO ₂ (%)	4.04	5.85	28.09	5.51	5.27	4.27	9.94	3.52	10.89	2.39	0.2	0.22	0.21
Al ₂ O ₃	61.75	57.83	51.14	57.12	59.94	63.78	49.84	61.33	51.25	59	0.05	0.05	0.13
Fe ₂ O _{3t}	14.21	18.48	3.16	17.50	13.64	12.35	22.38	16.89	21.00	19.61	0.14	0.17	0.15
MgO	0.08	0.09	0.07	0.11	0.07	0.11	0.19	0.09	0.15	0.08	0.24	0.24	0.37
CaO	0.054	0.052	0.073	0.072	0.062	0.173	0.063	0.083	0.052	0.052	56.244	55.939	56.431
Na ₂ O	0.058	0.045	0.025	0.049	0.037	0.037	0.051	0.057	0.061	0.196	0.02	0.055	0.096
K ₂ O	0.012	0.01	0.01	0.029	0.01	0.01	0.056	0.015	0.04	0.02	0.012	0.016	0.015
MnO	0.016	0.015	0.025	0.022	0.021	0.012	0.019	0.02	0.026	0.015	0	0.001	0.003
P ₂ O ₅	0.03	0.03	0.05	0.08	0.08	0.17	0.05	0.2	0.05	0.07	0	0	0
TiO ₂	3.59	3.26	2.55	3.56	3.62	2.51	3.47	2.34	3.5	2.97	0.01	0	0
La (ppm)	15	18	64	42	41	38	59	161	16	61	1	1	5
Ce	57	73	214	126	82	61	96	274	66	72	2	2	3
Pr	2.9	2.8	9.1	7.4	5.1	7	8.8	20.1	2.6	6.3	0.2	0.2	0.9
Nd	10.7	9.9	24.4	26.7	14.7	24.5	30.5	52.8	12.6	18.3	0.8	0.8	3.6
Sm	5.2	3.8	5.2	9.4	5.2	6.4	6.8	8.2	5	3.6	0.2	0.2	0.5
Eu	1.19	0.79	0.9	1.75	1.18	1.33	1.2	1.62	0.98	0.77	0.04	0.03	0.12
Gd	6.81	4.54	4.49	9.3	7.66	8.49	8.21	8.8	5.82	5.12	0.26	0.2	0.64
Tb	1.93	1.29	1.34	2.32	2.77	2.6	2.14	2.48	1.62	1.79	0.05	0.04	0.1
Dy	13.6	9	9.2	14.8	22.1	23.7	15	18.5	11	16.5	0.3	0.3	0.6
Ho	2.83	1.98	1.94	3.04	5.11	6.21	3.5	4.43	2.21	3.86	0.07	0.06	0.13
Er	8.96	6.13	6.51	9.42	18.1	22.3	11.23	15.47	7.06	13.82	0.21	0.17	0.67
Tm	1.87	1.17	1.34	1.89	3.67	4.4	2.13	3.12	1.4	2.66	0.04	0.02	0.06
Yb	12.3	7.7	9.5	12.3	25.9	28.1	12.9	20.2	9.5	17.4	0.2	0.2	0.4
Lu	1.87	1.16	1.4	1.81	3.94	4.49	1.85	3.1	1.33	2.64	0.03	0.03	0.06
ΣREE	141.88	141.15	352.86	268.38	238.93	239.4	259.08	593.75	143.34	225.55	4.84	4.96	16.21
ΣLREE	91.99	108.29	317.6	213.25	149.18	138.23	202.3	517.72	103.18	161.97	4.24	4.23	13.12
ΣHREE	50.17	32.97	35.72	54.88	89.25	100.29	56.96	76.1	39.94	63.79	1.16	1.02	2.66
ΣLREE/ΣHREE	1.81	3.26	8.87	3.85	1.66	1.37	3.53	6.78	2.56	2.53	3.62	4.12	4.89

The major elements of the ferrallitic samples of Western Guangxi region presented in Table 28, demonstrate a wide range in value. Al_2O_3 ranges from 27.13 wt.% to 68.16 wt.%, with an average value of 54.08 wt.%, SiO_2 ranges from 1.38 wt.% to 28.09 wt.% with average of 6.77 wt.%, Fe_2O_3t varies from 3.16 wt.% to 54.86 wt.% with an average of 21.10 wt.% and TiO_2 ranges from 1.77 wt.% to 4.5 wt.% with an average value of 3.28 wt.%.

Table 29: Correlation between major elements and rare earth elements (REE), Western Guangxi, China.

	SiO_2	Al_2O_3	Fe_2O_3t	MgO	CaO	Na_2O	K_2O	MnO	P_2O_5	TiO_2
La	0.04	-0.44	0.37	0.75	-0.04	-0.01	0.12	0.07	0.41	-0.16
Ce	0.02	-0.75	0.67	0.59	0.09	-0.18	0.27	0.26	0.62	-0.04
Pr	0.01	-0.55	0.48	0.78	0.00	-0.02	0.21	0.11	0.48	-0.12
Nd	-0.01	-0.58	0.52	0.79	-0.01	-0.03	0.19	0.10	0.47	-0.11
Sm	-0.06	-0.57	0.54	0.77	-0.05	-0.06	0.10	0.09	0.44	-0.10
Eu	-0.08	-0.58	0.56	0.76	-0.07	-0.06	0.07	0.08	0.46	-0.11
Gd	-0.06	-0.51	0.48	0.78	-0.06	-0.05	0.08	0.06	0.41	-0.10
Tb	-0.10	-0.45	0.45	0.71	-0.05	-0.03	0.04	0.02	0.41	-0.10
Dy	-0.16	-0.31	0.34	0.57	-0.02	0.06	-0.01	-0.05	0.41	-0.13
Ho	-0.18	-0.14	0.20	0.44	0.01	0.15	-0.05	-0.13	0.38	-0.17
Er	-0.19	0.02	0.06	0.29	0.02	0.26	-0.09	-0.17	0.34	-0.21
Tm	-0.20	0.13	-0.03	0.20	0.01	0.34	-0.10	-0.18	0.27	-0.21
Yb	-0.20	0.18	-0.07	0.15	-0.02	0.38	-0.12	-0.17	0.22	-0.22
Lu	-0.20	0.19	-0.08	0.15	-0.01	0.37	-0.12	-0.18	0.23	-0.22
ΣREE	0.00	-0.60	0.53	0.74	0.01	-0.06	0.18	0.13	0.53	-0.12
ΣLREE	0.02	-0.62	0.54	0.74	0.01	-0.08	0.20	0.15	0.53	-0.11
ΣHREE	-0.17	-0.19	0.24	0.52	-0.02	0.17	-0.03	-0.09	0.39	-0.18

In the table of correlations (Table 29) from the samples of the ferrallitic soils of the Dajia Salento-type bauxite deposits, western Guangxi, China, the majority of the rare earth elements (REE) demonstrate a medium to highly positive correlation with MgO , Ce demonstrates a medium to highly positive correlation with Fe_2O_3t and P_2O_5 , while having a highly negative correlation with Al_2O_3 . In fact, all light rare earth elements (LREE) show at least a medium negative correlation with Al_2O_3 .

7.3.4 Henan

Another karstic bauxite deposit that has been examined is the one in western Henan, located in the North China Block and north of the North Qinling orogenic belt. The bauxite deposit, in this case, lies between ferric clay consisting, mainly, of diaspore, illite and anatase, and top clay consisting, mainly, of illite, hematite and goethite. These three layers, the ferric clay, the bauxite ore and the top clay, compose the lower part of the Benxi Formation, which was covered by a coal-bearing formation and carbonate rocks. As mentioned before, in the previous regions in China, due to tectonic movements during the Mesozoic and Cenozoic era, the bauxite deposits were uplifted and exposed to the surface (Liu *et al.*, 2013).

Table 30: Major (wt.%) and rare earth elements (ppm) concentrations of analyzed samples of Henan, China (Liu *et al.*, 2013).

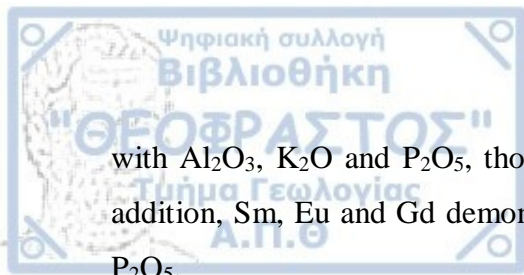
Element	G1	G2	G3	G4	G5	G6	G7	G8	G9	G10	G11
SiO ₂ (%)	7.83	7.97	7.37	7.92	7.27	6.84	29.51	25.45	33.55	12.85	2.61
Al ₂ O ₃	1.99	1.67	0.72	1.29	0.78	0.40	31.90	31.30	34.97	62.61	78.07
Fe ₂ O _{3t}	7.69	5.26	1.80	1.84	10.74	11.25	25.02	28.63	17.14	5.08	0.86
MgO	0.760	1.260	0.240	0.270	0.380	0.560	0.700	0.540	0.540	0.000	0.000
CaO	44.830	46.040	49.660	48.570	48.400	48.140	0.390	0.250	0.240	0.030	0.000
Na ₂ O	0.05	0.03	0.02	0.02	0.02	0.02	0.06	0.05	0.08	0.28	0.11
K ₂ O	0.21	0.35	0.21	0.30	0.18	0.13	5.96	5.31	6.32	2.89	0.30
MnO	0.201	0.093	0.087	0.259	0.814	0.377	0.004	0.007	0.001	0.000	0.000
P ₂ O ₅	0.02	0.04	0.01	0.02	0.02	0.02	0.26	0.16	0.20	0.26	0.15
TiO ₂	0.03	0.07	0.02	0.06	0.04	0.03	1.09	0.93	1.19	4.03	3.43
La (ppm)	2.64	5.18	1.81	3.92	3.01	1.96	161.54	137.56	185.81	381.08	127.92
Ce	5.46	11.69	3.22	5.96	5.99	3.20	265.10	309.54	510.51	366.65	303.21
Pr	0.74	1.52	0.39	0.87	1.04	0.50	34.36	30.60	42.39	76.32	25.17
Nd	4.07	7.29	1.55	3.58	5.54	2.67	134.65	118.83	163.18	242.34	82.78
Sm	2.13	2.24	0.37	0.93	1.90	1.03	26.08	25.41	41.84	33.31	12.20
Eu	0.68	0.57	0.10	0.29	0.54	0.38	5.56	5.08	8.45	5.56	2.04
Gd	4.91	3.44	0.65	2.17	3.97	3.42	24.06	22.75	37.37	22.51	9.39
Tb	1.22	0.70	0.13	0.45	0.79	0.80	2.65	3.18	5.25	3.46	1.61
Dy	8.60	4.45	0.78	3.15	5.44	6.02	10.67	17.23	27.92	16.69	8.91
Ho	1.89	0.88	0.15	0.67	1.30	1.42	1.71	3.14	4.89	3.05	1.81
Er	5.10	2.30	0.38	1.76	3.69	3.82	4.54	8.16	12.34	8.99	5.44
Tm	0.85	0.35	0.06	0.27	0.56	0.58	0.73	1.32	1.97	1.47	0.92
Yb	4.92	2.04	0.34	1.34	3.00	3.14	4.75	8.15	12.26	10.17	6.35
Lu	0.79	0.33	0.06	0.23	0.52	0.51	0.74	1.31	1.96	1.58	1.01
ΣREE	44	42.99	9.99	25.57	37.29	29.44	677.16	692.27	1056.14	1173.17	588.76
ΣLREE	15.04	27.92	7.33	15.26	17.48	9.36	621.74	621.94	943.73	1105.26	553.32
ΣHREE	28.28	14.49	2.56	10.03	19.28	19.70	49.86	65.24	103.96	67.92	35.44
ΣLREE/ΣHREE	0.53	1.93	2.86	1.52	0.91	0.48	12.47	9.53	9.08	16.27	15.62

The major elements of the samples of Henan region, China, demonstrate as well as the previous ones, a wide range in value (Table 30). Specifically, Al_2O_3 ranges from 0.40 wt.% to 78.07 wt.% with an average value of 22.34 wt.%. SiO_2 ranges between 2.61 wt.% and 33.55 wt.%, with an average of 13.56 wt.%, while Fe_2O_{3t} ranges between 0.86 wt.% and 28.63 wt.% with an average of 10.48 wt.%. TiO_2 varies between 0.02 wt.% and 4.03 wt.% with an average value of 0.99 wt.%.

Table 31: Correlation between major elements and rare earth elements (REE), Henan, China.

	SiO_2	Al_2O_3	Fe_2O_{3t}	MgO	CaO	Na_2O	K_2O	MnO	P_2O_5	TiO_2
La	0.47	0.80	0.24	-0.24	-0.84	0.91	0.62	-0.54	0.91	0.86
Ce	0.71	0.81	0.44	-0.26	-0.95	0.61	0.81	-0.60	0.89	0.70
Pr	0.53	0.79	0.29	-0.24	-0.86	0.89	0.67	-0.55	0.92	0.83
Nd	0.62	0.78	0.38	-0.25	-0.89	0.83	0.75	-0.57	0.95	0.79
Sm	0.82	0.66	0.55	-0.24	-0.89	0.61	0.90	-0.56	0.91	0.60
Eu	0.88	0.60	0.62	-0.24	-0.87	0.51	0.94	-0.54	0.89	0.50
Gd	0.89	0.57	0.65	-0.24	-0.86	0.47	0.94	-0.52	0.87	0.46
Tb	0.83	0.59	0.57	-0.24	-0.84	0.53	0.88	-0.50	0.83	0.51
Dy	0.78	0.54	0.54	-0.23	-0.77	0.48	0.82	-0.43	0.73	0.45
Ho	0.71	0.53	0.51	-0.25	-0.74	0.48	0.75	-0.37	0.68	0.45
Er	0.66	0.59	0.47	-0.27	-0.77	0.56	0.72	-0.37	0.71	0.53
Tm	0.65	0.62	0.46	-0.28	-0.78	0.58	0.72	-0.39	0.72	0.56
Yb	0.63	0.69	0.41	-0.27	-0.82	0.65	0.71	-0.45	0.77	0.64
Lu	0.63	0.68	0.42	-0.28	-0.82	0.64	0.71	-0.43	0.76	0.62
ΣREE	0.66	0.81	0.40	-0.26	-0.93	0.77	0.78	-0.59	0.94	0.78
ΣLREE	0.64	0.82	0.38	-0.26	-0.93	0.78	0.77	-0.59	0.94	0.80
ΣHREE	0.80	0.59	0.57	-0.25	-0.83	0.52	0.86	-0.47	0.81	0.51

In the table of correlations (Table 31) from the samples of the bauxite deposits from Henan, China, the majority of the rare earth elements (REE) demonstrate a medium to highly positive correlation with SiO_2 , Al_2O_3 , TiO_2 and Na_2O , a low to medium positive correlation with Fe_2O_{3t} and a highly positive correlation with K_2O and P_2O_5 , while having a highly negative correlation with CaO . La, Pr and Nd, specifically, show a very highly positive correlation with Al_2O_3 , Na_2O , P_2O_5 and TiO_2 , while Ce shows a very highly positive correlation



with Al_2O_3 , K_2O and P_2O_5 , though having a very highly negative correlation with CaO . In addition, Sm, Eu and Gd demonstrate a very highly positive correlation with SiO_2 , K_2O and P_2O_5 .

7.4 MONTENEGRO

The mineralogy and the geochemistry of the Montenegrin karstic bauxites, as well as the bauxite residue (red mud) have been studied and examined in research of the existence and the economic potential of rare earth elements (REE) and relevant critical metals.

All the karstic bauxites' deposits and occurrences are part of the metallogenetic province of Dinaric. The red karstic bauxites have developed in three different eras, the Middle Triassic, Jurassic and Paleogene, while the white karst bauxites are of Cretaceous age. The Triassic bauxite appears on top of limestones and formations of sediments of volcanic genesis. The Jurassic bauxites belong to a high karst zone that consists of karstified limestones and rare dolomites. The Cretaceous white bauxites were formed on a karst of limestones, dolomitic limestones and dolomites. Paleogene bauxites are found on a paleorelief made of limestones and dolomites (Radusinović and Papadopoulos, 2021).

Table 32: Major (wt.%) and rare earth elements (ppm) concentrations of analyzed samples of Montenegro (Radusinović and Papadopoulos, 2021).

Element	PI-II/1	VM-III/1	VM-III/2	VMP-III&IV/1	VM-III/3	P-IV/1	VMP-III&IV/2	P-IV/2	VMP-III&IV/3	VM-III/4	WMO-V&VII/1	WM-V/1	WMC-V&VI/1	WMC-V&VI/2	BK-VIII/1	U-IX/1
SiO ₂ (%)	6.83	30.42	8.82	11.90	14.12	17.40	19.89	16.22	18.04	25.06	13.28	12.00	22.60	23.70	13.07	9.48
Al ₂ O ₃	62.5	43.18	54.10	51.18	50.28	47.65	43.67	47.91	46.48	41.57	40.97	44.16	43.82	42.28	47.37	48.31
Fe ₂ O ₃	12.85	7.55	19.53	19.44	19.08	18.08	18.20	18.22	18.33	16.73	16.67	22.97	13.32	14.77	19.1	21.49
MgO	0.13	0.24	0.34	0.46	0.35	0.49	0.48	0.97	0.86	0.51	0.46	0.46	0.44	0.39	0.37	0.3
CaO	0.07	0.49	0.33	0.47	1.54	0.15	0.13	0.17	0.15	1.67	7.96	2.36	0.52	0.22	1.11	0.79
Na ₂ O	<0.01	0.03	<0.01	0.05	0.05	0.02	0.07	0.03	0.07	0.09	<0.01	0.03	0.02	0.05	<0.01	<0.01
K ₂ O	0.07	0.14	0.39	0.55	0.52	0.69	0.77	0.66	0.62	0.84	0.27	0.33	0.71	0.47	0.74	0.21
TiO ₂	2.31	1.20	2.63	2.51	1.98	2.21	2.17	2.12	2.03	1.44	1.78	2.01	2.22	2.22	2.77	2.79
P ₂ O ₅	<0.01	0.019	0.049	0.047	0.041	0.045	0.071	0.020	0.028	0.049	0.017	0.02	0.040	0.03	0.060	0.090
MnO	0.07	0.09	0.19	0.17	0.13	0.14	0.13	0.14	0.14	0.08	0.10	0.11	0.01	0.02	0.08	0.09
La (ppm)	54	109	194	199	47	241	283	313	245	71	104	22	57	6	90	108
Ce	311	313	351	365	100	384	355	365	343	111	187	52	124	20	164	226
Pr	10	25	38	39		38	38.23	42	33		19	6	11	2	16	20
Nd	35	97	139	142		137	136	157	123		69	22	36	7	55	67
Sm	8	19	27	26		25	24	26	21		13	5	7	2	10	11
Eu	2	3	6	5		6	5	6	5		3	1	1	0.4	2	2
Gd	9	18	24	25		26	25	27	22		12	4	7	1	8	9
Tb	2	3	4	4		4	4	4	4		2	1	1	0.3	1	2
Dy	12	17	22	23		22	23	26	23		13	5	8	2	8	9
Ho	3	3	5	5		4	5	6	5		3	1	2	0.5	2	2
Er	10	10	13	14		13	14	17	16		8	3	5	2	5	6
Tm	2	1	2	2		2	2	2	2		2	1	1	0.3	1	1
Yb	10	9	13	13		12	13	15	15		8	3	5	2	6	6
Lu	2	1	2	2		2	2	2	2		1	1	1	0.3	1	1
ΣREE	470	628	840	864		916	891	1008	859		444	127	266	44	369	470
ΣLREE	420	566	755	776		831	803	909	770		395	108	236	37	337	434
ΣHREE	50	62	85	88		85	88	99	89		49	19	30	7	32	36
ΣLREE/ ΣHREE	8.40	9.13	8.88	8.82		9.78	9.13	9.18	8.65		8.06	5.68	7.87	5.29	10.53	12.06

The major elements of the samples of karstic bauxites and bauxite residue of Montenegro demonstrate, similarly to the above, a wide range in value (Table 32). Al_2O_3 ranges from 40.97 wt.% to 62.5 wt.% with an average value of 47.21 wt.%. SiO_2 ranges between 6.83 wt.% and 30.42 wt.%, with an average of 16.43 wt.%, while Fe_2O_3 ranges between 7.55 wt.% and 22.97 wt.% with an average of 17.27 wt.%. TiO_2 varies between 1.20 wt.% and 2.79 wt.% with an average value of 2.15 wt.%.

Table 33: Correlation between major elements and rare earth elements (REE), Montenegro.

	SiO_2	Al_2O_3	Fe_2O_3	MgO	CaO	Na_2O	K_2O	MnO	P_2O_5	TiO_2
La	-0.04	0.07	0.20	0.63	-0.27	0.15	0.37	0.68	0.18	0.13
Ce	-0.17	0.42	-0.07	0.24	-0.33	-0.09	-0.01	0.66	0.06	0.14
Pr	-0.04	0.13	0.20	0.49	-0.23	0.28	0.39	0.83	0.24	0.04
Nd	-0.01	0.12	0.17	0.50	-0.23	0.29	0.37	0.84	0.20	-0.01
Sm	-0.02	0.16	0.13	0.42	-0.23	0.26	0.32	0.85	0.16	-0.03
Eu	-0.11	0.21	0.21	0.50	-0.19	0.24	0.35	0.87	0.11	0.02
Gd	0.02	0.16	0.09	0.47	-0.25	0.32	0.35	0.82	0.11	-0.08
Tb	-0.05	0.24	0.11	0.42	-0.26	0.34	0.23	0.85	0.1	-0.08
Dy	-0.01	0.21	0.06	0.50	-0.23	0.33	0.31	0.8	0.03	-0.1
Ho	-0.12	0.28	0.11	0.54	-0.21	0.31	0.32	0.78	0.03	-0.01
Er	-0.06	0.30	0.04	0.53	-0.27	0.36	0.27	0.76	-0.04	-0.09
Tm	-0.41	0.43	0.18	0.34	0.09	0.09	0.13	0.73	-0.1	0.02
Yb	-0.12	0.36	0.06	0.49	-0.25	0.31	0.26	0.77	-0.01	-0.03
Lu	-0.36	0.58	0.20	0.34	-0.33	0.21	0.24	0.75	0.02	0.15
ΣREE	-0.12	0.25	0.06	0.43	-0.29	-0.02	0.14	0.7	0.1	0.17
ΣLREE	-0.12	0.25	0.07	0.43	-0.30	-0.01	0.15	0.7	0.12	0.16
ΣHREE	-0.15	0.25	0.02	0.43	-0.25	-0.10	0.06	0.65	-0.02	0.18

In the table of correlations (Table 33) within major elements and rare earth elements (REE) from the samples of Montenegro it is noticed that there is a highly positive correlation between the majority of the rare earth elements (REE) and MnO, a medium positive correlation between the majority of the rare earth elements (REE) and MgO, a low to medium positive correlation between the majority of the rare earth elements (REE) with K_2O and Na_2O , while there is a low negative correlation with CaO. Furthermore, there is a medium negative correlation between Tm and Lu with SiO_2 .



8 DISCUSSION

The simultaneous extraction and exploitation of bauxites and REE would be financially and environmentally beneficial, both for the mining industry and the planet. Bauxite deposits have proven to be great sources of REE, especially in provinces of China (Liu *et al.*, 2010, 2013, 2016). Therefore, 23 samples from the bauxite mines of Imerys Bauxites S.A., Fokida, Central Greece were analysed to examine the presence, the amount of REE and their exploitability.

Firstly, the study confirmed the presence of rare earth elements (REE) in the bauxite deposits. This indicates a particular potential role, that of financial importance of these elements in the context of bauxite mining.

Secondly, an attempt was made to correlate the colour of the samples with the percentage of pisoliths and the concentration of REE. The analysis showed no clear connection between the colour of the samples (classified as brownish-red, orange-red, and yellow) and the REE concentration or the percentage of pisoliths. Similarly, no clear relation between the size of pisoliths and the REE concentration was found. As a result, it was concluded that colour cannot be used as a reliable factor in sample selection. However, given the limited number of samples used in this study, further research is recommended to explore this potential relationship more comprehensively. Additionally, studies from China that were compared to the present study, have not examined the relationship among the REE and the major elements, the colour, size of pisoliths and the percentage of pisoliths (Liu *et al.*, 2010, 2013, 2016;). However, it is suggested that the evident differentiation of rare earth elements (REE) results from their distinct chemical properties under surface conditions, during the weathering processes (Liu *et al.*, 2013), which is something that has not been examined in this thesis, but it could be an alternative analytical framework to examine potential links of the samples' origin and/or colour with REE content. Radusinović and Papadopoulou (2021) suggest that the Cretaceous white bauxites of the examined deposits in Montenegro indicate low average REE contents, though they are significantly richer in lithium.

Additionally, mineralogical analyses of the collected samples, using X-ray Diffraction (XRD), identified two main major minerals among the samples, creating two clusters. One cluster was dominated by diaspore, while the other cluster had boehmite as the main mineral. Hematite was the second mineral in abundance among the samples, followed by anatase and amorphous material. This distinction could have implications for processing and refining

methods in the future. The study of Liu *et al.* (2013) proposes that goethite absorbs Dy, Ho, Er, Tm, Yb and Lu, which could be a promising source of REE. Our XRD analysis indicated that only two samples (S.6_2, S.6_3) had high concentrations in goethite. These two samples have not different REE concentrations relative to the rest.

The study also investigated major elements in the samples. SiO₂ showed relatively consistent levels across most samples, except for higher values in the Koromilia samples (S.3). In contrast, iron oxide (Fe₂O₃) exhibited a decreasing trend with increasing aluminum oxide (Al₂O₃), although the S.3 samples deviated from this trend. This deviation highlighted the unique characteristics of the S.3 samples, which warranted further examination. It must be stressed here that, Radusinović and Papadopoulos (2021) suggest that low-quality bauxite deposits having a high SiO₂ content are associated with increased values of LREE.

Moreover, when clustering the samples based on major element content, clusters 1, 2, 4, and 5 exhibited higher values in ΣLREE and ΣHREE compared to cluster 3, which did not include any S.3 samples. This relationship suggested a potential link between major element composition and REE concentration.

Trace element analysis further differentiated the S.3 samples, particularly in the case of lithium (Li). One specific sample, S.5_1 (526 mine), stood out with significantly elevated values in most of the trace elements. Consequently, it was recommended to conduct additional research in this specific area to determine if this observation was an anomaly or if higher trace element concentrations actually existed in that part of the mine. Moreover, sample S.5_1 exhibited the highest values in all REEs among all clusters, while S.3 samples showed higher values in lanthanium (La) compared to most other samples.

Gamaletsos *et al.* (2019) concluded that the Fe-rich karst-type bauxites (red) have higher concentration in REE than the Fe-depleted bauxites (white). They contain mainly LREE³⁺ fluorocarbonate minerals (bastnäsite/parasite group), while the Fe-depleted contain, rarely, LREE³⁺ hydroxyphosphate (florencite) and scandian zircons. LREE are also, dispersed everywhere between pisoliths, oolites, cavities and/or into AlOOH matrix. In addition (Gamaletsos *et al.*, 2019) REE content in Greek bauxite is comparable to the globe, the EU, Mediterranean & Iranian bauxites, while is less than the content of Chinese bauxites. It is, also, increased compared to geological reference materials (chondrites, UCC, PAAS, NASC, ES), but reduced compared to other REE active mining sites (eg. Bayan Obo) and bauxite residue (red mud). Finally, Fe-rich bauxites (red) from central Greece have higher content (including Sc+Y), with an average of 569 ppm, comparable to the current thesis samples which show an

average of 400 ppm (including Sc+Y), while the Fe-depleted bauxites (white) have lower REE content (including Sc+Y), with an average value of 268 ppm (Gamaletsos *et al.*, 2019).

A correlation analysis using Pearson's method was conducted to explore potential relationships between numeric variables, including SiO₂, Al₂O₃, Fe₂O₃, TiO₂, CaO, pisoliths_size, pisoliths_percent, and the variables ΣREE, ΣLREE, and ΣHREE. While both positive and negative correlations were observed, none of them reached a statistically significant threshold. To investigate the possibility of correlations between ΣREE, ΣLREE, ΣHREE and two categorical variables, namely colour and region, an ANOVA test was applied. The results of the test indicated that neither region nor colour exhibited statistically significant evidence of a correlation with the REE sums (ΣREE, ΣLREE, and ΣHREE). The yellow bauxite samples, though, seem to lack in REE concentration, which could simply be explained from a geological point of view, as the depleted and deteriorated samples, which were weathered from the roof's water.

The geochemical analysis identified correlations between ΣREE and SiO₂, CaO in samples from Longhe and Henan, with a strong correlation between ΣREE and CaO in Henan samples. High correlations were observed between ΣLREE and SiO₂, CaO in Longhe and Henan samples, as well as between ΣLREE and Al₂O₃ in W. Guangxi and Henan samples. Henan samples also displayed a high correlation with TiO₂. An intensively high correlation was found between ΣHREE, and the five major oxides analyzed in Henan samples. No correlation coefficient between ΣREE, ΣLREE, ΣHREE and the major elements presents similar behavior among the six karst-bauxite deposits tested (Figure 11, Figure 12, Figure 13).

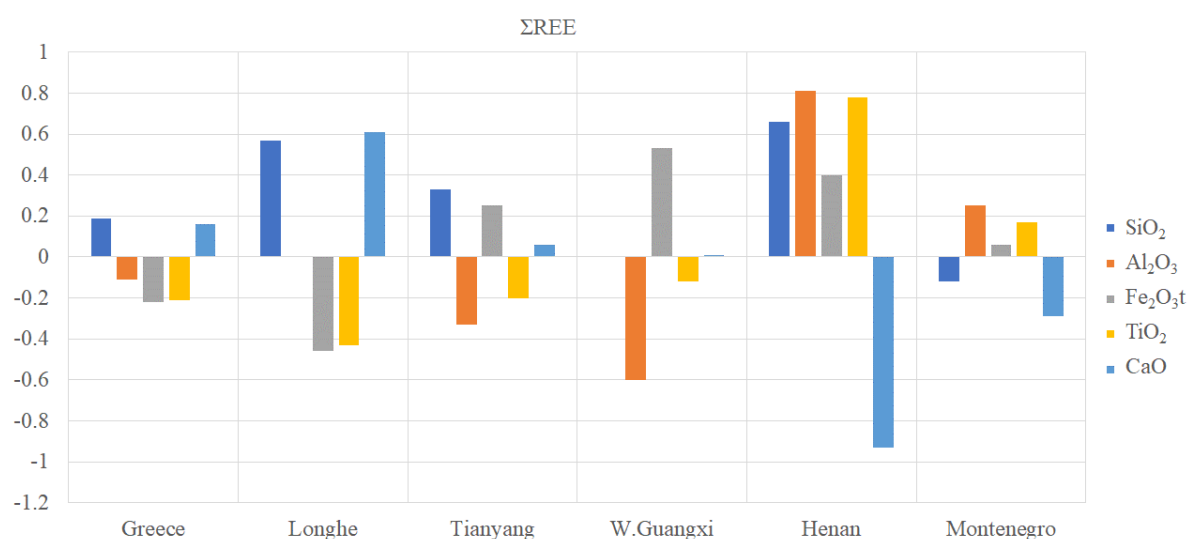


Figure 11: Bar graph of the major elements and the total rare earth elements (ΣREE) for every area of study.

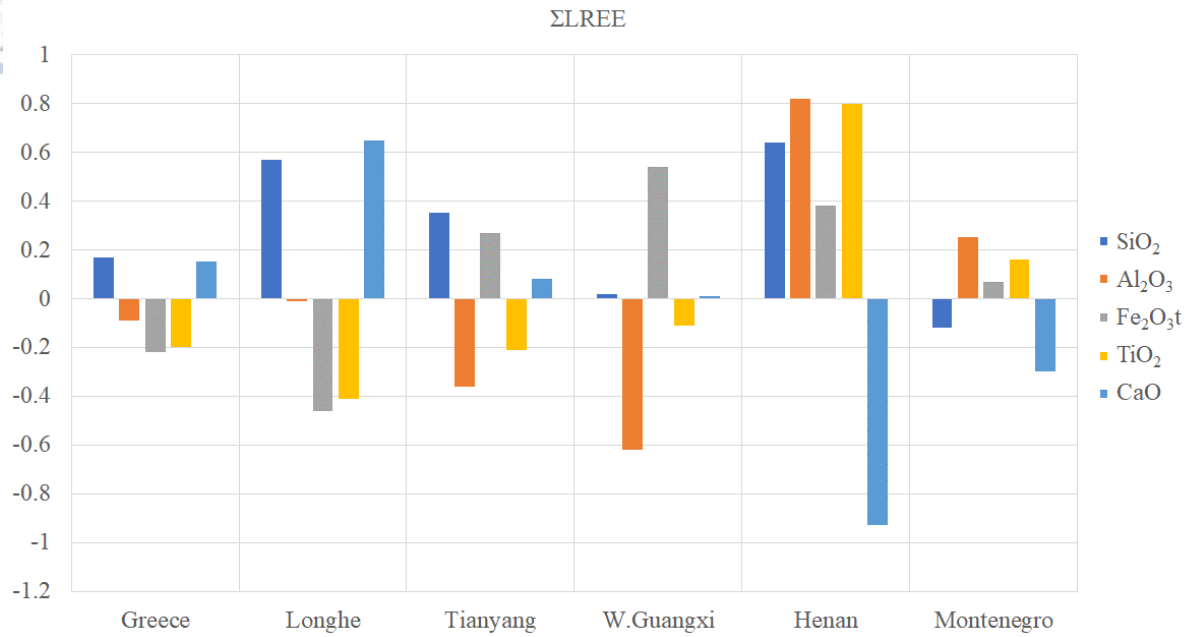


Figure 12: Bar graph of the major elements and the total light rare earth elements (ΣΛREE) for every area of study.

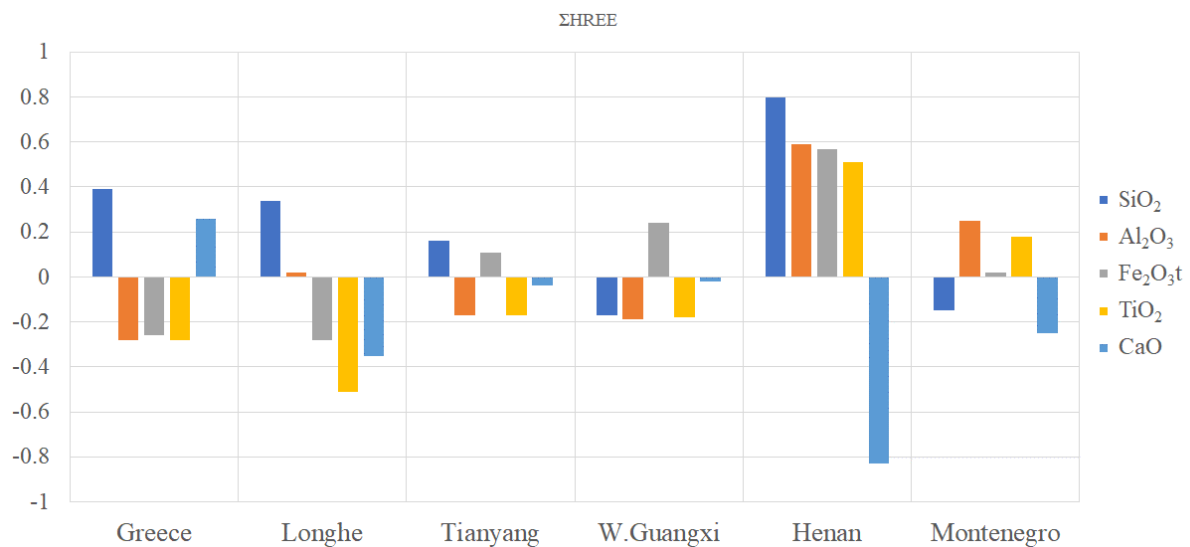
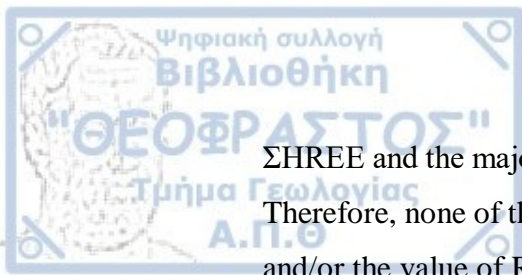


Figure 13: Bar graph of the major elements and the total heavy rare earth elements (ΣΗREE) for every area of study.

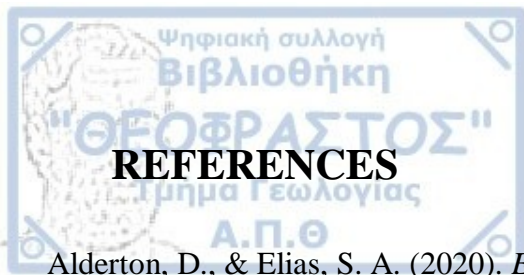
9 CONCLUSIONS

The data obtained in this study have revealed several significant findings.

- 1) The study confirmed the presence and concentration of rare earth elements (REE) in the bauxite deposits collected from various mines operated by Imerys Bauxites S.A. in Fokida, Central Greece.
- 2) Mineralogical analyses reveal that diaspore and boehmite are the major minerals in the bauxite ores.
- 3) The colour of the bauxite samples vary between yellow, orange-red and brownish-red.
- 4) The samples from Koromilia mine differentiate themselves from the rest having the highest Li and La concentrations.
- 5) The sample S.5_1, from 526 mine presents most of the highest values in traces and rare earth elements ($\Sigma\text{REE} = 877.38$ ppm) among our samples. This value is lower than all the other values of ΣREE from different bauxite mines that were examined, which are >1000 ppm. In particular, Longhe's highest value of ΣREE is 1035.23 ppm, Tianyang's is 2133.48 ppm, Western Guangxi's is 2134.37 ppm, Henan's is 1173.17 ppm and Montenegro's is 1008 ppm. Tianyang's and Western Guangxi's highest ΣREE values are approximately 2.5 times higher than the ones in this study.
- 6) Chondrite-normalized rare earth element diagrams of all bauxite deposits in Parnassos-Giona Zone show a positive Ce anomaly.
- 7) Our study results show no statistically significant relationship between ΣREE , ΣLREE , ΣHREE and the concentration of major elements, the pisoliths' size and percentage, the region and the colour. However, considering the small number of samples analyzed for this thesis, we recommend further and more extensive research of the bauxite deposits and their rare earth element (REE) concentrations.
- 8) Finally, the correlation comparison between Greece, China and Montenegro bauxite deposits, shows that the regions from China have the highest positive and negative correlations among the three countries, while Montenegro comes in second place and Greece last. In detail, intensively high correlations (mostly > 0.6 , absolute value) were found between ΣREE , ΣLREE , ΣHREE and the five major oxides analyzed in Henan samples. On the contrary, all the other correlation coefficients, for the rest five karst-bauxite deposits tested, between ΣREE , ΣLREE ,



ΣΗREE and the major elements show, in general, lower than 0.5 (absolute) values. Therefore, none of the major elements can be used as an indicator for the presence and/or the value of REE, LREE and HREE, according to this research.



REFERENCES

- Alderton, D., & Elias, S. A. (2020). *Encyclopedia of Geology* (2nd ed.). Academic Press.
- Aubouin, J. (1959). Granuloclasement vertical (graded bedding) et figures de courants (current marks) dans les calcaires purs; les breches de flanc des sillons geosynclinaux. *Bulletin de La Société Géologique de France*, S7-I(6), 578–582. <https://doi.org/10.2113/gssgfbull.S7-I.6.578>
- Aubouin, J. (1977). Brève présentation de la géologie de la Grèce. *Bull. Soc. Géol. France*, 7(XIX), 6–10.
- Bárdossy, G. (1984). *European bauxite deposits*. (In: Leonard Jr., J. (Ed.)).
- Bárdossy, G. (2013). *Karst Bauxites*. Elsevier.
- Bárdossy, G., & Aleva, G. J. J. (1990). *Lateritic Bauxites. Developments in Economic Geology*, 27. Elsevier Science Publishers.
- Bárdossy, G. Y., & Combes, P. J. (1999). *Karst bauxites: Interfingering of deposition and palaeoweathering*. Association of Sedimentologists, Special Publications, 27, Blackwell Science,.
- Bullerjahn, F., & Bolte, G. (2022). Composition of the reactivity of engineered slags from bauxite residue and steel slag smelting and use as SCM for Portland cement. *Construction and Building Materials*, 321, 126331.
- Celet, P. (1958). Existence d'une serie cretacee allochtone dans la region occidentale du Parnasse (Grece). *Bulletin de La Société Géologique de France*, 6(5), 471–486.
- Celet, P. (1962). *Contribution à l'étude géologique du Parnasse-Kiona et d'une partie des régions méridionales de la Grèce continentale*. Athènes : Laboratoire de géologie de l'Université.
- Celet, P. (1977). Les bordures de la zone du Parnasse (Grèce). Evolution paléogéographique au Mésozoïque et caractères structuraux. *6th Coll. Geol. Aegean Region, Athens.*, 725–740.
- Celet, P., Clement, B., & Ferriere, J. (1976). La zone béotienne en Grèce: Implications paléogéographiques et structurales. *Eclogae Geol. Helv.*, 69(3), 577–599.

- Chao, X., Zhang, T., Lv, G., Chen, Y., Li, X., & Yang, X. (2022). Comprehensive application technology of bauxite residue treatment in the ecological environment: A review. *Bulletin of Environmental Contamination and Toxicology*, 109(1), 209–214.
- Clement, B. (1977). Relations structurales entre la zone du Parnasse et la zone Pelagonienne en Beotie (Grèce continentale). *6th Coll. Aegean Geol. Athens*, 237–251.
- Day, J., Geiger, H., Troll, V. R., Perez-Torrado, F. J., Aulinas, M., Gisbert, G., & Carracedo, J. C. (2022). Bouncing Spallation Bombs During the 2021 La Palma Eruption, Canary Islands, Spain. *Earth Science, Systems and Society*, 16.
- Day, J. M., Troll, V. R., Aulinas, M., Deegan, F. M., Geiger, H., Carracedo, J. C., Pinto, G. G., & Perez-Torrado, F. J. (2022). Mantle source characteristics and magmatic processes during the 2021 La Palma eruption. *Earth and Planetary Science Letters*, 597, 117793.
- Deady, E., Mouchos, E., Goodenough, K., Williamson, B., & Wall, F. (2014). Rare earth elements in karst-bauxites: A novel untapped European resource? *ERES 2014*.
- Dercourt, J. (1964). *Contribution à l'étude géologique d'un secteur du Péloponnèse septentrional*. Athènes : Laboratoire de géologie et paléontologie ; Paris : Faculté des sciences,.
- Dercourt, J. (1980). *Grèce: Introduction à la géologie générale*. Guide.
- Dolg, M., Stoll, H., Savin, A., & Preuss, H. (1989). Energy-adjusted pseudopotentials for the rare earth elements. *Theoretica Chimica Acta*, 75(3), 173–194.
<https://doi.org/10.1007/BF00528565>
- Eliopoulos, D., Economou, G., Tzifas, I., & Papatrechas, C. (2014). The potential of rare earth elements in Greece. *ERES2014*, 4–7.
- Fleury, J.-J. (1980). Les zones de Gavrovo-Tripolitza et du Pinde-Olonos (Grèce continentale et Péloponnèse du Nord). Evolution d'une plate-forme et d'un bassin dans leur cadre alpin. *Villeneuve d'Ascq : S.G.N.*



Gamaletsos, P. (2014). *Mineralogy and geochemistry of bauxites from Parnassos—Ghiona mines and the impact on the origin of the deposits* [Διδακτορική Διατριβή, Εθνικό και Καποδιστριακό

Πανεπιστήμιο Αθηνών (ΕΚΠΑ). Σχολή Θετικών Επιστημών. Τμήμα Γεωλογίας και Γεωπεριβάλλοντος]. <https://doi.org/10.12681/eadd/42199>

Gamaletsos, P. N., Godelitsas, A., Filippidis, A., & Pontikes, Y. (2019). The rare earth elements potential of Greek bauxite active mines in the light of a sustainable REE demand. *Journal of Sustainable Metallurgy*, 5, 20-47.

Gándara, M. F. (2013). Aluminium: The metal of choice. *Mater. Tehnol*, 47(3), 261–265.

Gow, N. N., & Lozej, G. P. (1993). Bauxite. *Geoscience Canada*. <https://journals.lib.unb.ca/index.php/GC/article/view/3785>

Gregou, S. (1996). *THE PRE - FLYSCH AND BASAL SHALY FLYSCH DEPOSITION IN THE PARNASSUS - GHIONA ZONE, CENTRAL GREECE* [Doctoral Dissertation, Sweden. Lund University]. <https://doi.org/10.12681/eadd/8617>

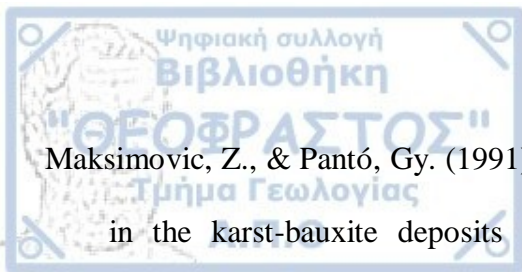
Harder, E. C. (1949). *Stratigraphy and Origin of Bauxite Deposits*. 60, 887. [https://doi.org/10.1130/0016-7606\(1949\)60\[887:SAOOBD\]2.0.CO;2](https://doi.org/10.1130/0016-7606(1949)60[887:SAOOBD]2.0.CO;2)

Hauke, J., & Kossowski, T. (2011). Comparison of values of Pearson's and Spearman's correlation coefficients on the same sets of data. *Quaestiones Geographicae*, 30(2), 87–93.

Ismail, N. J., Othman, M. H. D., Kamaludin, R., Esham, M. I. M., Ali, N. A., Rahman, M. A., Jaafar, J., & Bakar, S. A. (2019). Characterization of Bauxite as a Potential Natural Photocatalyst for Photodegradation of Textile Dye. *Arabian Journal for Science and Engineering*, 44, 10031–10040.

Jain, A. K., Murty, M. N., & Flynn, P. J. (1999). Data clustering: A review. *ACM Computing Surveys (CSUR)*, 31(3), 264–323.

- Kantiranis, N., Stergiou, A., Filippidis, A., & Drakoulis, A. (2004). CALCULATION OF THE PERCENTAGE OF AMORPHOUS MATERIAL USING PXRD PATTERNS. *Bulletin of the Geological Society of Greece*, 36(1), 446–453. <https://doi.org/10.12681/bgsg.16734>
- Karadağ, M. M., Küpeli, Ş., Arık, F., Ayhan, A., Zedef, V., & Döyen, A. (2009). Rare earth element (REE) geochemistry and genetic implications of the Mortaş bauxite deposit (Seydişehir/Konya–Southern Turkey). *Geochemistry*, 69(2), 143–159.
- Kehagia, F. (2010). A successful pilot project demonstrating the re-use potential of bauxite residue in embankment construction. *Resources, Conservation and Recycling*, 54(7), 417–421.
- Kodinariya, T., & Makwana, P. (2013). Review on Determining of Cluster in K-means Clustering. *International Journal of Advance Research in Computer Science and Management Studies*, 1, 90–95.
- Kossmat, F. (1924). Geologie der Zentralen Balkanhalbinsel: Die Kriegsschauplätze 1914-1918, geologisch dargestellt, 12. *Bornträger, Berlin*.
- Lehman, A. (2005). *JMP for basic univariate and multivariate statistics: A step-by-step guide*. 481p.
- Liu, X., Wang, Q., Deng, J., Zhang, Q., Sun, S., & Meng, J. (2010). Mineralogical and geochemical investigations of the Dajia Salento-type bauxite deposits, western Guangxi, China. *Journal of Geochemical Exploration*, 105(3), 137–152.
- Liu, X., Wang, Q., Feng, Y., Li, Z., & Cai, S. (2013). *Genesis of the Guangou karstic bauxite deposit in western Henan, China*. *Ore Geology Reviews*, 55, 162-175. (n.d.).
- Liu, X., Wang, Q., Zhang, Q., Zhang, Y., & Li, Y. (2016). Genesis of REE minerals in the karstic bauxite in western Guangxi, China, and its constraints on the deposit formation conditions. *Ore Geology Reviews*, 75, 100–115.
- MacQueen, J. (1967). Classification and analysis of multivariate observations. *5th Berkeley Symp. Math. Statist. Probability*, 281–297.



Maksimovic, Z., & Pantó, Gy. (1991). Contribution to the geochemistry of the rare earth elements in the karst-bauxite deposits of Yugoslavia and Greece. *Geoderma*, 51(1–4), 93–109.

[https://doi.org/10.1016/0016-7061\(91\)90067-4](https://doi.org/10.1016/0016-7061(91)90067-4)

Mountrakis, D. (2010). *Geologia kai Geotektoniki exeliki tis Elladas* (1st ed.). UNIVERSITY STUDIO PRESS A.E.

Mymrin, V., Guidolin, M. A., Klitzke, W., Alekseev, K., Guidolin, R. H., Avanci, M. A., Pawlowsky, U., Winter Jr, E., & Catai, R. E. (2017). Environmentally clean ceramics from printed circuit board sludge, red mud of bauxite treatment and steel slag. *Journal of Cleaner Production*, 164, 831–839.

Nopcsa, F. B. (1921). Geologische Grundzüge der Dinariden. *Geologische Rundschau*, 12(1), 1–19.

Nyamsari, D. G. & Yalcin M. G. (2017). Statistical analysis and source rock of the Minim-Martap plateau bauxite, Cameroon. *10(18)*, 1–16.

Orescanin, V., Nad, K., Mikelic, L., Mikulic, N., & Lulic, S. (2006). Utilization of bauxite slag for the purification of industrial wastewaters. *Process Safety and Environmental Protection*, 84(4), 265–269.

Papastamatiou, J. (1960). La geologie de la region montagneuse du Parnasse-Kiona-Oeta [with discussion]. *Bulletin de La Société Géologique de France*, 7(4), 398–409.

Patil, K. C. (1993). Advanced ceramics: Combustion synthesis and properties. *Bulletin of Materials Science*, 16, 533–541.

Pomoni-Papaioannou, F., & Solakius, N. (1991). Phosphatic hardgrounds and stromatolites from the limestone/shale boundary section at Prossilion (Maastrichtian-Paleocene) in the Parnassus-Ghiona Zone, Central Greece. *Palaeogeography, Palaeoclimatology, Palaeoecology*, 86(3–4), 243–254.

Radusinović, S., & Papadopoulos, A. (2021). The potential for REE and associated critical metals in karstic bauxites and bauxite residue of Montenegro. *Minerals*, 11(9), 975.

Richter, D., Müller, C., & Mihm, A. (1991). Die faziellen Beziehungen zwischen Parnass-und Pindos-Zone sowie die Vulkanite im Gebiet nördlich von Eratini (Kontinentalgriechenland).

Zeitschrift Der Deutschen Geologischen Gesellschaft, 67–86.

Robb, L. (2005). *Introduction to ore-forming processes* (2nd ed.). Wiley-Blackwell.

Robertson, A. H. F., Clift, P. D., Degnan, P. J., & Jones, G. (1991). Palaeogeographic and palaeotectonic evolution of the Eastern Mediterranean Neotethys. *Palaeogeography, Palaeoclimatology, Palaeoecology*, 87(1), 289–343. [https://doi.org/10.1016/0031-0182\(91\)90140-M](https://doi.org/10.1016/0031-0182(91)90140-M)

Solakius, N., Larsson, K., & Pomoni-Papaioannou, F. (1992). Planktic foraminiferal biostratigraphy of the carbonate/flysch transitional beds at Prossilion, in the Parnassus-Ghiona Zone, Central Greece. *Acta Geologica Hungarica*, 35, 441–445.

Soler, J. M., & Lasaga, A. C. (1996). A mass transfer model of bauxite formation. *Geochimica et Cosmochimica Acta*, 60(24), 4913–4931.

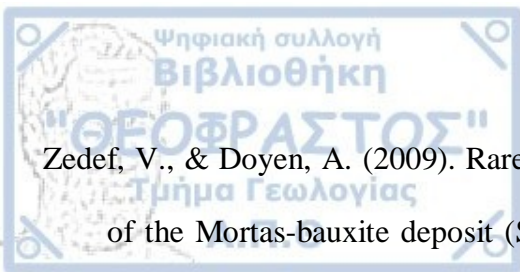
St, L., & Wold, S. (1989). Analysis of variance (ANOVA). *Chemometrics and Intelligent Laboratory Systems*, 6(4), 259–272.

Sun, S.-S., & McDonough, W. F. (1989). Chemical and isotopic systematics of oceanic basalts: Implications for mantle composition and processes. *Geological Society, London, Special Publications*, 42(1), 313–345.

Taylor, G., & Eggleton, R. A. (2008). Genesis of pisoliths and of the Weipa Bauxite deposit, northern Australia. *Australian Journal of Earth Sciences*, 55(S1), S87–S103.

Verma, A. S., Suri, N. M., & Kant, S. (2017). Applications of bauxite residue: A mini-review. *Waste Management & Research*, 35(10), 999–1012.

Wilschefski, S. C., & Baxter, M. R. (2019). Inductively coupled plasma mass spectrometry: Introduction to analytical aspects. *The Clinical Biochemist Reviews*, 40(3), 115.



Zedef, V., & Doyen, A. (2009). Rare earth element (REE) geochemistry and genetic implications of the Mortas-bauxite deposit (Seydis-ehir/Konya–Southern Turkey). *Chemie Der Erde*, 69, 143–159.

Internet sources:

<https://www.usgs.gov/media/images/bauxite-deposit-world-map> (retrieved 14/02/2022)